**CLELTON APARECIDO DOS SANTOS**

# "ESTUDOS ESTRUTURAIS E FUNCIONAIS DE PROTEÍNAS RELACIONADAS À PATOGENICIDADE DE *XYLELLA FASTIDIOSA*"

**CAMPINAS**
**2013**

# UNIVERSIDADE ESTADUAL DE CAMPINAS

INSTITUTO DE BIOLOGIA

**CLELTON APARECIDO DOS SANTOS**

# "ESTUDOS ESTRUTURAIS E FUNCIONAIS DE PROTEÍNAS RELACIONADAS À PATOGENICIDADE DE *XYLELLA FASTIDIOSA*"



Tese apresentada ao Instituto de Biologia da UNICAMP para obtenção do Título de Doutor em Genética e Biologia Molecular, na área de Genética de Microorganismos.

Orientadora: Profa. Dra. ANETE PEREIRA DE SOUZA
Coorientador: Prof. Dr. RICARDO APARICIO

**CAMPINAS,**
**2013**

FICHA CATALOGRÁFICA ELABORADA POR
MARA JANAINA DE OLIVEIRA – CRB8/6972
BIBLIOTECA DO INSTITUTO DE BIOLOGIA - UNICAMP

Sa59e

Santos, Clelton Aparecido dos, 1984-
Estudos estruturais e funcionais de proteínas relacionadas à patogenicidade de Xylella fastidiosa / Clelton Aparecido dos Santos. – Campinas, SP: [s.n.], 2013.

Orientador: Anete Pereira de Souza.
Coorientador: Ricardo Aparício.
Tese (doutorado) – Universidade Estadual de Campinas, Instituto de Biologia.

1. Xylella fastidiosa. 2. Biofilme. 3. DsbC. 4. 5'-nucleotidase. 5. Sistema Tol-Pal. I. Souza, Anete Pereira de, 1962-. II. Aparicio, Ricardo, 1971-. III. Universidade Estadual de Campinas. Instituto de Biologia. IV. Título.

Informações para Biblioteca Digital

**Título em Inglês**: Structural and functional characterization of proteins related to the pathogenicity of *Xylella fastidiosa*
**Palavras-chave em Inglês**:
*Xylella fastidiosa*
Biofilm
DsbC
5'-Nucleotidase
Tol-Pal system
**Área de concentração:** Genética de Microrganismos
**Titulação:** Doutor em Genética e Biologia Molecular
**Banca examinadora:**
Anete Pereira de Souza [Orientador]
Luís Antonio Peroni
Laurival Antonio Vilas-Bôas
Ljubica Tasic
Jörg Kobarg
**Data da defesa:** 22-02-2013
**Programa de Pós Graduação:** Genética e Biologia Molecular

Campinas, 22 de fevereiro de 2013

**BANCA EXAMINADORA**

Profa. Dra. Anete Pereira de Souza (orientadora)

Assinatura

Prof. Dr. Laurival Antonio Vilas-Bôas

Assinatura

Profa. Dra. Ljubica Tasic

Assinatura

Dr. Jörg Kobarg

Assinatura

Dr. Luis Antônio Peroni

Assinatura

Dra. Katlin Brauer Massirer

Assinatura

Prof. Dr. Carlos Henrique Inacio Ramos

Assinatura

Prof. Dr. Flavio Henrique da Silva

Assinatura

**"Et si sensus deficit, ad firmandum cor sincerum sola fides sufficit..."**

*do latin, em português algo como:*

*"Para além do entendimento, do sincero coração a fé (e o amor) é o suficiente..."*

# AGRADECIMENTOS

*Utilizando-me de algumas palavras eu gostaria de expressar a minha gratidão a todos que de alguma forma me encorajaram durante meus estudos de doutorado.*

*Eu tive o privilégio de durante os anos de 2009 a 2012, estar rodeado por pessoas maravilhosas, que não só contribuíram com meus conhecimentos científicos, mais me ensinaram valores morais e pessoais que sem dúvida fizeram a diferença na minha formação.*

*Muito obrigado,* ***Profa. Anete P. Souza*** *por ter me aceitado como aluno de doutorado, pela motivação e pela incansável persistência que demonstra com seus alunos e projetos. O seu exemplo é algo muito bonito que eu pretendo cultivar.*

*Agradeço também o* ***Prof. Ricardo Aparicio****, com quem tive o prazer de passar muitas horas coletando dados de biologia estrutural e discutindo resultados. Obrigado pelas brilhantes ideias e por toda amizade.*

*Aos* ***Amigos do LAGM*** *e de outros lugares que passei durante esses anos: estar com vocês foi tão bom que hoje eu me sinto a vontade para dizer que o sucesso deste trabalho é devido à ótima convivência e ajuda que vocês me proporcionaram. Sentirei muitas saudades de vocês e deste tempo!*

*O meu gosto pela ciência vem de longa data, porém ele foi estimulando ainda mais por algumas pessoas com quem eu pude compartilhar um pouco da minha vivência durante esta caminhada. Dentre estas pessoas eu não poderia deixar de agradecer duas pessoas que sempre*

*serão muito especiais para mim:* ***Profa. Olivia M. N. Arantes*** *e* ***Gislayne T. F. Vilas-Bôas****. Muito obrigado queridas por serem luz na minha vida.*

*Existe um antigo e sábio provérbio que diz que por trás de um grande homem, existe sempre uma grande mulher. Apesar da utilização do termo "grande homen" de uma forma despretenciosa para me autodesignar, pra mim o nome dessa grande mulher (de forma pretenciosa que o termo se remete) é* ***Lilian L. Beloti****. Obrigado coração!*

*À todos do Centro de Biologia Molecular e Engenharia Genética CBMEG/ UNICAMP e à FAPESP pela bolsa de doutorado que me foi concedida, o meu muito obrigado.*

*Não poderia deixar de agradecer ao meu pai* ***Felisberto Aparecido dos Santos*** *e à minha mãe* ***Neusa Zambianco dos Santos*** pela ternura e pela bravura que enfrentam a vida. Não existe riqueza maior do que aquela que é conquistada com os pequenos gestos de amor, esperança e integridade. Obrigado por terem cuidado tão bem de mim.

*Termino esta etapa confiante e com a esperança de poder deixar uma pequena contribuição à ciência e a sociedade por todo investimento feito à minha pessoa.*

*Clelton A. Santos*
*Fevereiro/2013*

**SUMÁRIO**

## Lista de Figuras

## Lista de Abreviações

| | |
|---|---|
| CD | Dicroísmo circular (*Circular Dichroism*) |
| C-terminal | Extremidade carboxi terminal da proteína |
| CVC | Clorose variegada dos citros |
| DLS | Espalhamento dinâmico de luz (*Dynamic Light Scattering*) |
| *D*max | Máxima distância intramolecular |
| DsbC | Proteína dissulfeto isomerase |
| EPS | Exopolissacarídeos |
| K*m* | Constante de Michaelis-Menten |
| N-terminal | Extremidade amino terminal da proteína |
| OD | Densidade ótica (*Optical Density*) |
| ORF | Quadro de leitura aberta (*Open Reading Frame*) |
| PAL | Lipoproteína associada ao peptidoglicano (*Peptidoglycan-Associated Lipoprotein*) |
| PDB | Banco de dados de estrutura de proteínas (*Protein Data Bank*) |
| pI | Ponto isoelétrico |
| PMSF | Fluoreto de fenilmetilsufonila |
| *p*NPP | *p*-Nitrofenil fosfato |
| Rg | Raio de giro |
| SAXS | Espalhamento de raios-X a baixos ângulos (*Small-Angle X-ray Scattering*) |
| SDS-PAGE | Eletroforese em gel de poliacrilamida com dodecil sulfato de sódio (*Sodium Dodecyl Sulfate-Polyacrylamide Gel Electrophoresis*) |
| SEC | Cromatografia de exclusão molecular (*Size Exclusion Chromatography*) |
| TCEP | Tris(2-carboxietil) fosfina |

| | |
|---|---|
| *Xf*5'-Nt | Proteína 5'-nucleotidase de *Xylella fastidiosa* |
| *Xf*DsbC | DsbC de *Xylella fastidiosa* |
| *Xf*DsbC$_{N\text{-}Red}$ | *Xf*DsbC não-reduzida |
| *Xf*DsbC$_{Red}$ | *Xf*DsbC reduzida |
| *Xf*Pal | PAL de *Xylella fastidiosa* |
| *Xf*TolB | Proteína de translocação B de *Xylella fastidiosa* |

# RESUMO

*Xylella fastidiosa* é uma bactéria responsável por inúmeras doenças de plantas em culturas economicamente importantes ao redor do mundo, incluindo a clorose variegada dos citros. Após a infecção de seu hospedeiro, as células de *X. fastidiosa* são aptas a formarem uma estrutura de biofilme que bloqueia os vasos xilemáticos, levando a uma condição de estresse hídrico na planta hospedeira e desencadeando o desenvolvimento da doença. Tendo como estímulo a relevância econômica da citricultura para o Brasil e, visando reduzir os prejuízos provocados pelos problemas fitossanitários que acometem esta cultura, foi realizado um consórcio de pesquisa com o intuito de se conhecer completamente o genoma da linhagem 9a5c de *X. fastidiosa*. Inúmeras proteínas associadas com patogenicidade, adaptação e sobrevivência bacteriana foram identificadas, incluindo *Xf*DsbC (proteína disulfeto isomerase), *Xf*5'-Nt (5'-nucelotidase), *Xf*TolB (proteína de translocação B) e *Xf*Pal (lipoproteina associada ao peptidoglicano) que foram caracterizadas neste estudo. Empregando ferramentas de caracterização de proteínas, aspectos funcionais e estruturais destas quatro proteínas alvos foram avaliados. Dentre os resultados destaca-se a imunodetecção de *Xf*DsbC, *Xf*5'-Nt, *Xf*TolB e *Xf*Pal durante as diferentes fases de formação e desenvolvimento do biofilme de *X. fastidiosa,* que é tido como o principal mecanismo de patogenicidade deste fitopatógeno, confirmando a predição inicial de tais proteínas como associadas a patogenicidade bacteriana. Adicionalmente, resultados funcionais e estruturais revelaram detalhes finos do papel biológico desempenhado por cada uma das proteínas estudadas. Juntos, os resultados apresentados neste trabalho contribuem para o melhor entendimento de patogenicidade bacteriana, especialmente com respeito ao fitopatógeno *X. fastidiosa*.

## ABSTRACT

*Xylella fastidiosa* is a plant pathogen bacterium responsible for numerous economically important crops diseases around the world, including the citrus variegated chlorosis. Following the host infection, the *X. fastidiosa* cells are able to form a biofilm structure which block the xylem vessels, leading to a hydric stress condition in the host plant and triggers the desease development. Given the economic relevance of citriculture for Brazil and in order to reduce the damage caused by phytosanitary problems that affect the citrus production, a research consortium was established with the aim to elucidate the complete genome sequence of the *X. fastidiosa* 9a5c strain. Numerous proteins associated with bacterial pathogenicity, adaptation and survival have been identified, including *Xf*DsbC (protein disulfide isomerase), *Xf*5'-Nt (5'-nucleotidase), *Xf*TolB (protein translocation B) and *Xf*Pal (peptidoglycan-associated lipoprotein) which were characterized in this study. Using tools for protein characterization, structural and functional aspects of these four protein targets were evaluated. Among the results, we highlight the immunodetection of *Xf*DsbC, *Xf*5'-Nt, *Xf*TolB and *Xf*Pal during the different stages of *X. faastidiosa* biofilm formation and development which is considered the primary mechanism of pathogenicity of this pathogen. These findings, confirming the initial prediction that relates such proteins as associated with bacterial pathogenicity. Additionally, structural and functional results revealed accurate details of the biological role played by each protein studied. Taken together, the findings presented in this study contribute to a better understanding of bacterial pathogenesis, especially with regard to the plant pathogen *X. fastidiosa*.

# 1. INTRODUÇÃO

## 1.1. *Xylella fastidiosa*: genoma e citricultura

Dentro do cenário agrícola do Brasil, a citricultura permanece como uma cultura de destaque do agronegócio brasileiro. Em nota, a Associação Nacional de Exportadores de Suco Cítricos (Citrus/BR) estima que a safra 2011/2012 rendeu aproximadamente US$ 1,5 bilhão, sendo o Estado de São Paulo o maior produtor do país.

Tendo como estímulo a relevância econômica da citricultura para o Estado de São Paulo e para o Brasil e, visando reduzir os prejuízos provocados pelos problemas fitossanitários que acometem esta cultura, foi realizado um consórcio de pesquisa (ONSA – Organização para Sequenciamento e Análise de Nucleotídeos) com a finalidade de conhecer completamente o genoma da linhagem de *Xylella fastidiosa* 9a5c, agente etiológico da Clorose Variegada dos Citros (CVC) (Lee *et al.,* 1991; Chang *et al*., 1993), isolada em 1992 em pomares de laranja Valência (*Citrus sinensis* (L.) Osbeck) afetados pela CVC no Estado de São Paulo (Chang *et al*., 1993).

*X. fastidiosa* é um bacilo Gram-negativo (Wells *et al.,* 1987) que se multiplica no xilema das plantas hospedeiras (Hopkins, 1989) e no lúmen do canal alimentar de insetos vetores (cigarrinhas) (Alves *et al*., 2008) responsáveis pela transmissão da bactéria às plantas (Roberto *et al*., 1996). Além do citros, linhagens distintas de *X. fastidiosa* podem atacar outras culturas (Almeida *et al*., 2008) incluindo lavouras economicamente importantes como café, ameixa e uva (Purcell & Hopkins, 1996).

A análise do sequenciamento da linhagem de *X. fastidiosa* 9a5c (Simpson *et al*., 2000), revelou que seu genoma apresenta um conteúdo GC de 52.7% e contém, além do cromossomo principal de 2.679.305 pares de bases (pb), dois plasmídeos, p*XF*51 com 51.158 pb e p*XF*1.3

com 1.285 pb. Um total de 2.904 ORFs (*Open Reading Frames*) foram anotadas, sendo deste total, 47% semelhantes a proteínas já descritas em outros organismos. Contudo, ressalta-se a anotação de sequências codificantes para proteínas ainda não caracterizadas, muitas das quais, podem estar envolvidas com a patogenicidade desta bactéria.

As proteínas homólogas foram classificadas em diferentes grupos funcionais (http://www.lbi.ic.unicamp.br/*Xf*/). Dentre estas categorias, 220 proteínas foram consideradas envolvidas com os mecanismos de patogenicidade, virulência e adaptação. Entretanto, apesar do sequenciamento completo do genoma de *X. fastidiosa* ter trazido muitas informações genéticas sobre esse fitopatógeno, apenas os estudos funcionais poderão levar a um melhor entendimento dos mecanismos de patogenicidade desta bactéria.

Neste sentido, a análise estrutural e funcional de proteínas de *X. fastidiosa*, principalmente aquelas envolvidas com a patogenicidade, virulência e adaptação é de extrema importância. Apesar de alguns estudos já terem sido realizados (Azzoni *et al*., 2004; Rosselli *et al*., 2006; Tranvensolo *et al.,* 2008; Saraiva *et al.,* 2009; Caserta *et al.*, 2010; Toledo *et al*., 2011; Rosselli-Murai *et al.,* 2012), as informações geradas pelo projeto de sequenciamento desta bactéria nos permite investigações mais detalhadas. Tais esforços tem contribuido significativamente para o entendimento do comportamento deste fitopatógeno no ambiente, bem como ajudado na elucidação dos seus mecanismos de patogenicidade.

### 1.2. *Xylella fastidiosa*: formação de biofilme e patogenicidade

Bactérias fitopatogênicas como *X. fastidiosa* apresentam, na maioria das vezes, um restrito espectro de hospedeiros, sendo geralmente confinadas a uma única espécie ou gênero de planta (da Silva *et al.,* 2002; Vojnov *et al.,* 2010). Esta especificidade é garantida pelo produto

dos genes de avirulência denominados de *avr*, presentes no patógeno. Os genes *avr* desempenham papel importante na patogenicidade, pois são estes que vão determinar o desenvolvimento ou a resistência à doença (Collmer, 1998).

Uma peculiaridade da análise do genoma da linhagem 9a5c de *X. fastidiosa* foi a descoberta da ausência dos genes *avr* (Simpson *et al.*, 2000). Pelo fato de tais genes modularem a fase de reconhecimento genético entre a planta e o patógeno, a ausência desses genes indicava que outros mecanismos de patogenicidade, não envolvendo a presença dos genes *avr*, poderiam estar presentes em *X. fastidiosa*. Dentre estes, a oclusão física do xilema decorrente da colonização de *X. fastidiosa*, o sequestro de nutrientes, a produção de toxinas e o desequilíbrio fitormonal, poderiam afetar o sistema fotossintético de uma planta susceptíveis, sendo apontados como mecanismos de patogenicidade (Hopkins, 1989).

Fortes evidências suportavam a ideia de que, uma vez que as células de *X. fastidiosa* eram injetadas nos vasos xilemáticos de plantas hospedeiras, pelos insetos vetores (Homoptera, Cicadellidae, subfamily Cicadellinae) (Roberto *et al*., 1996; Alves *et al*., 2008), elas poderiam se aderir fortemente à parede do xilema (Purcell & Hopkins, 1996), chegando a obstruir mecanicamente tais vasos (Chang *et al*., 1993). Estas evidências foram reforçadas após o sequenciamento do genoma da linhagem de *X. fastidiosa* 9a5c, no qual se observou a grande diversidade de genes relacionados à produção de exopolissacarídeo (EPS), além da presença de inúmeros genes para a produção de proteínas de adesão (Simpson *et al.*, 2000).

Subsequentemente, com novos estudos na área da microscopia e proteômica, não demorou muito tempo para se chegar à conclusão de que *X. fastidiosa* poderia apresentar, além do crescimento planctônico, uma forma de crescimento em biofilme no interior dos vasos do xilema, sendo tal estrututa o principal mecanismo de patogenicidade desta bactéria.

A descoberta dos biofilmes microbianos trouxe enorme revolução na microbiologia e ecologia microbiana. Durante muitos anos, os microrganismos foram comumente descritos como organismos planctônicos, ou seja, suspensão de células individuais e de vida livre. Contudo, atualmente é consenso que diversas espécies de microrganismos crescem predominantemente em biofilmes em ambientes naturais (Sauer *et al*., 2002)

Biofilmes podem ser definidos como comunidades microbianas associadas a uma superfície, sendo muitas vezes denominados de agregados microbianos, nas quais a posição e as relações espaciais de cada célula do sistema são predeterminadas por um ciclo de desenvolvimento coordenado, mediado por moléculas sinalizadoras e alguns mecanismos de posicionamento celular (Stoodley *et al*., 2002).

As fases de desenvolvimento do biofilme microbiano já foram estabelecidas (Figura 1.1), compreendendo: i) a fase de adesão inicial, caracterizada pela adesão de algumas células ou grupos de células à superfície a ser colonizada; ii) início da maturação, quando se inicia a fase de estruturação e arquitetura do biofilme; iii) biofilme maduro, quando a densidade celular atinge seu maior grau e a arquitetura do biofilme é altamente complexa; e iv) fase de dispersão, na qual alguns grupos de células se destacam do biofilme maduro para colonizarem outras partes do hospedeiro (Sauer *et al*., 2002).

Souza *et al*. (2004) realizaram um estudo da expressão global de genes de *X. fastidiosa* comparando as condições de crescimento em biofilme e na forma planctônica. Neste estudo, as fases de desenvolvimento do biofilme de *X. fastidiosa* linhagem 9a5c foram estabelecidas *in vitro*. Os autores descreveram que entre 3-5 dias de crescimento as células haviam começado a aderir ao substrato, formando pequenos agregados. Após 10 dias de desenvolvimento, houve o início da formação das micro-colônias, embora alguns grupos pequenos de células se mantivessem ainda livres. O desenvolvimento da arquitetura inicial do biofilme foi vista após 15

dias, tendo atingido seu auge com 20 dias, quando foi observada a maior densidade celular, caracterizando, desta forma a fase de biofilme maduro. A última fase de desenvolvimento, correspondendo à fase de dispersão do biofilme foi visto após 30 dias da adesão inicial das células ao substrato, sendo caracterizada pela desagregação de grupos de células e re-colonização de outras superfícies.

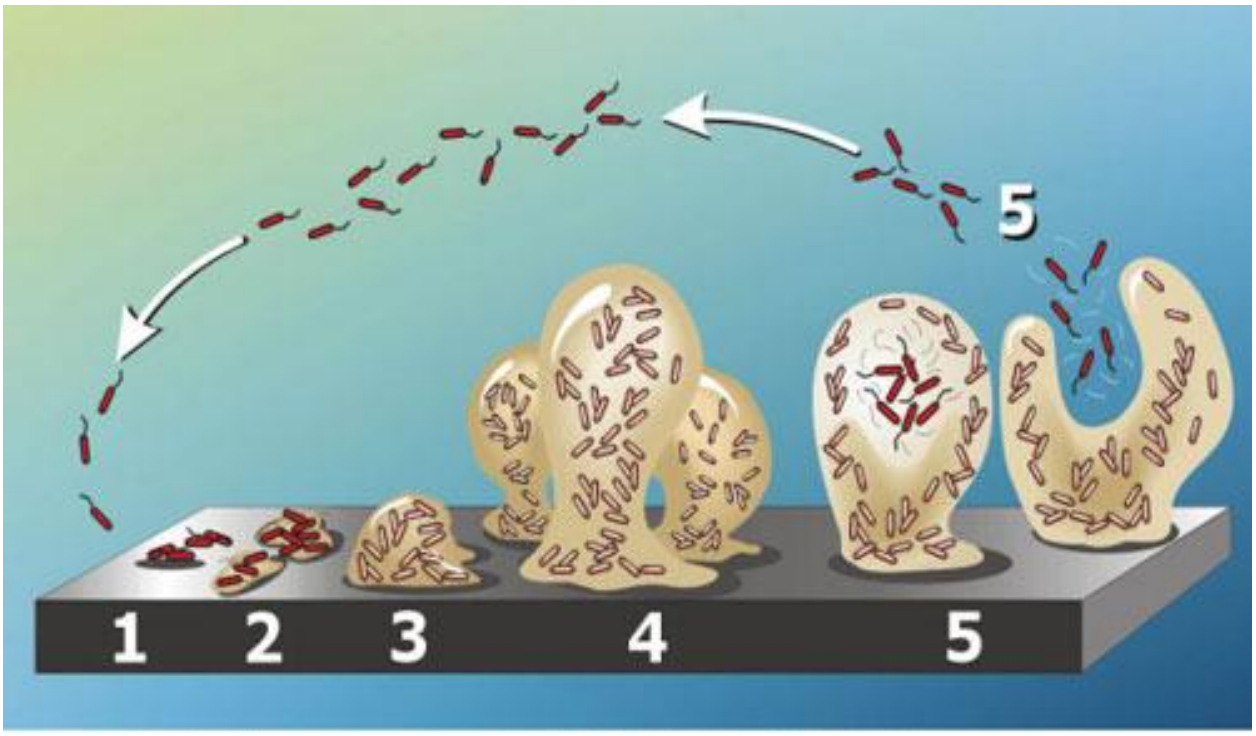


**Figura 1.1.** Fases de desenvolvimento do biofilme microbiano. Fase 1: adesão inicial de células a superfície. Fase 2: produção de EPS resultando na adesão firme e irreversível a superfície. Fase 3: desenvolvimento inicial da arquitetura do biofilme. Fase 4: maturação da arquitetura do biofilme. Fase 5: dispersão de células do biofilme. Adaptado de Sauer *et al*. (2002).

Estudos focando no perfil de expressão gênica entre a forma de crescimento em biofilme e planctônica já foram realizados. Souza *et al*. (2004), utilizando microarranjos de DNA, demonstraram que 202 genes foram induzidos na condição de crescimento em biofilme, enquanto 32 genes foram reprimidos nesta mesma condição. Os genes induzidos foram relacionados a funções regulatórias, metabolismo de proteínas, manutenção de plasmídeo e biossíntese de aminoácidos, cofatores, polissacarídeos de superfície, lipopolissacarídeos e proteínas de transporte. Em adição, a expressão de genes que codificam para *pili* e para proteínas envolvidas na adesão da bactéria ao substrato, também foi observada. Posteriormente, Caserta *et al.* (2010) demonstraram a imunodetecção de proteínas de adesão (XadA1 e XadA2) e *pili* (PilC) no biofilme de *X. fastidiosa.* Contudo, pouco se sabe sobre o papel de outras proteínas na formação e desenvolvimento de biofilmes microbianos.

Silva *et al*. (2011), analisaram o proteoma do biofilme maduro (com 20 dias de formação) de *X. fastidiosa*. Os autores encontraram um total de 456 proteínas expressas nesta condição, que correspondem a aproximadamente 10% do total de proteínas presentes no genoma. A análise do biofilme mostrou 144 proteínas (37%) diferentes das encontradas na condição de crescimento planctônico. Análises de espectrometria de massas foram utilizadas para identificar esras proteínas e, os resultados revelaram que a maioria das proteínas expressas no biofilme maduro de *X. fastidiosa* estavam associadas com metabolismo, adesão celular, patogenicidade e com resposta a condição de estresse.

Neste contexo, o estudo de proteínas que estejam direta ou indiretamente envolvidas com a formação e desenvolvimento do biofilme de *X. fastidiosa*, abre novas perspectivas para a compreensão dos mecanismos de patogenicidade deste fitopatógeno.

## 1.3. ORFs selecionadas para o estudo

A anotação das ORFs de *X. fastidiosa* linhagem 9a5c, pode ser obtida no site http://www.xylella.lncc.br/, que disponibiliza também, além da linhagem 9a5c, o genoma de cinco outras linhagens de *X. fastidiosa* completamente sequenciados.

A seleção das ORFs alvo deste estudo foi baseada na análise de Simpson *et al*. (2000), sendo que as ORFs selecionadas estavam incluídas entre as proteínas envolvidas com patogenicidade, virulência e adaptação. As características das quatro ORFs selecionadas para este estudo são detalhadas a seguir. Detalhes adicionais sobre as proteínas codificadas por tais ORFs podem ser encontrados nos capítulos 1, 2 e 3.

### 1.3.1 ORF *Xf*1177

A ORF *Xf*1177 possui 789 pb e, segundo análises de similaridade de sequencias, parece codificar uma proteína periplasmática com 263 aminoácidos e 28,5 kDa. Essa proteína apresenta similaridade superior a 70% com uma enzima DsbC (dissulfeto isomerase) da família Dsb de várias *Xanthomonas* spp.

As proteínas da família Dsb (*Disulfide bond*) são responsáveis pela formação e isomerização das ligações de dissulfeto no periplasma bacteriano e contribuem para a estabilidade, atividade e enovelamento de muitas proteínas secretadas ou domínios extra-citoplasmáticos de proteínas de membrana ricos em resíduos de cisteína (Kadokura & Beckwith, 2010).

Quimicamente, o processo de formação da ligação de dissulfeto é uma reação oxidante em que dois elétrons são removidos da proteína. Por outro lado, a quebra de uma ligação de dissulfeto é uma reação redutora, na qual dois elétrons são doados para a proteína. As enzimas

que interagem diretamente com o enovelamente protéico por introduzirem ou romperem as ligações de dissulfeto são, na maioria dos casos, oxidorredutases pertencentes à superfamília das tiorredoxinas e possuem o motivo CXXC (cisteínas separadas por dois aminoácidos) no sítio ativo.

Em *E. coli*, o sistema de formação e isomerização das ligações de dissulfeto é formado por cinco proteínas: DsbA, DsbB, DsbC, DsbD e DsbG (Kadokura *et al.,* 2003) sendo DsbB e DsbD proteínas integrais de membrana. A ORF *Xf*1177 tem o domínio funcional de uma DsbC e está envolvida na isomerização e redução das ligações de dissulfeto (Figura 1.2).

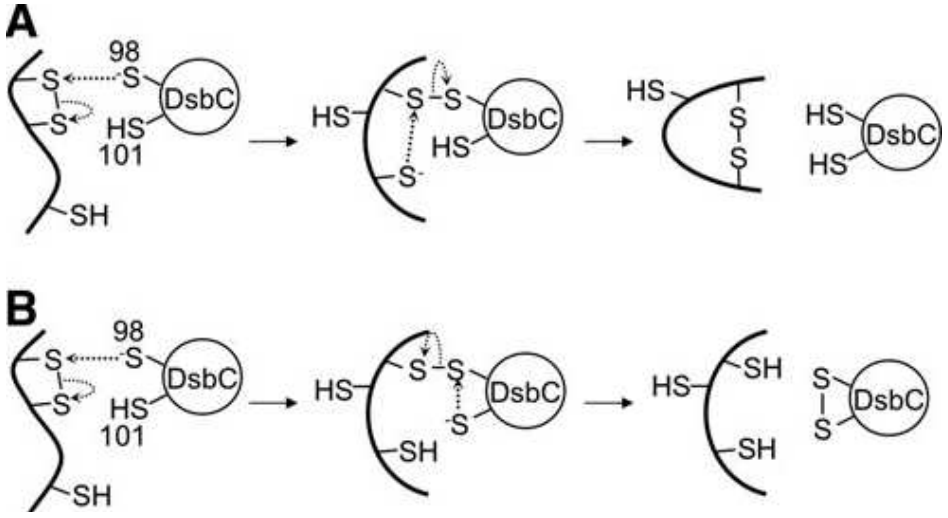


**Figura 1.2**. Isomerização (A) e redução (B) das ligações de dissulfeto catalisada pela proteína DsbC. Na etapa de isomerização a ligação de dissulfeto não nativa é rearranjada para que a proteína assuma sua estrutura corretamente enovelada, já na etapa de redução, DsbC reduzida doa 2 elétrons para a proteína rompendo a ligação. Na figura é apresentado o grupo tiol das cisteínas 98 e 101 do sítio ativo da proteína DsbC (Kadokura & Beckwith, 2010).

Apesar do mecanismo de isomerização catalisado pela proteína DsbC ser muito estudado, ainda não foi elucidado completamente o modo pelo qual DsbC repara as ligações de dissulfeto

formadas incorretamente. Dois modelos são propostos (Rietsch *et al.,* 1997; Kadokura *et al*., 2003) e, em ambos os casos, a reação inicia-se com o ataque nucleofílico pela cisteína-98 da proteína DsbC à ligação de dissulfeto incorreta (Figura 1.2). Esta reação resulta na formação de uma ligação de dissulfeto entre DsbC e o substrato que pode ser resolvido por duas vias. No primeiro modelo (Figura 1.2 A), a ligação de dissulfeto formada entre o substrato e DsbC é atacada por uma terceira cisteína do substrato, resolvendo o complexo DsbC-substrato, gerando uma ligação de dissulfeto mais estável no substrato e restaurando o estado reduzido da proteína DsbC. Neste caso DsbC age como uma verdadeira dissulfeto isomerase. O segundo modelo (Figura 1.2 B), propõe que a ligação de dissulfeto formada entre DsbC-substrato é atacada pela cisteína-101 da proteína DsbC, gerando um substrato reduzido e uma proteína DsbC oxidada. O substrato, por sua vez, tem a chance de ser novamente oxidado pela proteína DsbA e formar suas ligações de dissulfeto. Vale destacar que neste último modelo DsbC age como uma redutase de ligação de dissulfeto. Em ambos os modelos, o sítio ativo da proteína DsbC deve estar reduzido para realizar o primeiro passo para o reparo das ligações de dissulfeto não nativas, ou seja, incorretas.

A estrutura tridimensional da proteína DsbC (PDB:1EEJ) de *E. coli,* resolvida por McCarthy *et al.* (2000), com 1,9 Å de resolução, revelou dois monômeros de 23 kDa que formam um homodímero em forma de "V" com enovelamento similar a tiorredoxina (Figura 1.3).

Em mutantes de *E. coli,* cujo o gene *dsbc* foi interrompido ou deletado, observa-se que proteínas ricas em resíduos de cisteínas apresentam atividade reduzida ou são degradadas (Hiniker & Bardwell, 2004; Berkmen *et al*., 2005; Messens *et al*., 2007; Vertommen *et al*., 2008). Entre essas proteínas destacam-se a endorribunuclease periplasmática (RNaseI), a endopeptidase (MepA), a fosfatase ácida periplasmática (AppA), e a endonuclease-1

periplasmática (End1). Além disso, é bem conhecido que mutantes nulos para *dsbc* apresentam um aumento de sensibilidade ao cobre (Hiniker *et al*., 2005), que possui a capacidade de oxidar proteínas na presença do oxigênio molecular. O aumento da sensibilidade ao referido metal, apresentado por estes mutantes, seria devido à incapacidade dos mesmos repararem as ligações de dissulfeto formadas incorretamente em proteínas no periplasma bacteriano quando em condições oxidantes.

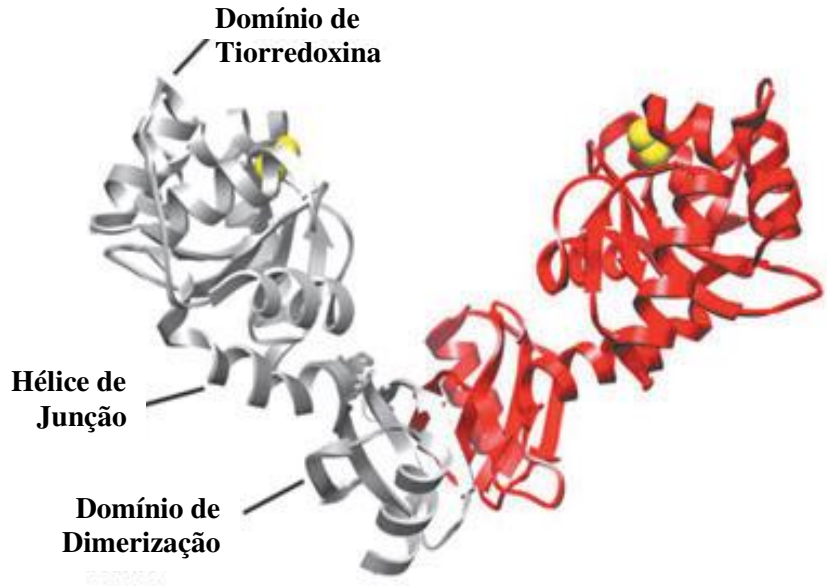


**Figura 1.3.** Estrutura tridimensional da proteína DsbC de *E. coli* (PDB:1EEJ). DsbC é um homodímero e cada um dos seus monômeros contém um domínio N-terminal de dimerização e um domínio C-terminal similar a tiorredoxina, sendo estes dois domínios conectados por uma hélice de junção. Em amarelo é apresentado as duas cisteínas (98 e 101) do sítio ativo.

Em adição à atividade de isomerização e redução, DsbC apresenta atividade de chaperonina, que permite que esta proteína se ligue a proteínas desenoveladas impedindo a agregação protéica (Bassette *et al*., 1999), sendo que esta propriedade é independente do sítio ativo (CXXC) (Liu & Wang, 2001). A soma de todas as características apresentadas por DsbC tem permitido seu emprego biotecnológico, com estudos recentes demonstrando o papel

preponderante desta proteína na produção de proteínas eucarióticas, corretamente enoveladas e solúveis, em sistemas de expressão/co-expressão simples, como o procariótico (Ponniah *et al*., 2010; Shouldice *et al*., 2010).

### 1.3.2 ORF *Xf*1808

O gene correspondendo à ORF *Xf*1808 (960 pb) codifica uma proteína com 320 aminoácidos e 34,9 kDa, com cerca de 87% de similaridade como uma 5'-Nucleotidase de *Xanthomonas campestris* pv. *vesicatoria*.

As 5´-Nucleotidases são enzimas que, por possuírem significante homologia de sequência em seu sítio catalítico, são incluídas na família de proteínas fosfatases. Estas fosfatases hidrolisam uma ampla gama de substratos incluindo todos os 5´-ribo e 5´-desoxirribonucleotídeos di ou trifosfatados, açúcares uridina difosfato e uma variedade de substratos sintéticos como o bis (*p*-nitrofenol) fosfato (Kohn & Reis, 1963). Algumas destas enzimas também apresentam atividade de fosfotransferase, transferindo o fosfato inorgânico para substratos desfosforilados.

Uma nucleotidase de *X. fastidiosa* (*Xf*SurE) foi recentemente caracterizada pelo nosso grupo (Saraiva *et al*., 2009). Os resultados desta caracterização demonstraram que esta nucleotidase apresenta atividade para os quatro substratos canônicos (naturais) (3´-AMP, 5´-dAMP, 5´-AMP e 5´-GMP), além disso a caracterização estrutural, empregando espalhamento de raios-X a baixos ângulos (SAXS), permitiu correlacionar aspectos funcionais inerentes ao comportamento alostérico apresentado por esta enzima. Outro achado de extrema relevância foi o fato de ter sido sugerido que *Xf*SurE parece ser uma enzima *house-cleaning*, ou seja, uma enzima que intercepta e hidrolisa nucleotídeos não canônicos, impedindo danos ao DNA,

confirmando, desta forma, a contribuição de estudos de caracterização estrutural/funcional de proteínas.

### 1.3.3 ORF *Xf*1624 e *Xf*1625

A ORF *Xf*1624 possui 432 pb e a proteína correlata apresenta 15.8 kDa (144 aminoácidos). A predição, baseada em BLAST-P, revela similaridade superior a 95% com a proteína precursora 6 de membana externa (Omp6), também chamada de lipoproteína associada ao peptídoglicano (Pal), de várias linhagens de *X. campestris*. A ORF *Xf*1625 possui 1320 pb e codifica uma proteína de 440 aminoácidos e 47.6 kDa. Os resultados de comparação entre essa proteína e outras já depositadas em bancos de dados (BLAST-P), revelaram sua similaridade (81%) com a proteína TolB de *Xanthomonas axonopodis* pv. *citri.*

As proteínas da família Tol se associam com a proteína denominada Pal formando o complexo Tol-Pal (Dubuisson *et al.*, 2002). O sistema Tol-Pal é bem conservado em bactérias Gram-negativas e seus componentes são necessários para a manutenção da integridade da membrana externa desses microrganismos (Sturgis, 2001). Este sistema é composto, até agora, por cinco proteínas. TolQ, TolR, TolA são proteínas da membrana plasmática, com domínios periplasmáticos, TolB é periplasmática e Pal, está associada ao peptidoglicano, sendo abundante na membrana externa (Cascales *et al*., 2002).

Apesar do sistema Tol-Pal ter sido intensivamente estudado em *E. coli*, seu papel fisiológico ainda é pouco conhecido. Acredita-se que esse sistema esteja envolvido na coesão do envelope bacteriano (Walburger *et al.,* 2002). Pelo fato destas proteínas estarem localizadas, especificamente, no sítio de constrição celular em *E. coli*, isso sugere que esse sistema constitui um sub-complexo do mecanismo de divisão celular das bactérias Gram-negativas, sendo

empregado para assegurar a correta invaginação da membrana externa durante a fissão binária (Gerding *et al*., 2007). Além disso, suas interações permitem a importação de colicinas do grupo A (Lazzaroni *et al.,* 2002) e DNA filamentoso de fagos como f1, fd, M13 e CTXphi (Click & Webster, 1997) para a intoxicação/infecção da célula. Em acréscimo, mutações nos genes *tol-pal* levam ao aumento da sensibilidade da célula a uma variedade de drogas e detergentes, podendo causar o extravasamento dos componentes periplasmáticos, ao mesmo tempo que torna esses mutantes resistentes a diferentes colicinas (Bonsor *et al.,* 2009 ).

A análise do genoma da linhagem de *X. fastidiosa* 9a5c, parece indicar a provável organização em *operon* das ORF *Xf*1624, *Xf*1625 (Figura 1.4). A organização transcricional dos genes de *E. coli* que codificam as proteínas do sistema Tol-Pal caracterizados com mais detalhes, revela a organização destes em dois *operons* adjacentes, estando posicionados no cromossomo na seguinte ordem: (*ybgC-tolQ-tolR-tolA*) e (*tolB-pal-ybgF*) (Webster, 1991), apesar de um transcrito *ybgC-ybgF* já ter sido observado (Vianney *et al*., 1996). Em *X. fastidiosa,* com exceção do gene *ybgF* que não foi encontrado no seu genoma, os genes do sistema Tol-Pal parecem seguir a mesma organização apresentada em *E. coli* (Figura 1.4).

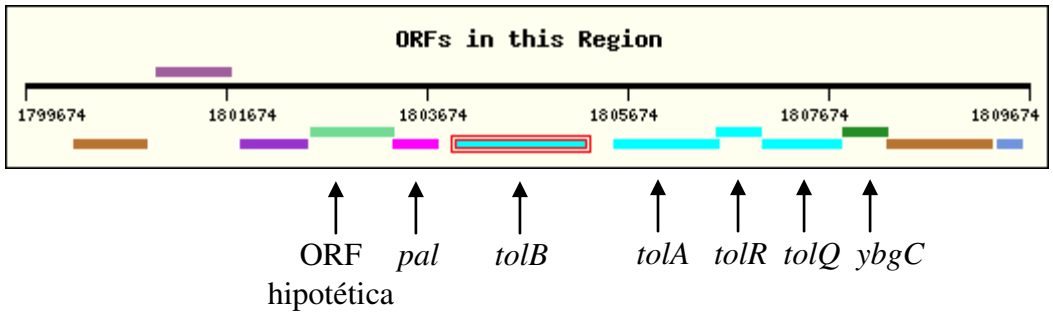


**Figura 1.4.** Disposição dos genes codificantes para o sistema Tol-Pal no cromossomo de *X. fastidiosa* 9a5c.

## 1.4. OBJETIVOS

### 1.4.1. Objetivos Gerais

- Contribuir para o conhecimento dos mecanismos de patogenicidade de *X. fastidiosa*, caracterizando quatro ORFs que codificam proteínas, supostamente, relacionadas à sua patogenicidade.

### 1.4.2. Objetivos Específicos

- Efetuar a clonagem e a expressão heteróloga das ORFs *Xf*1177 (*Xf*DsbC), *Xf*1808 (*Xf*5´-Nt), *Xf*1624 (*Xf*Pal), *Xf*1625 (*Xf*TolB), assim como realizar a purificação das proteínas recombinantes produzidas;

- Realizar a caracterização bioquímica e biofisica das proteínas recombinantes expressas / purificadas;

- Elucidar a provável função desempenhada pelas proteínas alvos estudadas.

## 2 CAPÍTULO 1 – ARTIGO

# "Functional and structural studies of the disulfide isomerase DsbC from the plant pathogen *Xylella fastidiosa* reveals a redox-dependent oligomeric modulation *in vitro*"

**Autores:** Clelton A. Santos, Marcelo A. S. Toledo, Daniela B. B. Trivella, Lilian L. Beloti, Dilaine R. S. Schneider, Antonio M. Saraiva, Aline Crucello, Adriano R. Azzoni, Alessandra A. Souza, Ricardo Aparicio, Anete P. Souza

**Publicado na Revista *FEBS Journal***

**Volume 279 (20), páginas 3828–3843, Outubro 2012**


# Functional and structural studies of the disulfide isomerase DsbC from the plant pathogen *Xylella fastidiosa* reveals a redox-dependent oligomeric modulation in *vitro*

Clelton A. Santos, Marcelo A. S. Toledo, Daniela B. B. Trivella, Lilian L. Beloti, Dilaine R. S. Schneider, Antonio M. Saraiva, Aline Crucello, Adriano R. Azzoni, Alessandra A. Souza, Ricardo Aparicio and Anete P. Souza

DOI: 10.1111/j.1742-4658.2012.08743.x

the FEBS Journal

# Functional and structural studies of the disulfide isomerase DsbC from the plant pathogen *Xylella fastidiosa* reveals a redox-dependent oligomeric modulation *in vitro*

Clelton A. Santos[1], Marcelo A. S. Toledo[1], Daniela B. B. Trivella[2], Lilian L. Beloti[1], Dilaine R. S. Schneider[1], Antonio M. Saraiva[1], Aline Crucello[1], Adriano R. Azzoni[1,3], Alessandra A. Souza[4], Ricardo Aparicio[2] and Anete P. Souza[1,5]

1 Centro de Biologia Molecular e Engenharia Genética, Universidade Estadual de Campinas, Brazil
2 Laboratório de Biologia Estrutural e Cristalografia, Instituto de Química, Universidade Estadual de Campinas, Brazil
3 Departamento de Engenharia Química, Escola Politécnica, Universidade de São Paulo, Brazil
4 Centro APTA Citros Sylvio Moreira/IAC, Cordeirópolis, Brazil
5 Departamento de Biologia Vegetal, Instituto de Biologia, Universidade Estadual de Campinas, Brazil

**Keywords**
biofilm formation; DsbC; oligomeric assembly; SAXS; *Xylella fastidiosa*

**Correspondence**
A. P. Souza, Centro de Biologia Molecular e Engenharia Genética (CBMEG), Universidade Estadual de Campinas, Rua Candido Rondon 400, Cidade Universitária 'Zeferino Vaz', CP 6010, 13083-875, Campinas, São Paulo, Brazil
Fax: +55 19 3521 1089
Tel: +55 19 3521 1089
E-mail: anete@unicamp.br

(Received 23 May 2012, revised 1 August 2012, accepted 6 August 2012)

doi:10.1111/j.1742-4658.2012.08743.x

*Xylella fastidiosa* is a Gram-negative bacterium that grows as a biofilm inside the xylem vessels of susceptible plants and causes several economically relevant crop diseases. In the present study, we report the functional and low-resolution structural characterization of the *X. fastidiosa* disulfide isomerase DsbC (XfDsbC). DsbC is part of the disulfide bond reduction/isomerization pathway in the bacterial periplasm and plays an important role in oxidative protein folding. In the present study, we demonstrate the presence of XfDsbC during different stages of *X. fastidiosa* biofilm development. XfDsbC was not detected during *X. fastidiosa* planktonic growth; however, after administering a sublethal copper shock, we observed an overexpression of XfDsbC that also occurred during planktonic growth. These results suggest that *X. fastidiosa* can use XfDsbC *in vivo* under oxidative stress conditions similar to those induced by copper. In addition, using dynamic light scattering and small-angle X-ray scattering, we observed that the oligomeric state of XfDsbC *in vitro* may be dependent on the redox environment. Under reducing conditions, XfDsbC is present as a dimer, whereas a putative tetrameric form was observed under nonreducing conditions. Taken together, our findings demonstrate the overexpression of XfDsbC during biofilm formation and provide the first structural model of a bacterial disulfide isomerase in solution.

**Structured digital abstract**

- XfDsbC and XfDsbC bind by x ray scattering (View Interaction: 1, 2)
- XfDsbC and XfDsbC bind by molecular sieving (View interaction)
- XfDsbC and XfDsbC bind by comigration in non denaturing gel electrophoresis (View interaction)
- XfDsbC and XfDsbC bind by cross-linking study (View Interaction: 1, 2)
- XfDsbC and XfDsbC bind by dynamic light scattering (View Interaction: 1, 2)

**Abbreviations**
DLS, dynamic light scattering; EcDsbC, *Escherichia coli* DsbC; HiDsbC, *Haemophilus influenzae* DsbC; PDB, Protein Data Bank; Rg, radius of gyration; SAXS, small-angle X-ray scattering; TCEP, *tris*(2-carboxyethyl)phosphine; XcDsbC, *Xanthomonas campestris* DsbC; XfDsbC, *Xylella fastidiosa* disulfide isomerase DsbC; $XfDsbC_{N\text{-}Red}$, nonreduced XfDsbC; $XfDsbC_{Red}$, reduced XfDsbC.

## Introduction

Disulfide bond formation is a critical step for the correct folding of many proteins that are rich in cysteine residues. In addition to conferring a stable structure, disulfide bonds play a regulatory role by changing the shape, surface charge or reactivity of some proteins [1]. Among the Gram-negative bacteria, the Dsb protein family constitutes the oxidative protein folding machinery and plays an important role in disulfide bond formation in the periplasm [2–5]. The enzymatic pathway of the Dsb protein family is well characterized in *Escherichia coli* and is composed of five members: DsbA, DsbB, DsbC, DsbD and DsbG [5]. These proteins are typically oxidoreductases and contain a CXXC motif (cysteine residues separated by two amino acids) in the catalytic site, similar to thioredoxin-like proteins [6].

Chemically, DsbA, which is a strong thiol oxidant, catalyzes disulfide bond formation [7,8]. DsbA rapidly oxidizes cysteine residues in proteins that are located in the periplasm by introducing a disulfide bond that is more energetically favourable for correct protein folding [9]. However, two cysteines can be incorrectly joined in a disulfide bond that does not appear in the native protein conformation. When mis-oxidized, the non-native disulfide bond may be reduced or rearranged to ensure that correct protein folding is achieved. DsbC catalyzes this step in the reduction/isomerization pathway [4,10,11].

Two models have been proposed to explain how *E. coli* DsbC (EcDsbC) reshuffles proteins containing incorrect disulfide bonds [5]. However, the biological role of DsbC in other bacteria is not completely understood. In addition to isomerase activity, DsbC exhibits certain chaperone-like properties [12], and this function appears to be independent of the two cysteines in the active site CXXC motif [13]. The isomerase and chaperone activities of DsbC are important for bacterial pathogenicity because these activities ensure the correct folding in a wide range of proteins, including secreted virulence factors and surface components such as adhesins and pili [14].

An interesting aspect of the disulfide bond isomerization mechanism is that the active-site cysteine residues must remain reduced for DsbC activity. This characteristic is particularly intriguing because DsbC acts in the bacterial periplasm, which is an oxidizing environment. DsbD, a transmembrane protein that transfers reducing equivalents from the cytosol to the periplasm, is responsible for maintaining DsbC in the reduced and active state [10,15].

Interestingly, a study of eukaryotic protein disulfide isomerase, which is topologically analogous to prokaryotic DsbC, revealed an intramolecular structural rearrangement between the catalytic and noncatalytic domains that was dependent on the environmental redox state [16]. Protein disulfide isomerase is composed of two catalytic domains (a and a′) that are separated by two noncatalytic domains (b and b′) and a third domain (c) [17]. Correspondingly, EcDsbC is described as a V-shaped homodimeric protein in which each monomer contains an N-terminal dimerization domain that is joined by a hinged linker to the C-terminal catalytic domain [18].

In *E. coli* mutants lacking *dsbC*, many cysteine-rich proteins exhibited reduced activity or were degraded [11,19,20]. However, the most expressive phenotype observed in *dsbC*-null mutants is an increased sensitivity to copper (a redox-active metal), which indicates that DsbC is required for the oxidative stress response [21].

In the present study, we report the functional and structural characterization of DsbC from the 9a5c strain of *Xylella fastidiosa* (XfDsbC) by small-angle X-ray scattering (SAXS). *X. fastidiosa* is a Gram-negative bacterium that grows as a biofilm in the xylem vessels of susceptible plants and causes many diseases in commercial crops around the world, including citrus variegated chlorosis, an economically important crop disease that compromises sweet orange production in Brazil [22,23]. We characterized XfDsbC to evaluate its role in biofilm formation, which blocks the xylem and causes the onset of disease. The results obtained demonstrate that XfDsbC expression occurs during bacterial biofilm formation and is enhanced under oxidative stress conditions. In addition, using modelling approaches based on the SAXS data, we provide evidence for a possible redox-dependent oligomeric modulation of XfDsbC *in vitro*.

## Results

### XfDsbC is involved in biofilm formation and the copper stress response

We investigated the involvement of XfDsbC in *X. fastidiosa* biofilm formation and development. XfDsbC was successfully cloned, and the protein was purified by affinity chromatography. XfDsbC has a molecular mass of 29.5 kDa, which corresponds to the 263-amino acid sequence encoded by ORF *Xf*1177 plus the C-terminal $His_6$-Tag added by the pET29a(+) vector. Titration of the number of free cysteines revealed that the recombinant XfDsbC was purified in an oxidized

state as reported previously [24]. Polyclonal antibodies against XfDsbC were produced and used for western blot analysis. We observed a differential expression pattern of XfDsbC during *X. fastidiosa* biofilm formation and planktonic cell growth (Fig. 1). XfDsbC was expressed during all phases of biofilm development. However, during the planktonic growth phase of *X. fastidiosa*, XfDsbC was poorly expressed and could not be detected by western blotting (Fig. 1A). However, after administering a sublethal copper shock, the planktonic cells overexpressed XfDsbC (Fig. 1B). The samples were normalized against total protein concentration before gel loading to ensure that the same amount of protein was evaluated for each condition. These results suggest that *X. fastidiosa* can use XfDsbC *in vivo* under oxidative stress conditions similar to those induced by copper. The statistical analysis of the ratio of the intensity and area (pixels) of the bands visualized on nitrocellulose membranes revealed statistically significant differences ($P < 0.05$) in the expression profiles of XfDsbC (Fig. 1C, D). Under copper-induced oxidative stress, the expression of XfDsbC was only significantly greater in biofilms than in planktonic cells after 5, 10 and 30 days of biofilm growth (Fig. 1D). The intensities of the protein bands corresponding to XfDsbC in the different phases of biofilm formation in the presence or absence of copper stress were similar to the profiles observed for planktonic cells and biofilms exposed to copper shock. At 15 and 20 days, there were no significant differences ($P < 0.05$) in XfDsbC expression between biofilms in the presence or absence of copper. However, at 3 and 5 days, XfDsbC was expressed in larger quantities in the biofilms that were not treated with copper, whereas, at 10 and 30 days, XfDsbC was expressed in larger quantities in the biofilm cells that were subjected to copper stress (Fig. 1C, D).

## XfDsbC expression complements the *dsbC*-defective *E. coli* mutant

The thiol-disulfide reductase activity of purified nonreduced XfDsbC ($XfDsbC_{N\text{-}Red}$) was confirmed *in vitro* using the rate of insulin disulfide reduction (Fig. 2A). As expected, the activity of XfDsbC was comparable to that of EcDsbC. The insulin reduction rate of XfDsbC was 0.0126 ($\Delta A_{650} \cdot min^{-2}$), which was approximately 88% of the activity of EcDsbC [0.0143 ($\Delta A_{650} \cdot min^{-2}$)]. In addition to the reductase activity, the disulfide bond isomerase activity of XfDsbC was assessed *in vivo* in a *dsbC E. coli* mutant. This *dsbC*-defective *E. coli* mutant was used because an appropriate methodology for the construction of the *X. fastidiosa* 9a5c mutants is not yet available. DsbC isomerase activity is required for

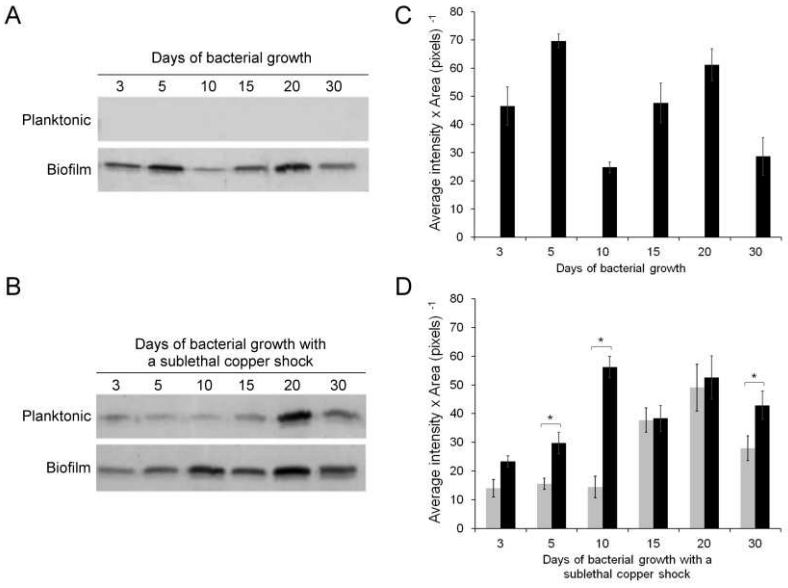


**Fig. 1.** XfDsbC expression in *X. fastidiosa* is elevated during biofilm formation and the oxidative stress response. Total protein samples were isolated from different biofilm growth phases and planktonic cells (see Experimental procedures), normalized using BCA quantification, and evaluated by western blot analysis using polyclonal antibodies against XfDsbC in the absence (A) or presence (B) of oxidative stress induced by copper. (C) The XfDsbC expression profiles of biofilm (black bars) and planktonic (grey bars) cells in the absence or (D) presence of copper were quantified using EDAS software. The bars represent the mean of three independent experiments. The error bars indicate the SE obtained from triplicate experiments. Asterisks indicate statistically significant differences ($P < 0.05$, *t*-test).

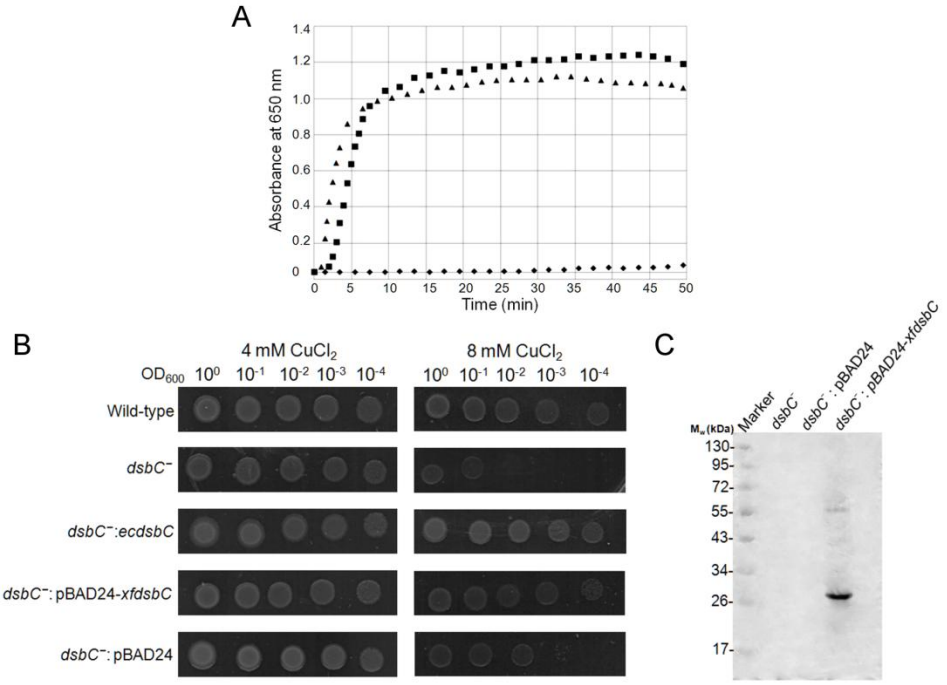


**Fig. 2.** XfDsbC functionally complements a *dsbC*-null *E. coli* mutant. (A) The $XfDsbC_{N\text{-}Red}$ (▲) thiol-reductase activity was confirmed *in vitro* using the insulin disulfide reduction assay. EcDsbC (■) and a test without catalyst (♦) were used as positive and negative controls, respectively. (B) The XfDsbC disulfide bond isomerase activity was assessed *in vivo* for its ability to complement an *E. coli* mutant lacking *dsbC* (*dsbC*⁻). The *dsbC* phenotypes of the various strains (wild-type, *dsbC*⁻, *dsbC*⁻ containing pBAD24-*xfdsbC*, and *dsbC*⁻ with a wild-type *ecdsbC* gene or empty vector) were evaluated by spotting 5 μL of 10-fold serial dilutions onto BHI agar plates with the appropriate antibiotic and containing 4 or 8 mM $CuCl_2$ with 0.002% (w/v) L-arabinose. The plates were incubated overnight at 37 °C, and the ability of XfDsbC to restore the wild-type phenotype was analyzed. (C) The expression of XfDbsC in the *dsbC*⁻ strain was confirmed by western blot analysis.

tolerance to copper, a redox-active metal [21]. Copper is a nonspecific thiol oxidant that leads to protein misfolding through the establishment of non-native disulfide bonds. The DsbC reduction/isomerization pathway acts to reverse protein misfolding by rearranging the disulfide bonds and promoting native protein folding. XfDsbC expression complemented the *dsbC*⁻ *E. coli* mutant under the oxidative stress conditions induced by copper (i.e. the transformation of the *dsbC*⁻ mutant strain with pBAD24-*xfdsbC* restored the wild-type phenotype) (Fig. 2B). In addition, western analysis of XfDsbC in *dsbC*⁻ cells containing pBAD24-*xfdsbC* that were grown on plates containing 8 mM $CuCl_2$ (Fig. 2C) strongly suggests that the increased cell viability under this condition is correlated with the presence of XfDsbC. Our findings show that the basal expression of *xfdsbC* can support the growth of the *dsbC*⁻ *E. coli* mutant strain even in the absence of L-arabinose, which induces the arabinose operon in the pBAD24 vector (data not shown).

## Initial characterization of XfDsbC

The initial analysis of the amino acid sequence of XfDsbC revealed the presence of 21 N-terminal amino acid residues that are not present in the homologous EcDsbC and *Erwinia chrysanthemi* proteins (Fig. S1). Interestingly, these additional N-terminal amino acids are also found in the bacterium *Xanthomonas campestris* DsbC (XcDsbC), which has host specificity for the same citrus plants infected by *X. fastidiosa*. Four cysteine residues similar to those observed in the 3D structure of EcDsbC [18] are present in the thioredoxin-like domains of XfDsbC. The Cys143 and Cys146 residues of XfDsbC (active site) correspond to Cys98 and Cys101 of the EcDsbC crystal structure [Protein Data Bank (PDB) code: 1EEJ], and the Cys186 and Cys208 residues of XfDsbC (non-active site) correspond to Cys141 and Cys163 of EcDsbC. These cysteine residues are strongly conserved between DsbC homologues and, because DsbC can undergo structural changes that are dependent on the redox environment, these cysteine residues may be directly or indirectly involved in structural rearrangements and function. Therefore, we evaluated whether the redox environment caused changes in the structure of XfDsbC *in vitro*. XfDsbC samples in the presence or absence of reducing agents were analyzed using SDS/PAGE, native gel electrophoresis, CD, size-exclusion chromatography, fluorimetry, chemical cross-linking and dynamic light scattering (DLS).

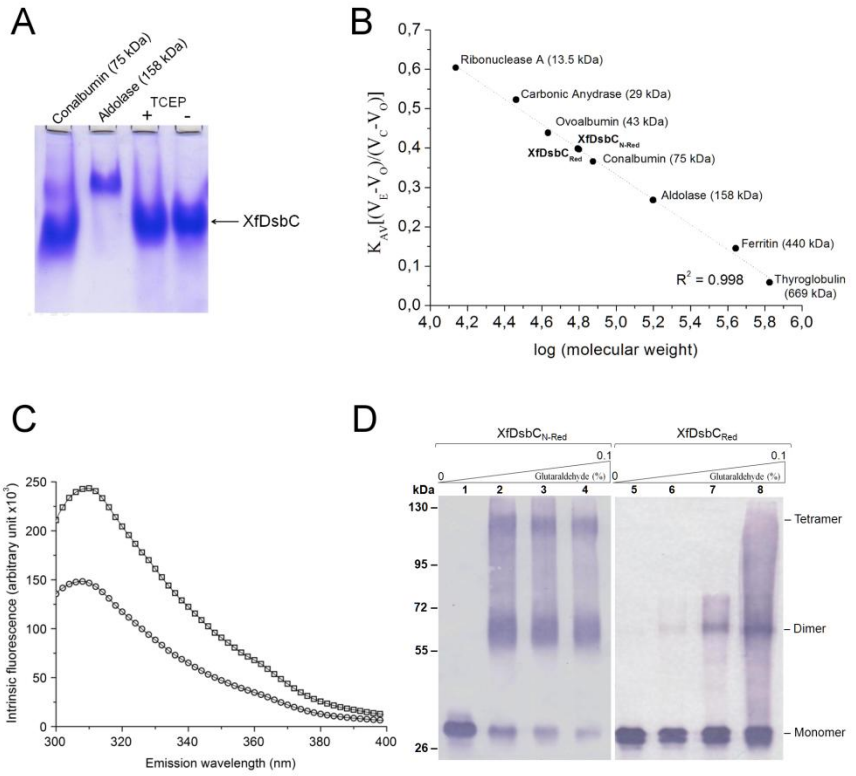


**Fig. 3.** Initial characterization of XfDsbC. (A) XfDsbC nondenaturing polyacrylamide gel electrophoresis in the presence (+) and absence (–) of TCEP. (B) Size-exclusion chromatography calibration curves for $XfDsbC_{Red}$ and $XfDsbC_{N\text{-}Red}$. The monomeric molecular mass for XfDsbC is 29.5 kDa, and the expected molecular mass for the XfDsbC dimer is 59 kDa. The estimated molecular masses for $XfDsbC_{Red}$ and $XfDsbC_{N\text{-}Red}$ were 60.2 and 61.7 kDa, respectively. (C) XfDsbC fluorimetry spectra of $XfDsbC_{Red}$ and $XfDsbC_{N\text{-}Red}$ are shown as squares and circles, respectively. (D) Glutaraldehyde cross-linking of XfDsbC in the absence ($XfDsbC_{N\text{-}Red}$) and presence ($XfDsbC_{Red}$) of TCEP. The XfDsbC samples (5 μM) were treated with increasing concentrations of glutaraldehyde (0%, 0.025%, 0.05% and 0.1%), and the products were evaluated by western blot analysis using polyclonal antibodies against XfDsbC.

Under denaturing conditions in the presence and absence of β-mercaptoethanol, XfDsbC was present in the gel as a single band at approximately 29 kDa, which corresponds to the molecular mass of the monomer. Under nondenaturing conditions, XfDsbC samples exhibited the same gel migration profile in the presence and absence of *tris*(2-carboxyethyl)phosphine (TCEP). This profile was more similar to that of conalbumin (75 kDa) than that of aldolase (158 kDa) (Fig. 3A). The CD analysis revealed a typical protein spectrum with a predominantly α-helical structure (38% helical/18% sheet), similar to that for EcDsbC calculated from its crystal structure [18]. There were no significant differences in the secondary structure content of XfDsbC in the presence or absence of TCEP (data not shown).

Analytical size-exclusion chromatography of reduced and nonreduced XfDsbC confirmed the native gel results, indicating that there were no differences between the two tested conditions (Fig. 3B). Both the reduced and nonreduced protein samples eluted as single peaks in the gel filtration assays, with retention times that corresponded to apparent molecular masses of 60.2 and 61.7 kDa, respectively (Fig. 3B). Different buffer and pH conditions, as well as XfDsbC oxidation under atmospheric oxygen, were evaluated, and no differences were observed in the elution profiles of the samples in the presence or absence of the reducing agent (data not shown).

The conformational changes in the XfDsbC protein samples under reducing or nonreducing conditions were next analyzed by fluorimetry, and tryptophan emission was used as a probe to monitor DsbC folding. XfDsbC contains a tryptophan residue that neighbours Cys186, which is distal from the active site (Fig. S1). This cysteine residue can establish a disulfide bond with Cys208 and likely plays a role in XfDsbC folding. The fluorescence spectra recorded upon excitation at 280 nm showed that reduction with TCEP increased the intrinsic fluorescence intensity and shifted the maximum emission wavelength from 307 to 310 nm (Fig. 3C).

Although XfDsbC can exist predominantly as dimers in solution, and SDS/PAGE, nondenaturing gel electrophoresis, CD and size-exclusion chromatography did not reveal any redox-dependent structural

changes in XfDsbC, higher-order oligomeric species that appear to correspond to tetramers were observed *in vitro* under the nonreduced condition of XfDsbC (Fig. 3D, lanes 1–4) after chemical cross-linking with glutaraldehyde, along with dimeric and monomeric species (Fig. 3D, lanes 2–4). However, only dimeric forms, in addition to monomeric species, were observed under the reduced condition (Fig. 3D, lanes 5–8). These slow-migrating species were not observed in the absence of glutaraldehyde (Fig. 3D, lanes 1 and 5).

We also used DLS analysis to assess the redox-dependent oligomeric modulation of XfDsbC. The results of this analysis showed that, under both nonreduced and reduced conditions, XfDsbC showed a low index of polydispersity (%Pd; 9.5 and 5.8, respectively) (Table 1). In addition, the molecule in solution under the nonreduced condition presents a hydrodynamic diameter ($D_h$) of 4.6 nm and differs from that observed under the reduced condition which has a $D_h$ of 3.8 nm, indicating of the presence of a high oligomer form of XfDsbC under the nonreduced condition.

## SAXS analysis suggests a redox-dependent oligomeric assembly of XfDsbC *in vitro*

XfDsbC SAXS scattering curves collected in the presence and absence of reducing agent were analyzed. The scattering curves of 4- and 7-mg·mL$^{-1}$ protein samples in the presence of 3 mM TCEP [reduced XfDsbC (XfDsbC$_{Red}$)] were collected. The 7-mg·mL$^{-1}$ samples exhibited interparticle interference effects that compromised further analysis, although the curves collected from 4-mg·mL$^{-1}$ samples did not exhibit this behaviour. Therefore, the scattering curves of XfDsbC at 4 mg·mL$^{-1}$ were selected for SAXS data analyses and model construction. The superimposition of the 20 scattering curves collected for XfDsbC$_{Red}$ at 4 mg·mL$^{-1}$ revealed a transition during the data collection that may be the result of conformational changes arising from radiation damage. Therefore, only the first curve was used for further analysis (Fig. 4A). As shown in Fig. 4A (inset), the constructed XfDsbC$_{Red}$ Guinier plot demonstrated a linear behaviour, indicating sample monodispersity. The Guinier analysis revealed a radius of gyration (Rg) of 31.2 Å. XfDsbC$_{Red}$ Kratky plots were also constructed (Fig. 4B) and displayed a well-defined maximum, which is expected for the native state of a compact globular protein. The molecular mass of the scattering particles was estimated to be 66 kDa by SAXS MOW software [25]. This suggests that XfDsbC$_{Red}$ is a dimer in solution, similar to other DsbC proteins [18,26]. The XfDsbC$_{Red}$ distance distribution function, $P(r)$, showed a maximum intramolecular distance ($D_{max}$) of 100 Å (Fig. 4D). The Rg calculated from the $P(r)$ was 31.5 Å, which is consistent with the values obtained from the Guinier analysis.

Scattering curves were collected from 1, 4 and 13 mg·mL$^{-1}$ XfDsbC in the absence of TCEP (XfDsbC$_{N\text{-}Red}$). However, the curves at 1 mg·mL$^{-1}$ were too dilute for SAXS data collection and resulted in weak scattering curves. The molecular masses estimated from the 4- and 13-mg·mL$^{-1}$ samples were identical. For consistency with the XfDsbC$_{Red}$ samples, we selected the XfDsbC$_{N\text{-}Red}$ curves collected at 4 mg·mL$^{-1}$ for further analyses. As observed for XfDsbC$_{Red}$, the XfDsbC$_{N\text{-}Red}$ protein samples suffered radiation damage. Therefore, only the first curve was selected (Fig. 4C). The XfDsbC$_{N\text{-}Red}$ Guinier region is displayed in Fig. 4C (inset). From the Guinier analysis, an Rg of 35.4 Å was calculated. The Kratky plot was also evaluated (Fig. 4B) and showed a defined maximum with smaller $q$ values than those of the XfDsbC$_{Red}$ maximum, which indicates a larger XfDsbC$_{N\text{-}Red}$ scattering particle. The XfDsbC$_{N\text{-}Red}$ molecular mass obtained in the absence of TCEP was estimated to be 117 kDa, suggesting that, in the absence of reducing agent, an XfDsbC tetramer is formed in solution. The XfDsbC$_{N\text{-}Red}$ $P(r)$ had a $D_{max}$ of 130 Å (Fig. 4D), and the distance peak was concentrated at small distances, indicating a prolate XfDsbC$_{N\text{-}Red}$ structure. A second estimation of the Rg calculated from the $P(r)$ was 38.4 Å, which is consistent with the values obtained in the Guinier analysis.

**Table 1.** Hydrodynamic diameters ($D_h$), percentage of sample polydispersity (% Pd), estimated molecular weights from the measured radius (MW-R), percentage of sample intensity (% Int) and estimated relative amount of mass (% Mass) of each species determined from DLS analysis of XfDsbC in the presence (XfDsbC$_{N\text{-}Red}$) or absence (XfDsbC$_{Red}$) of a reducing agent.

| Sample | $D_h$ (nm) | % Pd | MW-R (kDa) | % Int | % Mass |
|---|---|---|---|---|---|
| XfDsbC$_{N\text{-}Red}$ | 4.6 | 9.5 | 119 | 73 | 99.6 |
| XfDsbC$_{Red}$[a] | 3.8 | 5.8 | 75 | 72 | 99.5 |

[a] To ensure complete protein reduction, XfDsbC was incubated with a freshly prepared solution of TCEP at a final concentration of 3 mM for 1 h before the DLS experiments.

## The XfDsbC tetramer appears to be compact and distinct from the joining of two dimers

The monomeric XfDsbC homology model constructed with the I-TASSER server exhibited similarities to the EcDsbC [18] and *Haemophilus influenzae* DsbC (HiDsbC) [27] proteins. The amino acid sequence

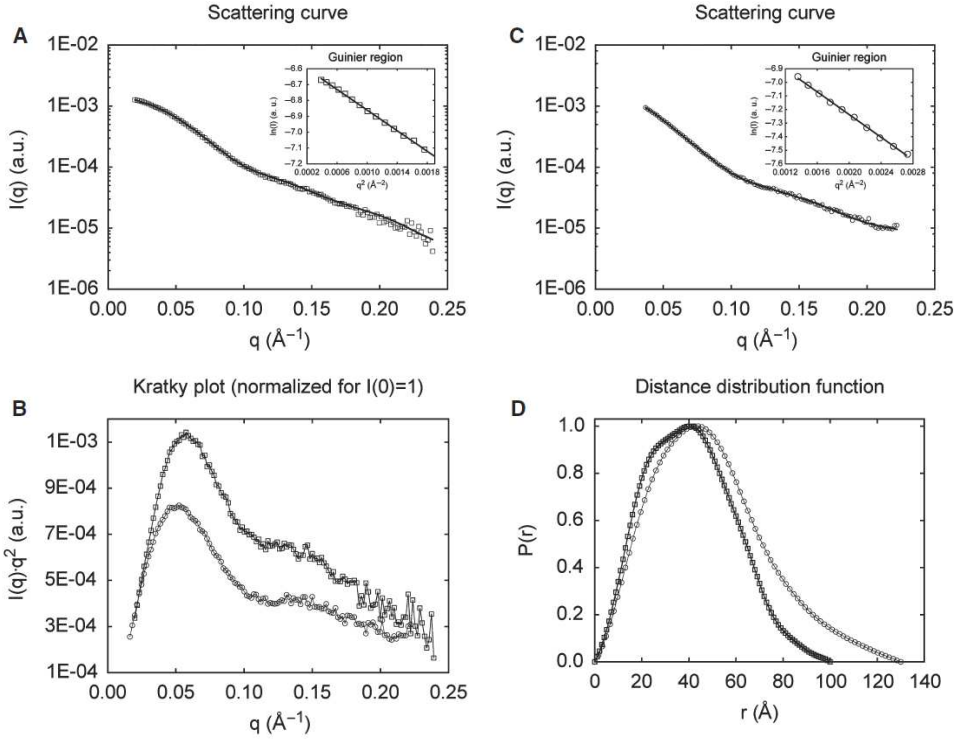


**Fig. 4.** XfDsbC SAXS analysis under reducing and nonreducing conditions. XfDsbC SAXS data analysis from samples collected in the presence ($XfDsbC_{Red}$) or absence ($XfDsbC_{N\text{-}Red}$) of TCEP. (A) $XfDsbC_{Red}$ scattering curve (open squares) and BUNCH curve (solid line) fitting. (B) Kratky plots. (C) $XfDsbC_{N\text{-}Red}$ scattering curve (open circles) and SASREF curve (solid line) fitting. The Guinier regions are shown in the insets A and C. (D) distance distribution functions [*P*(r)]. The Kratky plots and [P(r)] were calculated for *q* values in the range 0.0197–0.3008 Å$^{-1}$ for $XfDsbC_{Red}$ and 0.0351–0.2152 Å$^{-1}$ for $XfDsbC_{N\text{-}Red}$. The $XfDsbC_{Red}$ and $XfDsbC_{N\text{-}Red}$ plots are shown as squares and circles, respectively.

similarity of these two proteins to XfDsbC is approximately 35%. As observed in the structures of EcDsbC and HiDsbC, the constructed XfDsbC model displays two distinguishable domains: the dimerization and catalytic domains. The dimerization domain is small and is composed of 58 residues (residues 20–77) that form a β-strand, a turn and an α-helix. The catalytic domain is the largest domain and displays a thioredoxin-like fold. The XfDsbC catalytic domain is comprised of residues 86–244 and harbours the active site cysteine residues (Cys143 and Cys146 in XfDsbC, which correspond to Cys98 and Cys101 in EcDsbC). The catalytic domain is connected to the dimerization domain by a poorly modelled hinge. To construct the XfDsbC dimer, the 3D structure of the constructed monomer homology model was superimposed on the crystal structure of the EcDsbC dimer (PDB code: 1EEJ). A second XfDsbC chain was generated and superimposed on the remaining EcDsbC monomer. The putative XfDsbC dimer interface was proposed based on the high-resolution structures, chimeric constructs and site-directed mutagenesis of other DsbC dimeric proteins [18,26–28]. The dimerization domains of EcDsbC and HiDsbC are primarily connected by hydrogen-bond interactions formed by main chain residues from two external anti-parallel β-strands. An ionic interaction between EcDsbC His45 and Asp53 also contributes to the stability of the dimer and protein isomerase activity [26,29]. Therefore, the conservation of this characteristic interface in the XfDsbC structure was investigated. According to the XfDsbC homology model, XfDsbC has an external β-strand in its dimerization domain. The β-strand enables anti-parallel main chain contacts between the two XfDsbC dimerization domains and likely involves residues 68–77. An arginine (Arg68) and an aspartate (Asp77) residue are located on the extremities of this β-strand. Because Arg and Asp are oppositely charged, it is possible that ionic interactions help to stabilize the XfDsbC dimer, as observed in EcDsbC [26,29].

Based on this potential XfDsbC dimeric interface, the XfDsbC dimer was modelled according to the experimental XfDsbC low-resolution scattering curve. In this step, the XfDsbC dimerization domains and catalytic domains were provided as individual chains to the software suite BUNCH. Restraints were imposed to prevent the domains from being too far apart and to maintain the dimerization interface. A maximum distance from the centre of mass of each dimerization domain and catalytic domain to residues 68–77 of the two dimerization domains was set to maintain the dimerization interface and preserve the proximity of the catalytic domains and dimerization domains. The linker region (residues 78–85) that connects the dimerization and catalytic domains was removed from the input sequence, and the software was allowed to model these flexible regions. More than 40 XfDsbC atomic models were generated by BUNCH, and these models showed a good fit to the experimental SAXS curves, with chi-squared values of approximately 2.5. These models were visually inspected and sorted into three major groups that primarily differed in the orientation of the catalytic domains. In one of these groups, the catalytic Cys125 was turned away from the catalytic cleft and was exposed to the solvent, which would likely limit the activity of the protein. The cleft formed by the two catalytic domains has been suggested to play an important role in substrate recognition and protein activity [26] because the catalytic cysteine residue is oriented in the direction of this cleft in the known DsbC crystal structures. Therefore, the models with the cysteine facing away from the cleft were considered to have an improbable catalytic domain orientation and were discarded. The remaining models were carefully inspected and further clustered into two groups. The first group was comprised of models that followed the dimerization and catalytic domain orientations predicted by known DsbC crystal structures (Fig. 5A). The second group included models with intertwined dimerization and catalytic domains (named 'inverted dimers'; Fig. S2). It was difficult to evaluate the correctness of these two groups of XfDsbC dimer models because both models are possible given the low-resolution data. However, because the models in the first group were most similar to the reported DsbC crystal structures, one of the dimers from this group of models was selected for further analysis (Fig. 5A).

The selected XfDsbC SAXS dimer model is similar to the EcDsbC dimer crystal structure (PDB code: 1EEJ). The dimerization domains are connected by contacts mediated by two β-strand-like secondary structural elements on the surface of each dimerization domain. The dimer displays a V-shaped conformation,

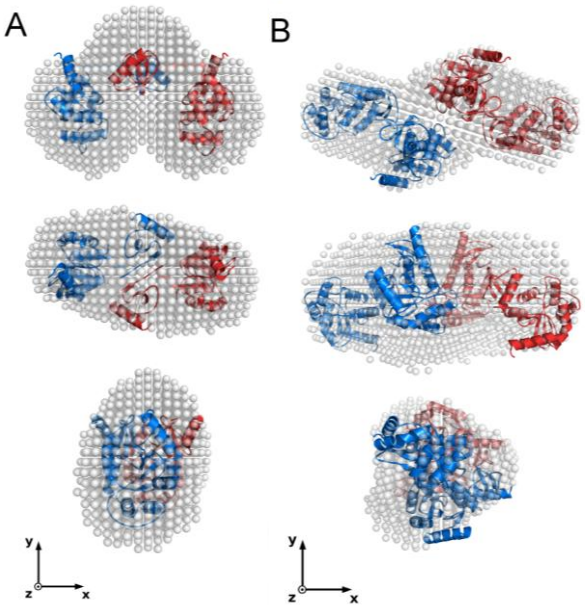


**Fig. 5.** The oligomeric assembly of XfDsbC responds to the environmental redox state *in vitro*. The suggested XfDsbC dimer (A) and tetramer (B) were modelled based on SAXS curves. The 3d XfDsbC atomic model for the dimer was generated using BUNCH, whereas the tetramer was modelled with SASREF. P2 symmetry was imposed in both cases. In both strategies, the dimerization and catalytic domains were inputted as independent entities, and only a few constraints were imposed for model generation. The low-resolution protein envelopes, which were constructed with DAMMIF software, are shown as semi-transparent whitish spheres superimposed on the atomic models. The middle views are rotated by 90° around the *x*-axis, clockwise in (A) and counterclockwise in (B). The bottom views in both panels are rotated 90° clockwise around the *y*-axis. The figures were generated USING PYMOL (Schrodinger LLC).

and a potential catalytic cleft is formed between the two catalytic domains. This cleft has an internal angle of approximately 60°, suggesting that XfDsbC is slightly closed in comparison to EcDsbC (internal cleft angle of approximately 70°). The catalytic XfDsbC cysteine residue (Cys143) and its disulfide bond partner (Cys146) are positioned close to the catalytic cleft. However, the adjacent structural cysteines (Cys186 and Cys208) are oriented in opposite directions and are slightly exposed to the solvent.

It was not possible to model the XfDsbC tetramer using a rigid-body fit for the SAXS-modelled XfDsbC dimer described above, which suggests that the XfDsbC dimer undergoes domain orientation and/or conformational changes to form the tetramer. Therefore, in an attempt to model a putative XfDsbC tetramer, four

XfDsbC dimerization and catalytic domains were inputted into SASREF software as individual chains. Using this strategy, SASREF was able to model an XfDsbC tetramer using only a few constraints.

The models obtained from different runs were judged to be similar by visual inspection. One of the XfDsbC tetrameric models is presented in Fig. 5B. The chi-squared value obtained for the comparison of the $XfDsbC_{N\text{-}Red}$ SAXS curve with the modelled tetramer is 1.6, which indicates an excellent fit and the correctness of the model. The modelled XfDsbC tetramer is formed by interchain contacts between two catalytic domains from different dimers and likely involves domain reorientation, as noted above.

Curiously, the XfDsbC tetrameric models were similar to the DsbC oligomeric structures generated by applying symmetric operations to DsbC crystal structures (Fig. S3). This observation may support the possibility that larger oligomers of DsbC proteins can form.

## Discussion

The XfDsbC protein was annotated in the *X. fastidiosa* 9a5c genome as being involved in pathogenicity, adaptation and survival [30]. Functional and structural studies of proteins in this category have helped determine how this bacterium has adapted to plant hosts and provide a better understanding of the mechanisms underlying pathogenicity and bacterial virulence [31–34].

Biofilm formation is considered to be the primary mechanism of pathogenicity by *X. fastidiosa* [35]. The phases of *X. fastidiosa* biofilm development have been defined previously [34,36]. The initial adhesion phase of the cells to the substrate occurs after 3–5 days. Within 10 days, micro-colonies are formed, followed by a maturation phase that occurs between 15 and 20 days after adhesion. The development of the biofilm architecture begins at approximately 15 days, and the biofilm is fully mature within 20 days. The last stage of biofilm formation, the dispersion phase, occurs between 25 and 30 days after adhesion.

We confirmed that XfDsbC is involved in bacterial pathogenicity by demonstrating its expression during *X. fastidiosa* biofilm formation. Interestingly, XfDsbC is poorly expressed during *X. fastidiosa* planktonic growth, suggesting that, under these conditions, the disulfide bond isomerization pathway is largely not required for bacterial survival. The frequency of the formation of non-native disulfide bonds by DsbA is low under normal bacterial growth conditions [37], which explains the minimal requirement for XfDsbC during *X. fastidiosa* planktonic growth. Biofilm growth provides greater adaptive advantages than planktonic growth by coordinating the growth rate, which provides the cells with increased resistance to antimicrobial agents, such as metals [38]. Thus, stress response pathways, including mechanisms that promote survival, have a major role in the success of bacterial biofilm formation [39]. The disulfide bond isomerization pathway in which XfDsbC plays its primary role comprises one such survival mechanism because it is directly involved in protein folding [2–5,10].

Cells exhibit different gene expression and metabolic profiles during biofilm and planktonic growth [34,40]. In the present study, we demonstrated, by direct immunodetection, that XfDsbC is differentially expressed during *X. fastidiosa* planktonic and biofilm growth. Interestingly, in response to metal stress, planktonic *X. fastidiosa* overexpresses XfDsbC, with expression levels similar to those observed in mature biofilms. Our findings reveal that *X. fastidiosa* can use XfDsbC *in vivo* as a response to oxidative stress, which is corroborated by the finding that XfDsbC is able to complement a *dsbC*-null *E. coli* mutant under similar stress conditions. However, during the mature biofilm stage, copper does not appear to affect the expression profile of XfDsbC. At this stage, the complete structure of the biofilm makes the cells less responsive to changes in the external environment [38–40]. Therefore, the expression of XfDsbC at the mature biofilm stage in the presence or absence of copper reflects the response to bacterial growth under biofilm growth conditions, as opposed to a specific response to metal stress. The initial stage of *X. fastidiosa* biofilm development is marked by the production of many cysteine-rich proteins, including pili and adhesin proteins [34]. The increased expression of XfDsbC during biofilm formation may be related to the increased expression of cysteine-rich proteins and the need to fold these proteins correctly. Moreover, the differences observed between biofilms in the presence and absence of copper appear to indicate that the bacterial cells are more susceptible to changes in the external environment during microcolony formation and biofilm dispersal; increased XfDsbC expression appears to be a coordinated cellular action in these phases. At the stage of cell adhesion to the substrate, the cells may rely on mechanisms outside of the isomerization pathway to respond to oxidative stress, resulting in a decreased level of XfDsbC expression under these conditions.

In addition to disulfide bond reductase and isomerase activity, DsbC proteins have chaperone activity [12,13]; however, the mechanism of this activity is not completely understood for DsbC. One intrinsic feature

of a chaperone-like protein is the formation of large oligomers that facilitate interactions between proteins and their substrates [41]. The detection of XfDsbC tetramers by DLS and SAXS under nonreducing conditions may be evidence of chaperone activity. However, whether this oligomeric state occurs *in vivo* is unclear.

DsbC homologues have always been described as homodimers [18,26–28], and their disulfide bond reduction/isomerization activity is partly correlated with this state [2–5]. However, Arredondo *et al.* [26] observed evidence for a linked EcDsbC with a single active thioredoxin domain in a tetrameric state using multi-angle light scattering. The hydrodynamic radius of the tetramer was 4.4 nm, which is not consistent with the radius of the dimer (3.8 nm) and suggests that the tetramer is a compact molecule [26]. These results are in accordance with our findings of DLS and, similarly, the compact form of EcDsbC tetramer appears to be consistent with the XfDsbC tetramer that we observed *in vitro* in the SAXS analysis.

We did not observe any differences between the reduced and nonreduced forms of XfDsbC by size-exclusion chromatography or native gel electrophoresis. However, DLS and SAXS analyses demonstrated the influence of a reducing agent in the folding state of XfDsbC. Thus, it is possible that the reducing agent-mediated XfDsbC dimer-tetramer modulation is not directly linked to disulfide bond formation at the tetramer interface. Rather, it appears that, under nonreducing conditions, certain amino acid residues may be exposed, promoting XfDsbC tetramer formation. By contrast, under reducing conditions, disulfide bond breakage hinders or hides this interface. The current low-resolution data do not clarify the mechanism that guides XfDsbC tetramer assembly.

Based on fluorimetry analysis in which the disulfide reduction increases fluorescence emission, we can assert that changes in the folding state of XfDsbC are related to disulfide bond formation between Cys186 and Cys208, which are equivalent to Cys141 and Cys163 in EcDsbC [18]. Interestingly, the disulfide bond formed between these cysteine residues has a substantial structural role in EcDsbC folding [24]. Therefore, the absence of differences in XfDsbC behaviour by size-exclusion chromatography and native gel electrophoresis could be explained by the weakness of the tetramerization interface, which may not be maintained under the drag and pressure conditions of chromatography and electrophoresis because a tetrameric form of XfDsbC was observed *in vitro* by chemical cross-linking at low protein concentration only under the nonreduced condition.

Previous studies in which amino acid residues important for EcDsbC dimerization were replaced have shown that the dimeric disulfide isomerase is converted into a monomeric protein that retains oxidase activity, similar to DsbA [29,42], suggesting that dimerization acts to protect the DsbC active sites from DsbB-mediated oxidation [29,43]. Tetramer formation may play a similar role for XfDsbC, for example, in preventing the reduction of the disulfide bonds. Bioinformatics estimates have revealed that more than 300 *E. coli* proteins that contain multiple cysteines are exported to the periplasm [44,45] and may be substrates for disulfide bond-forming enzymes [5]. Thus, the XfDsbC redox-dependent modulation observed *in vitro* may be involved in substrate recognition and specificity, comprising a role that has not been previously described for DsbC homologues.

## Experimental procedures

### Bacterial strain and *in vitro* growth conditions

*X. fastidiosa* subsp. *pauca* 9a5c [46] and *E. coli* strains DH5-α, C43 (DE3) (Avidis, Saint-Beauzire, France), JW2861 and BW25113 [47] were used in the present study. Before *in vitro* culture, the *X. fastidiosa* cells were inoculated into susceptible sweet orange trees to maintain their pathogenicity [34]. The infected plants developed symptoms typical citrus of variegated chlorosis, and the bacteria were isolated. *X. fastidiosa* was grown in Periwinkle Wilt media [48] at 130 r.p.m. and 28 °C, and the *E. coli* strains were cultured in LB or Brain-Heart Infusion Broth (BHI; HiMedia, Mumbai, India) media at 200–300 r.p.m. and 25–37 °C, with antibiotic supplementation as necessary. The *X. fastidiosa* biofilm and planktonic cells were obtained using a protocol established by De Souza *et al.* [36] and a sublethal copper shock with 1 mM $CuSO_4$ was applied for 24 h as indicated.

### Cloning, expression and purification

The coding sequence of the *xfdsbC* ORF *Xf*1177 (798 bp) was amplified from *X. fastidiosa* genomic DNA by PCR with the specific oligonucleotides Xf1177petF (5′-CC AAACATATGTACCGCCTTATCGTCGCCTTG-3′) and Xf1177petR (5′-AAACTCGAGGCCCCCTTTAGCTGTT GCGG-3′), which contained *Nde*I and *Xho*I restriction sites, respectively. The PCR amplification product was cloned into the pET29a(+) (Novagen, Madison, WI, USA) expression vector, which added a C-terminal six-histidine tag to the coding sequence. Sequence analysis of the cloned vector did not reveal any base substitutions. To overexpress XfDsbC in *E. coli* C43 (DE3) cells, the cells were grown at 37 °C in 1 L of LB containing 30 $\mu g \cdot mL^{-1}$ kanamycin until

$D_{600}$ of 0.6–0.8 was reached. The expression of the recombinant protein was induced by the addition of 5.6 mM lactose followed by cultivation for 18 h at 25 °C and 200 r.p.m. The culture was harvested by centrifugation (3000 ***g*** for 15 min at 4 °C) and then the cell pellets were resuspended in 50 mL of buffer A (50 mM Tris-HCl, pH 7.5, 300 mM NaCl) plus 1 $mg{\cdot}mL^{-1}$ lysozyme and 1 mM phenylmethanesulfonyl fluoride (Sigma, St Louis, MO, USA) and incubated on ice for 30 min. The cells were disrupted by sonication, and the unbroken cells and debris were removed by centrifugation (27 000 ***g*** for 40 min at 4 °C). The XfDsbC protein was purified in a single chromatographic step on a Ni-NTA column (Qiagen, Hilden, Germany) equilibrated in buffer A. The purified XfDsbC protein was eluted with five column volumes of buffer A containing 250 mM imidazole, and the purity was estimated using SDS/PAGE. The affinity-purified XfDsbC sample was dialyzed overnight against buffer B (50 mM Tris-HCl, pH 7.5, 150 mM NaCl) at 4 °C. The determination of the redox states of purified XfDsbC was achieved using Ellman's method [49]. The protein concentration was spectrophotometrically determined and calculated from the $A_{280}$ with a molar absorption coefficient ($\varepsilon_{280}$) of 23 630 $M^{-1}{\cdot}cm^{-1}$, assuming that all Cys residues were oxidized, or 23 380 $M^{-1}{\cdot}cm^{-1}$, assuming that all Cys residues were reduced.

## Biochemical assays and disulfide bond isomerization *in vivo*

The *in vitro* thiol-disulfide reductase activity of XfDsbC was determined by measuring the turbidity increase at 650 nm resulting from insulin reduction in accordance with published procedures [50]. EcDsbC purified from the JW2861 clone, as obtained from the ASKA library [51], was used as a positive control in these tests. Reductase activity was expressed as the ratio of the slope of the linear portion of the turbidity curve to the lag time [52]. In addition, the XfDsbC disulfide bond isomerase activity was assessed *in vivo* using a functional complementation assay based on copper sensitivity [21]. The *xfdsbC* gene was cloned into the pBAD24 vector [53] using the oligonucleotides Xf1177badF (5′-ATCCATGGGTTACCGCCTTATC GTCG-3′) and Xf1177badR (5′-AATGTCGACTCAGCC CCCTTTAGCT-3′), which contained *Nco*I and *Sal*I restriction sites, respectively. pBAD24-*xfdsbC* or pBAD24 empty vector was transformed into the *E. coli* JW2861 strain, which is a *dsbC* deletion mutant derived from the wild-type BW25113 strain. Both strains were kindly provided by the National BioResource Project (NIG, Mishima, Japan). For the copper sensitivity assay, the strains (wild-type, *dsbC*$^-$ and *dsbC*$^-$ containing pBAD24-*xfdsbC* or the empty vector) were grown overnight in LB containing 30 $\mu g{\cdot}mL^{-1}$ chloramphenicol, 100 $\mu g{\cdot}mL^{-1}$ ampicillin or 30 $\mu g{\cdot}mL^{-1}$ kanamycin (depending on the strain) at 37 °C and 300 r.p.m. The cultures were then diluted 1 : 100 in BHI media supplemented with the appropriate antibiotic and grown at 37 °C and 300 r.p.m. until $D_{600}$ of 0.8 was reached. The *dsbC* phenotype was tested by spotting 5 μL of 10-fold serial dilutions onto BHI agar plates with the appropriate antibiotic containing 0, 4 and 8 mM $CuCl_2$ with and without 0.002% w/v L-arabinose. The plates were incubated overnight at 37 °C, and the ability of XfDsbC to restore the wild-type phenotype was analyzed. We reintroduced wild-type EcDsbC, which was expressed from the pCA24N plasmid [51], into the *dsbC*$^-$ strain as a positive control for functional complementation. All of the spot titrations were performed in triplicate, and XfDsbC expression in the *dsbC*$^-$ strain was confirmed by western blot analysis.

## Extraction of total protein from *X. fastidiosa* biofilm and planktonic cells

*X. fastidiosa* biofilm and planktonic cells were collected after 3, 5, 10, 15, 20 and 30 days of growth. To assess the differential metal stress responses of the biofilm and planktonic cells, both cell types were exposed to a sublethal copper shock for 24 h with 1 mM $CuSO_4$. Biofilm and planktonic cells exposed or not exposed to $CuSO_4$ were sampled at various time points, and total protein was extracted from each sample. For total protein extraction, the biofilm and planktonic cells from each treatment were collected and resuspended in 1 mL of extraction buffer (50 mM Tris-HCl, pH 8.0, 25 mM NaCl, 5 mM EDTA and 2% Triton X-100) containing 1 $mg{\cdot}mL^{-1}$ lysozyme and 1 mM phenylmethanesulfonyl fluoride. The samples were placed on ice for 20 min and lysed by sonication, followed by centrifugation (10 000 ***g*** for 10 min at 4 °C). The total protein concentration of each protein sample was normalized with a micro BCA protein assay kit (Thermo Fisher Scientific Inc., Waltham, MA, USA) before SDS/PAGE analysis. A BSA standard curve was utilized for the total protein concentration comparison. The standard curve exhibited an $R^2$ of 0.989.

## XfDsbC immunodetection during *X. fastidiosa* biofilm and planktonic growth

Polyclonal antibodies against XfDsbC were produced by Rheabiotech (Campinas, Brazil) and used in the XfDsbC immunodetection assays. For western blot analysis, approximately 105 μg of total *X. fastidiosa* protein from different biofilm developmental phases and planktonic growth cultures were separated using 12% SDS/PAGE. After electrophoresis, the proteins were transferred to nitrocellulose membranes (Immobilon™-Nc; Sigma) using a Trans-Blot Semi-Dry Transfer Cell (Bio-Rad, Hercules, CA, USA) in accordance with the manufacturer's instructions. XfDsbC was detected with a 1 : 4000 dilution of anti-XfDsbC and a 1 : 8000 dilution of alkaline phosphatase-conjugated

anti-rabbit IgG (Santa Cruz Biotechnology Inc., Santa Cruz, CA, USA). The membranes were developed with NBT/BCIP chromogenic substrates (Promega, Madison, WI, USA). Three independent experiments were performed for each biological treatment to assess potential variations in protein transfer. The signal intensity was quantified using EDAS 290 software (Kodak, Rochester, NY, USA), and the resulting values were subjected to statistical analysis ($P \leq 0.05$, *t*-test).

### Native gel electrophoresis analysis

Nondenaturing PAGE was performed under the conditions previously described for a pH range of 8.6–10.6 [54]. XfDsbC (p*I* = 9.01) protein samples (approximately 60 μg) in the presence and absence of 3 mM TCEP reducing agent were analyzed using 7.5% native gel electrophoresis with aldolase (p*I* = 6.1, 158 kDa) and conalbumin (p*I* = 5.9, 75 kDa) (GE Healthcare, Uppsala, Sweden) as standards.

### CD

The CD spectra of the recombinant XfDsbC were collected on a Jasco J-810 Spectropolarimeter dichrograph (Japan Spectroscopic, Tokyo, Japan). The far-UV CD spectra were generated with XfDsbC at an approximate concentration of 5 μM in 10 mM sodium phosphate buffer at pH 7.5 with 0 or 3 mM TCEP. The assays were performed in a quartz cuvette with a path length of 1 mm, and 10 accumulations within the range 260–190 nm at a rate of 50 nm·min$^{-1}$ at 24 °C were recorded for each sample and the mean was determined. The deconvolution and statistical analysis of the CD spectra were performed using DICHROWEB [55].

### Size-exclusion chromatography

Gel filtration chromatography was performed using a prepacked Superdex 200 HR10/30 (GE Healthcare) column. After equilibration of the column with buffer B, samples (approximately 750 μg) containing 0 or 3 mM TCEP were loaded at a flow rate of 0.5 mL·min$^{-1}$. The Superdex column was calibrated using HMW and LMW calibration kits (GE Healthcare) as standard molecular weight markers.

### DLS

DLS measurements were performed on a DynaPro instrument (Protein Solutions Inc., Charlottesville, VA, USA). XfDsbC samples at a concentration of 1 and 4 mg·mL$^{-1}$ in the absence or presence of 3 mM TCEP were analyzed in buffer B. $XfDsbC_{N\text{-}Red}$ or $XfDsbC_{Red}$ samples (approximately 100 μL) were placed in a quartz cell and DLS measurements were taken at 4 °C. At least 100 acquisitions of 5 s were collected for each condition tested.

### Glutaraldehyde cross-linking

The oligomeric state of purified XfDsbC was determined *in vitro* by chemical cross-linking with glutaraldehyde. The protein samples (approximately 5 μM protein in 20 mM Hepes buffer, pH 7.5, in a total volume of 100 μL) in the presence or absence of 3 mM TCEP were incubated on ice for 5 min with increasing concentrations (0–0.1%) of a freshly prepared solution of glutaraldehyde. The reactions were stopped by adding 10 μL of 1 M Tris-HCl, pH 8.0, and the products were evaluated by SDS/PAGE and western blot analysis using polyclonal antibodies against XfDsbC.

### Tryptophan fluorescence measurements

The tryptophan fluorescence spectra of XfDsbC were measured on an ISS K2 Fluorescence Spectrometer (ISS, Champaign, IL, USA). Three independent experiments were performed using 5 μM XfDsbC in the presence and absence of 3 mM TCEP in buffer B. Excitation was performed at a fixed wavelength of 280 nm, and emission spectra were recorded in the range 300–400 nm. The fluorescence contribution from the blank solutions containing the reducing agent or not were subtracted from that of the samples reduced or nonreduced, respectively.

### SAXS data collection, processing and model construction

XfDsbC samples were submitted for SAXS data collection. XfDsbC at concentrations of 1, 4, 7 and 13 mg·mL$^{-1}$ in buffer B was incubated with 0 or 3 mM TCEP for 3 h before the SAXS experiments. The samples were centrifuged at 13 000 ***g*** at 4 °C before use in the SAXS experiments. The SAXS data collection was performed at the SAXS-1 beamline at the Brazilian National Synchrotron Light Laboratory (LNLS, Campinas, Brazil) [56] with a Pilatus (300 K; 84 × 107 mm) 2D detector (Dectris Ltd, Baden, Switzerland) and a monochromatic X-ray beam with a wavelength of 1.3808 Å. The sample-to-detector distance was adjusted to 1101.50 mm to cover a momentum transfer interval of $0.0158 < q < 0.4426$ Å$^{-1}$, where $q = [(4\pi)/(\lambda)]\sin\theta$ and $2\theta$ is the scattering angle. Individual XfDsbC samples were carefully loaded into cells made of two thin, parallel mica windows and maintained at 4 °C during the measurements. The protein samples and buffer solution were exposed to the X-ray beam in 1- to 5-min frames. At least 10 successive frames were recorded for each protein concentration and TCEP condition.

The data reduction was performed using FIT2D [57] with radial integration of the collected images, and normalization was performed relative to the intensity of the transmitted beam after buffer scattering subtraction. The SAXS data analyses were performed using ATSAS software [58].

The Rg and scattering intensity at zero angle [$I(0)$] were calculated using the indirect Fourier transform method implemented in GNOM software [58], which also calculates the distance distribution function $P(r)$ and allows the assessment of $D_{max}$ and molecule anisometry. Kratky plots [$q^2I(q) \times q$] [59] were also generated to evaluate the conformational variability of the protein in solution. The molecular weight of the protein was estimated using the SAXS MoW algorithm [25].

*Ab initio* dummy bead models were calculated from the experimental curves using DAMMIN and DAMMIF [56,60]. Different point-group symmetries (P1, P2 and P4) were imposed, and the best results were obtained with P2 symmetry. The final low-resolution 3D envelope, which represents the protein, was generated by averaging independent runs with DAMAVER and DAMFILT software [61] in automatic mode. The individual and mean SAXS envelopes were visually inspected.

In parallel with the *ab initio* methods used to construct the low-resolution envelope from the experimental curve, rigid-body modelling was performed. First, a monomeric XfDsbC 3D homology model was obtained using the I-TASSER server [62]. To assemble possible XfDsbC dimers and tetramers, the I-TASSER XfDsbC models were superimposed on the EcDsbC crystal structure (PDB code: 1EEJ) using PYMOL (Schrodinger LLC, New York, NY, USA). Possible XfDsbC dimerization interfaces were suggested based on the EcDsbC dimeric structure [18]. The theoretical dimeric XfDsbC atomic model was first modelled onto the SAXS curve using BUNCH [63]. In this procedure, an XfDsbC monomer was presented to the software with separate dimerization and catalytic domains, and few restraints were imposed in the reconstruction of the XfDsbC dimer.

The XfDsbC tetramer models were constructed using SASREF software [64]. For this task, the catalytic and dimerization domains were separately provided to the software, and restrictions on the shortest and longest distances for the independent domains were imposed. The dimerization interface was restricted based on the results obtained with the XfDsbC dimer model.

The discrepancy ($\chi$) between the experimental data and the theoretical scattering curves computed for each possible atomic model was assessed using CRYSOL software [64]. Conventionally, the $\chi$ parameter, which is provided by CRYSOL, is used as a measurement of the goodness of fit to the experimental data. The structural alignments were performed using SUPCOMB software [65].

## Acknowledgements

The work described in the present study was supported by grants from the Fundação de Amparo à Pesquisa do Estado de São Paulo (FAPESP, Process 01/07533-7). C.A.S. was the recipient of a graduate fellowship from FAPESP (Process 08/55690-3); A.P.S. and R.A. are recipients of a research fellowship from the Conselho Nacional de Desenvolvimento Científico e Tecnológico (CNPq). We gratefully acknowledge the Laboratório Nacional de Luz Síncrotron (LNLS, Campinas, Brazil) for providing beamline time. We would also like to thank Mateus B. Cardoso for help with the SAXS experiments and the Laboratório de Espectroscopia e Calorimetria (LEC) and Laboratório Nacional de Biociências (LNBio, Campinas, Brazil) for support with the spectroscopic studies. The authors declare that there are no conflicts of interest.

## References

1 Thakur KG, Praveena T & Gopal B (2010) Structural and biochemical bases for the redox sensitivity of *Mycobacterium tuberculosis* RslA. *J Mol Biol* **397**, 1199–1208.

2 Sato Y & Inaba K (2012) Disulfide bond formation network in the three biological kingdoms, bacteria, fungi and mammals. *FEBS J* **279**, 2262–2271.

3 Messens J & Collet JF (2006) Pathways of disulfide bond formation in *Escherichia coli*. *Int J Biochem Cell Biol* **38**, 1050–1062.

4 Gleiter S & Bardwell JC (2008) Disulfide bond isomerization in prokaryotes. *Biochim Biophys Acta* **1783**, 530–534.

5 Kadokura H & Beckwith J (2010) Mechanisms of oxidative protein folding in the bacterial cell envelope. *Antioxid Redox Signal* **13**, 1231–1246.

6 Pedone E, Limauro D, D'Ambrosio K, De Simone G & Bartolucci S (2010) Multiple catalytically active thioredoxin folds: a winning strategy for many functions. *Cell Mol Life Sci* **67**, 3797–3814.

7 Wunderlich M & Glockshuber R (1993) Redox properties of protein disulfide isomerase (DsbA) from *Escherichia coli*. *Protein Sci* **2**, 717–726.

8 Warwicker J (1998) Modeling charge interactions and redox properties in DsbA. *J Biol Chem* **273**, 2501–2504.

9 Hennecke J, Sebbel P & Glockshuber R (1999) Random circular permutation of DsbA reveals segments that are essential for protein folding and stability. *J Mol Biol* **286**, 1197–1215.

10 Rietsch A, Belin D, Martin N & Beckwith J (1996) An *in vivo* pathway for disulfide bond isomerization in *Escherichia coli*. *Proc Natl Acad Sci USA* **93**, 13048–13053.

11 Hiniker A & Bardwell JC (2004) *In vivo* substrate specificity of periplasmic disulfide oxidoreductases. *J Biol Chem* **279**, 12967–12973.

12 Chen J, Song JL, Zhang S, Wang Y, Cui DF & Wang CC (1999) Chaperone activity of DsbC. *J Biol Chem* **274**, 19601–19605.

13 Liu X & Wang CC (2001) Disulfide-dependent folding and export of *Escherichia coli* DsbC. *J Biol Chem* **276**, 1146–1151.
14 Heras B, Shouldice SR, Totsika M, Scanlon MJ, Schembri MA & Martin JL (2009) DSB proteins and bacterial pathogenicity. *Nat Rev Microbiol* **7**, 215–225.
15 Rietsch A, Bessette P, Georgiou G & Beckwith J (1997) Reduction of the periplasmic disulfide bond isomerase, DsbC, occurs by passage of electrons from cytoplasmic thioredoxin. *J Bacteriol* **179**, 6602–6608.
16 Nakasako M, Maeno A, Kurimoto E, Harada T, Yamaguchi Y, Oka T, Takayama Y, Iwata A & Kato K (2010) Redox-dependent domain rearrangement of protein disulfide isomerase from a thermophilic fungus. *Biochemistry* **49**, 6953–6962.
17 Wilkinson B & Gilbert HF (2004) Protein disulfide isomerase. *Biochim Biophys Acta* **1699**, 35–44.
18 McCarthy AA, Haebel PW, Törrönen A, Rybin V, Baker EN & Metcalf P (2000) Crystal structure of the protein disulfide bond isomerase, DsbC, from *Escherichia coli*. *Nat Struct Biol* **7**, 196–199.
19 Berkmen M, Boyd D & Beckwith J (2005) The nonconsecutive disulfide bond of *Escherichia coli* phytase (AppA) renders it dependent on the protein-disulfide isomerase, DsbC. *J Biol Chem* **280**, 11387–11394.
20 Vertommen D, Depuydt M, Pan J, Leverrier P, Knoops L, Szikora JP, Messens J, Bardwell JC & Collet JF (2008) The disulphide isomerase DsbC cooperates with the oxidase DsbA in a DsbD-independent manner. *Mol Microbiol* **67**, 336–349.
21 Hiniker A, Collet JF & Bardwell JC (2005) Copper stress causes an *in vivo* requirement for the *Escherichia coli* disulfide isomerase DsbC. *J Biol Chem* **280**, 33785–33791.
22 Lee RF, Derrick KS, Beretta MJG, Chagas CM & Rosetti V (1991) Citrus variegated chlorosis: a new destructive disease of citrus in Brazil. *Citrus Ind* **72**, 12–15.
23 Chang CJ, Garnier M, Zreik L, Rossetti V & Bové JM (1993) Culture and serological detection of the xylem-limited bacterium causing citrus variegated chlorosis and its identification as a strain of *Xylella fastidiosa*. *Curr Microbiol* **27**, 137–142.
24 Zapun A, Missiakas D, Raina S & Creighton TE (1995) Structural and functional characterization of DsbC, a protein involved in disulfide bond formation in *Escherichia coli*. *Biochemistry* **34**, 5075–5089.
25 Fischer H, Neto MD, Napolitano HB, Polikarpov I & Craievich AF (2010) Determination of the molecular weight of proteins in solution from a single small-angle X-ray scattering measurement on a relative scale. *J Appl Crystallogr* **43**, 101–109.
26 Arredondo SA, Chen TF, Riggs AF, Gilbert HF & Georgiou G (2009) Role of dimerization in the catalytic properties of the *Escherichia coli* disulfide isomerase DsbC. *J Biol Chem* **284**, 23972–23979.
27 Zhang M, Monzingo AF, Segatori L, Georgiou G & Robertus JD (2004) Structure of DsbC from *Haemophilus influenzae*. *Acta Crystallogr D Biol Crystallogr* **60**, 1512–1518.
28 Banaszak K, Mechin I, Frost G & Rypniewski W (2004) Structure of the reduced disulfide-bond isomerase DsbC from *Escherichia coli*. *Acta Crystallogr D Biol Crystallogr* **60**, 1747–1752.
29 Bader MW, Hiniker A, Regeimbal J, Goldstone D, Haebel PW, Riemer J, Metcalf P & Bardwell JC (2001) Turning a disulfide isomerase into an oxidase: DsbC mutants that imitate DsbA. *EMBO J* **20**, 1555–1562.
30 Simpson AJ, Reinach FC, Arruda P, Abreu FA, Acencio M, Alvarenga R, Alves LM, Araya JE, Baia GS, Baptista CS *et al.* (2000) The genome sequence of the plant pathogen *Xylella fastidiosa*. *Nature* **406**, 151–159.
31 Saraiva AM, Reis MA, Tada SF, Rosselli-Murai LK, Schneider DRS, Pelloso AC, Toledo MAS, Giles C, Aparicio R & de Souza AP (2009) Functional and small-angle X-ray scattering studies of a new stationary phase survival protein E (SurE) from *Xylella fastidiosa* – evidence of allosteric behaviour. *FEBS J* **276**, 6751–6762.
32 Toledo MAS, Schneider DRS, Azzoni AR, Favaro MTP, Pelloso AC, Santos CA, Saraiva AM & Souza AP (2011) Characterization of an oxidative stress response regulator, homologous to *Escherichia coli* OxyR, from the phytopathogen *Xylella fastidiosa*. *Protein Expr Purif* **75**, 204–210.
33 Santos CA, Beloti LL, Toledo MAS, Crucello A, Favaro MTP, Mendes JS, Santiago AS, Azzoni AR & Souza AP (2012) A novel protein refolding protocol for the solubilization and purification of recombinant peptidoglycan-associated lipoprotein from *Xylella fastidiosa* overexpressed in *Escherichia coli*. *Protein Expr Purif* **82**, 284–289.
34 Caserta R, Takita MA, Targon ML, Rosselli-Murai LK, de Souza AP, Peroni L, Stach-Machado DR, Andrade A, Labate CA, Kitajima EW *et al.* (2010) Expression of *Xylella fastidiosa* fimbrial and afimbrial proteins during biofilm formation. *Appl Environ Microbiol* **76**, 4250–4259.
35 de Souza AA, Takita MA, Coletta-Filho HD, Caldana C, Goldman GH, Yanai GM, Muto NH, de Oliveira RC, Nunes LR & Machado MA (2003) Analysis of gene expression in two growth states of *Xylella fastidiosa* and its relationship with pathogenicity. *Mol Plant Microbe Interact* **16**, 867–875.
36 de Souza AA, Takita MA, Coletta-Filho HD, Caldana C, Yanai GM, Muto NH, de Oliveira RC, Nunes LR & Machado MA (2004) Gene expression profile of the

plant pathogen *Xylella fastidiosa* during biofilm formation *in vitro*. *FEMS Microbiol Lett* **237**, 341–353.
37 Shouldice SR, Heras B, Walden PM, Totsika M, Schembri MA & Martin JL (2011) Structure and function of DsbA, a key bacterial oxidative folding catalyst. *Antioxid Redox Signal* **14**, 1729–1760.
38 Rodrigues CM, Takita MA, Coletta-Filho HD, Olivato JC, Caserta R, Machado MA & de Souza AA (2008) Copper resistance of biofilm cells of the plant pathogen *Xylella fastidiosa*. *Appl Microbiol Biotechnol* **77**, 1145–1157.
39 Sauer K, Rickard AH & Davies DG (2007) Biofilms and biocomplexity. *Microbe* **2**, 347–353.
40 Booth SC, Workentine ML, Wen J, Shaykhutdinov R, Vogel HJ, Ceri H, Turner RJ & Weljie AM (2011) Differences in metabolism between the biofilm and planktonic response to metal stress. *J Proteome Res* **10**, 3190–3199.
41 Hartl FU, Bracher A & Hayer-Hartl M (2011) Molecular chaperones in protein folding and proteostasis. *Nature* **475**, 324–332.
42 Ke H, Zhang S, Li J, Howlett GJ & Wang CC (2006) Folding of *Escherichia coli* DsbC: characterization of a monomeric folding intermediate. *Biochemistry* **45**, 15100–15110.
43 Inaba K, Murakami S, Suzuki M, Nakagawa A, Yamashita E, Okada K & Ito K (2006) Crystal structure of the DsbB-DsbA complex reveals a mechanism of disulfide bond generation. *Cell* **127**, 789–801.
44 Hiniker A, Ren G, Heras B, Zheng Y, Laurinec S, Jobson RW, Stuckey JA, Martin JL & Bardwell JC (2007) Laboratory evolution of one disulfide isomerase to resemble another. *Proc Natl Acad Sci USA* **104**, 11670–11675.
45 Dutton RJ, Boyd D, Berkmen M & Beckwith J (2008) Bacterial species exhibit diversity in their mechanisms and capacity for protein disulfide bond formation. *Proc Natl Acad Sci USA* **105**, 11933–11938.
46 Schaad NW, Postnikova E, Lacy G, Fatmi M & Chang CJ (2004) *Xylella fastidiosa* subspecies: *X. fastidiosa* subsp. [correction] fastidiosa [correction] subsp. nov., *X. fastidiosa* subsp. multiplex subsp. nov. & *X. fastidiosa* subsp. pauca subsp. nov. *Syst Appl Microbiol* **27**, 290–300.
47 Baba T, Ara T, Hasegawa M, Takai Y, Okumura Y, Baba M, Datsenko KA, Tomita M, Wanner BL & Mori H (2006) Construction of *Escherichia coli* K-12 in-frame, single-gene knockout mutants: the Keio collection. *Mol Syst Biol* **2**, 2006.0008.
48 Davis MJ, French WJ & Schaad NW (1981) Axenic culture of the bacteria associated with phony disease of peach and plum leaf scald. *Curr Microbiol* **5**, 311–316.
49 Ellman GL (1959) Tissue sulfhydryl groups. *Arch Biochem Biophys* **82**, 70–77.
50 Holmgren A (1979) Thioredoxin catalyzes the reduction of insulin disulfides by dithiothreitol and dihydrolipoamide. *J Biol Chem* **254**, 9627–9632.
51 Kitagawa M, Ara T, Arifuzzaman M, Ioka-Nakamichi T, Inamoto E, Toyonaga H & Mori H (2005) Complete set of ORF clones of *Escherichia coli* ASKA library (a complete set of *E. coli* K-12 ORF archive): unique resources for biological research. *DNA Res* **12**, 291–299.
52 Martínez-Galisteo E, Padilla CA, García-Alfonso C, López-Barea J & Bárcena JA (1993) Purification and properties of bovine thioredoxin system. *Biochimie* **75**, 803–809.
53 Guzman LM, Belin D, Carson MJ & Beckwith J (1995) Tight regulation, modulation & high-level expression by vectors containing the arabinose PBAD promoter. *J Bacteriol* **177**, 4121–4130.
54 Gallagher SR (2001) One-dimensional electrophoresis using nondenaturing conditions. *Curr Protoc Protein Sci* **10**, 10.3.1–10.3.11.
55 Whitmore L & Wallace BA (2004) DICHROWEB, an online server for protein secondary structure analyses from circular dichroism spectroscopic data. *Nucleic Acids Res* **32**, W668–W673.
56 Kellermann G, Vicentin F, Tamura E, Rocha M, Tolentino H, Barbosa A, Craievich A & Torriani I (1997) The small-angle X-ray scattering beamline of the Brazilian synchrotron light laboratory. *J Appl Crystallogr* **30**, 880–883.
57 Hammersley AP, Svensson SO, Hanfland M, Fitch AN & Hausermann D (1996) Two-dimensional detector software: from real detector to idealised image or two-theta scan. *High Press Res* **14**, 235–248.
58 Konarev PV, Petoukhov MV, Volkov VV & Svergun DI (2006) ATSAS 2.1, a program package for small-angle scattering data analysis. *J Appl Crystallogr* **39**, 277–286.
59 Doniach S (2001) Changes in biomolecular conformation seen by small angle X-ray scattering. *Chem Rev* **101**, 1763–1778.
60 Franke D & Svergun DI (2009) DAMMIF, a program for rapid ab-initio shape determination in small-angle scattering. *J Appl Crystallogr* **42**, 342–346.
61 Volkov VV & Svergun DI (2003) Uniqueness of *ab initio* shape determination in small-angle scattering. *J Appl Crystallogr* **36**, 860–864.
62 Roy A, Kucukural A & Zhang Y (2010) I-TASSER: a unified platform for automated protein structure and function prediction. *Nat Protoc* **5**, 725–738.
63 Petoukhov MV & Svergun DI (2005) Global rigid body modeling of macromolecular

complexes against small-angle scattering data. *Biophys J* **89**, 1237–1250.

64 Svergun D, Barberato C & Koch MHJ (1995) CRYSOL a program to evaluate X-ray solution scattering of biological macromolecules from atomic coordinates. *J Appl Crystallogr* **28**, 768–773.

65 Kozin MB & Svergun DI (2001) Automated matching of high- and low-resolution structural models. *J Appl Crystallogr* **34**, 33–41.

## Supporting information

The following supplementary material is available:

**Fig. S1.** CLUSTALW2 alignment of DsbC sequences from *X. fastidiosa* strain 9a5c (XfDsbC), *X. campestris* pv. *campestris* (XcDsbC), *E. chrysanthemi* (ErcDsbC) and *E. coli* (EcDsbC).

**Fig. S2.** The inverted $XfDsbC_{Red}$ dimer.

**Fig. S3.** Possible tetrameric assemblies of (A) EcDsbC (PDB code: 1EEJ) and (B) HiDsbC (PDB code: 1TDJ).

This supplementary material can be found in the online version of this article.

Please note: As a service to our authors and readers, this journal provides supporting information supplied by the authors. Such materials are peer-reviewed and may be reorganized for online delivery, but are not copy-edited or typeset. Technical support issues arising from supporting information (other than missing files) should be addressed to the authors.

# Functional and Structural Studies of the Disulfide Isomerase *Xf*DsbC from the Plant Pathogen *Xylella fastidiosa* Reveals a Redox-dependent Oligomeric Modulation *in vitro*

Clelton A. Santos[1], Marcelo A.S. Toledo[1], Daniela B.B. Trivella[2], Lilian L. Beloti[1], Dilaine R.S. Schneider[1], Antonio M. Saraiva[1], Aline Crucello[1], Adriano R. Azzoni[1,3], Alessandra A. Souza[4], Ricardo Aparicio[2] and Anete P. Souza[1,5,*]

[1]*Centro de Biologia Molecular e Engenharia Genética, Universidade Estadual de Campinas, Campinas, SP, Brazil*

[2]*Laboratório de Biologia Estrutural e Cristalografia, Instituto de Química, Universidade Estadual de Campinas, Campinas, SP, Brazil*

[3]*Departamento de Engenharia Química, Escola Politécnica, Universidade de São Paulo, São Paulo, SP, Brazil*

[4]*Centro APTA Citros Sylvio Moreira/IAC, Rodovia Anhanguera Km 158, Cordeirópolis, SP, Brazil*

[5]*Departamento de Biologia Vegetal, Instituto de Biologia, Universidade Estadual de Campinas, Campinas, SP, Brazil*

**Supplementary Figures S1-S3**

***Address correspondence to**: Anete P. Souza, Centro de Biologia Molecular e Engenharia Genética (CBMEG), Universidade Estadual de Campinas, Rua Candido Rondon 400, Cidade Universitária "Zeferino Vaz", CP 6010, 13083-875, Campinas, São Paulo, Brazil, Tel. and Fax: +55 19 3521-1089; E-mail: anete@unicamp.br

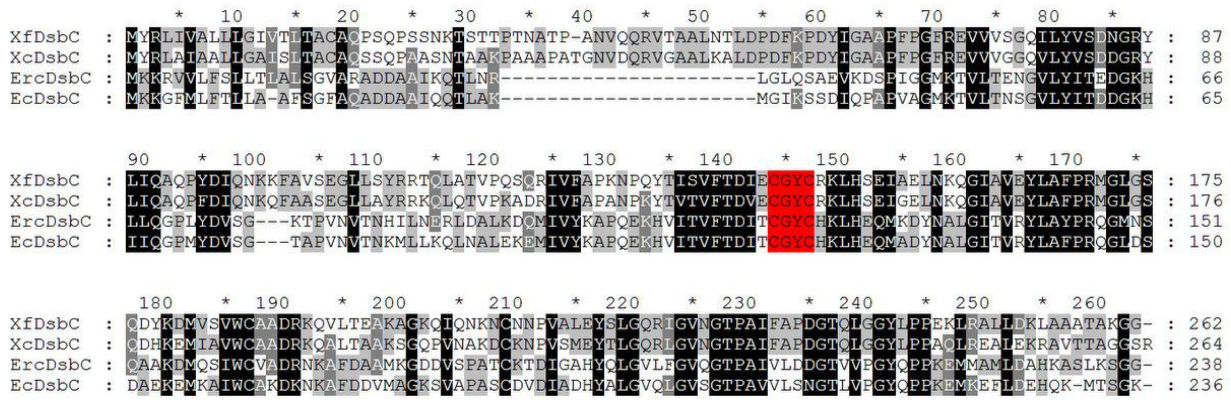


**Supplemental Figure S1.** ClustalW2 alignment of DsbC sequences from *Xylella fastidiosa* strain 9a5c (*Xf*DsbC), *Xanthomonas campestris* pv. *campestris* (XcDsbC), *Erwinia chrysanthemi* (ErcDsbC) and *Escherichia coli* (EcDsbC). The regions that are fully conserved in the four sequences (black) and the residues that are strongly similar between the sequences (gray) are highlighted. The oxi-redox switch, which is composed of the CGYC motif, is indicated in red in all sequences.

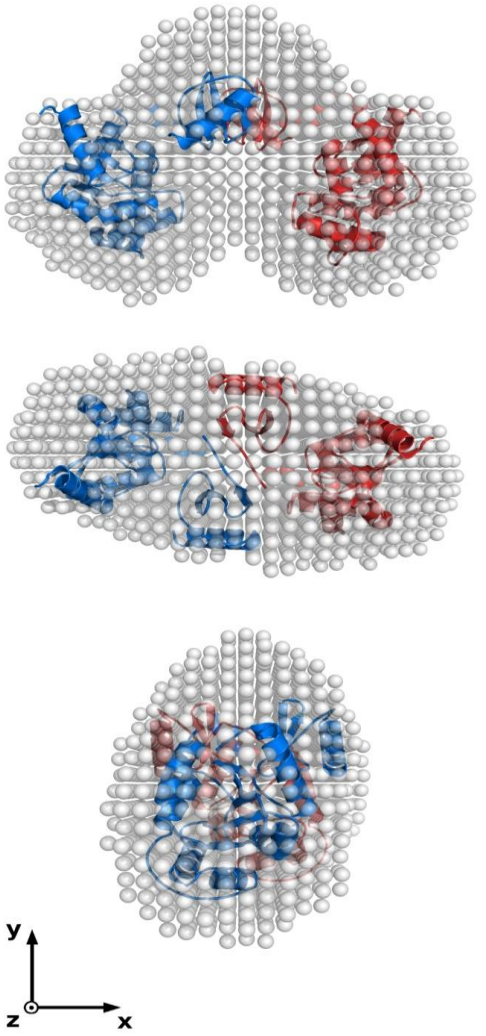


**Supplemental Figure S2**. The inverted *Xf*DsbC$_{Red}$ dimer. Three-dimensional atomic model for *Xf*DsbC dimer was generated as an output from BUNCH software. The low-resolution data obtained limits the interpretation of the correct *Xf*DsbC$_{Red}$ dimeric structure. Therefore, a second possible *Xf*DsbC$_{Red}$ dimer is also provided. The same low-resolution protein envelope constructed for the *Xf*DsbC$_{Red}$ dimer displayed in Fig. 5A is shown here as semi-transparent whitish spheres superimposed onto the inverted *Xf*DsbC$_{Red}$ dimer atomic model. The middle and bottom views are rotated clockwise by 90° around the x- and y-axes, respectively. The figure was generated with PyMOL software (Schrodinger, LLC).

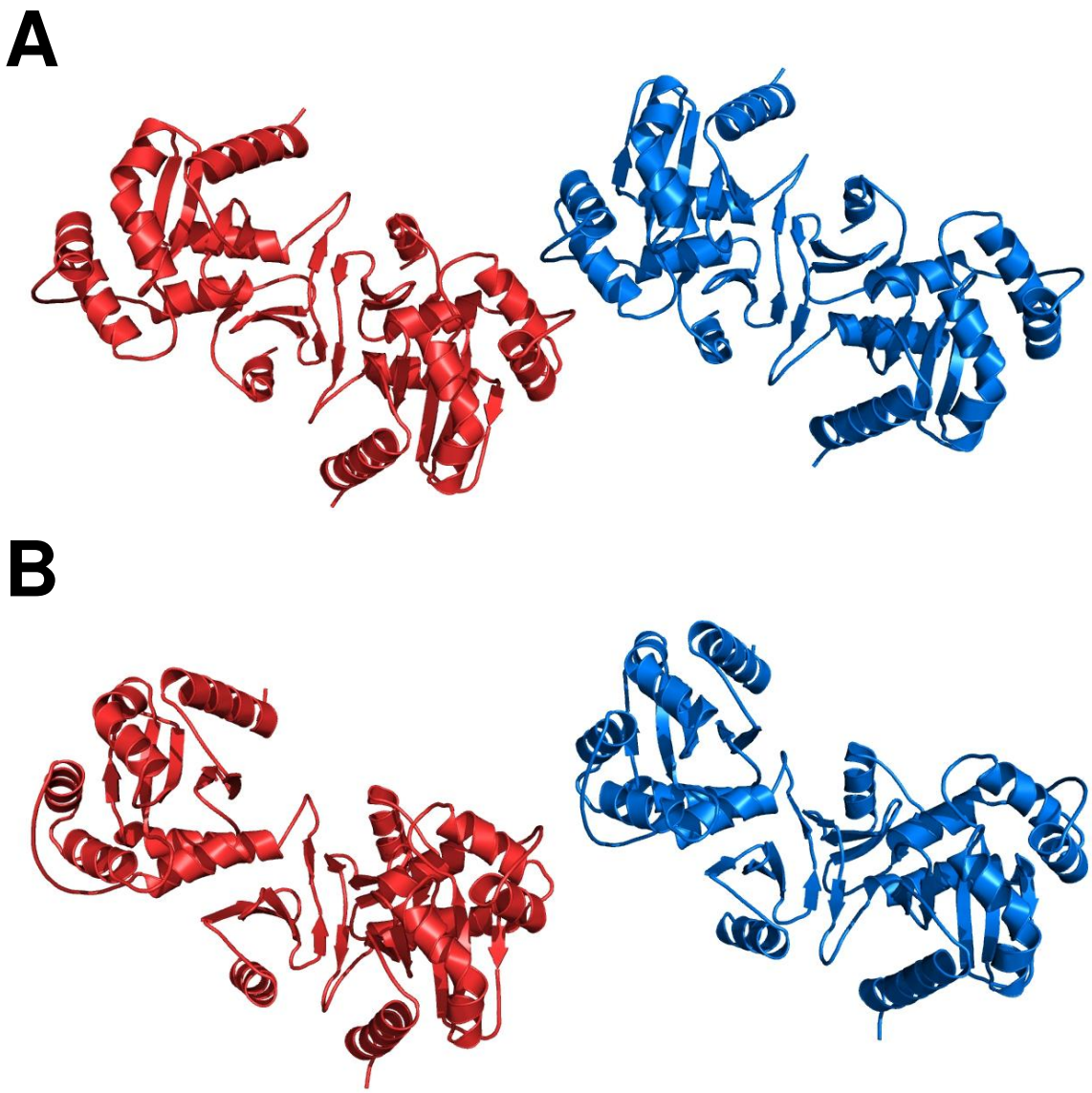


**Supplemental Figure S3.** Possible tetrameric assemblies of (A) EcDsbC (PDB ID 1EEJ) and (B) HiDsbC (PDB ID 1TDJ)**.** These oligomers were observed in the crystal structures by applying symmetric operations. The symmetric molecules and figures were generated with PyMOL software (Schrodinger, LLC).

# 3 CAPÍTULO 2 – ARTIGO

## "Initial biochemical and functional characterization of a 5'-nucleotidase from *Xylella fastidiosa* related to the human cytosolic 5'-nucleotidase I"

**Autores:** Clelton A. Santos, Antonio M. Saraiva, Marcelo A.S. Toledo, Lilian L. Beloti, Aline Crucello, Marianna T.P. Favaro, Maria A.C. Horta, André S. Santiago, Juliano S. Mendes, Alessandra A. Souza, Anete P. Souza

**Aceito para publicação na revista *Microbial Pathogenesis***

**Fevereiro/2013**

# Accepted Manuscript

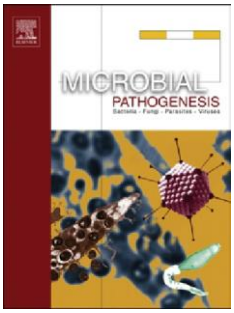


Initial biochemical and functional characterization of a 5'-nucleotidase from *Xylella fastidiosa* related to the human cytosolic 5'-nucleotidase I

Clelton A. Santos, Antonio M. Saraiva, Marcelo A.S. Toledo, Lilian L. Beloti, Aline Crucello, Marianna T.P. Favaro, Maria A.C. Horta, André S. Santiago, Juliano S. Mendes, Alessandra A. Souza, Anete P. Souza

PII: S0882-4010(13)00027-2

DOI: 10.1016/j.micpath.2013.02.007

Reference: YMPAT 1396

To appear in: *Microbial Pathogenesis*

Received Date: 6 December 2012

Revised Date: 18 February 2013

Accepted Date: 22 February 2013

Please cite this article as: Santos CA, Saraiva AM, Toledo MAS, Beloti LL, Crucello A, Favaro MTP, Horta MAC, Santiago AS, Mendes JS, Souza AA, Souza AP, Initial biochemical and functional characterization of a 5'-nucleotidase from *Xylella fastidiosa* related to the human cytosolic 5'-nucleotidase I, *Microbial Pathogenesis* (2013), doi: 10.1016/j.micpath.2013.02.007.

# Initial biochemical and functional characterization of a 5'-nucleotidase from *Xylella fastidiosa* related to the human cytosolic 5'-nucleotidase I

Clelton A. Santos[a], Antonio M. Saraiva[a,b], Marcelo A.S. Toledo[a], Lilian L. Beloti[a], Aline Crucello[a], Marianna T.P. Favaro[a], Maria A.C. Horta[a], André S. Santiago[a], Juliano S. Mendes[a], Alessandra A. Souza[c], Anete P. Souza[a,d,*]

[a] *Centro de Biologia Molecular e Engenharia Genética, Universidade Estadual de Campinas, Campinas, SP, Brazil*
[b] *Instituto Nacional de Metrologia, Qualidade e Tecnologia, Rio de Janeiro, RJ, Brazil*
[c] *Centro APTA Citros Sylvio Moreira, IAC, Rodovia Anhanguera Km 158, Cordeirópolis, SP, Brazil*
[d] *Departamento de Biologia Vegetal, Instituto de Biologia, Universidade Estadual de Campinas, Campinas, SP, Brazil*

**Running title**: *Characterization of a 5'-nucleotidase from Xylella fastidiosa*

*Abbreviations used: Xf*5'-Nt, 5'-nucleotidase from *X. fastidiosa*; cN-I, cytosolic 5'-nucleotidase I; CD, circular dichroism*; p*NPP, *p*-nitrophenyl phosphate.

***Address correspondence to**: Anete P. Souza, Centro de Biologia Molecular e Engenharia Genética (CBMEG), Universidade Estadual de Campinas, Av. Candido Rondon 400, Cidade Universitária "Zeferino Vaz", CP 6010, 13083-875, Campinas, São Paulo, Brazil; Tel. and Fax: +55 19 3521-1089; E-mail: anete@unicamp.br

## Abstract

The 5'-nucleotidases constitute a ubiquitous family of enzymes that catalyze either the hydrolysis or the transfer of esterified phosphate at the 5' position of nucleoside monophosphates. These enzymes are responsible for the regulation of nucleotide and nucleoside levels in the cell and can interfere with the phosphorylation-dependent activation of nucleoside analogs used in therapies targeting solid tumors and viral infections. In the present study, we report the initial biochemical and functional characterization of a 5'-nucleotidase from *Xylella fastidiosa* that is related to the human cytosolic 5'-nucleotidase I. *X. fastidiosa* is a plant pathogenic bacterium that is responsible for numerous economically important crop diseases. Biochemical assays confirmed the phosphatase activity of the recombinant purified enzyme and revealed metal ion dependence for full enzyme activity. In addition, we investigated the involvement of *Xf*5'-Nt in the formation of *X. fastidiosa* biofilms, which are structures that occlude the xylem vessels of susceptible plants and are strictly associated with bacterial pathogenesis. Using polyclonal antibodies against *Xf*5'-Nt, we observed an overexpression of *Xf*5'-Nt during the initial phases of *X. fastidiosa* biofilm formation that was not observed during *X. fastidiosa* planktonic growth. Our results demonstrate that the de/phosphorylation network catalyzed by 5'-nucleotidases may play an important role in bacterial biofilm formation, thereby contributing novel insights into bacterial nucleotide metabolism and pathogenicity.


**Keywords:** 5'-nucleotidase, cN-I, *Xylella fastidiosa*, biofilm formation, nucleotide metabolism

## 1. Introduction

From a biochemical perspective, life, including all of its subtleties, is controlled primarily by nucleic acids (DNA and RNA). All living organisms are constantly replicating and transmitting to their descendants the hereditary information contained in their genes. Therefore, enzymes that are involved in metabolic pathways (biosynthesis or degradation) controlling the assembly and composition of nucleic acids have a direct impact on life [1, 2].

In bacteria, DNA recycling is tailored to the needs of the cell and involves several specialized catabolic enzymes [1], including the 5'-nucleotidases (EC 3.1.3.5). The 5'-nucleotidases constitute a family of enzymes that catalyze either the hydrolysis or the transfer of esterified phosphate at the 5' position of nucleoside monophosphates and are known to regulate the nucleotide and nucleoside levels in the cell [3-6].

The mammalian 5'-nucleotidases are the most well-characterized enzymes from this phosphatase family [7]. Currently, seven mammalian 5'-nucleotidases have been reported [8-14]. Interestingly, despite sharing an identical catalytic mechanism and possessing conserved structural motifs required for enzymatic activity, these enzymes vary in their subcellular localization and substrate specificity [7]. Five of the known human 5'-nucleotidases enzymes act in the cytosol [9-11, 13, 14], one is mitochondrial [12] and one is anchored in the plasma membrane [8]. Although the microbial 5'-nucleotidases are poorly characterized, they may be suitable targets for the therapeutic treatment of tumors and viral infections, because the enzymes from this family have been reported to interfere with the phosphorylation-dependent activation of nucleoside analogs used in the treatment of these diseases [4].

Here, we report the initial biochemical and functional characterization of a recombinant 5'-nucleotidase from the 9a5c strain of *Xylella fastidiosa* (*Xf*5'-Nt) that is related to the human

cytosolic 5'-nucleotidase I. *X. fastidiosa* is a Gram-negative plant pathogenic bacterium that causes relevant crops diseases around the world [15]. Following the host infection, *X. fastidiosa* cells form a biofilm structure [16] that occludes the xylem vessels, leading to a hydric stress condition in the host plant that triggers disease development. Our results indicate that the de/phosphorylation network catalyzed by 5'-nucleotidases may play an important role in bacterial biofilm formation, thereby providing new insights into bacterial nucleotide metabolism and pathogenicity.

## 2. Materials and Methods

### *2.1. Cloning, expression and purification*

The coding sequence of the *Xf5′-Nt* ORF (960 bp), NCBI reference sequence **NP_299368.1**, was amplified from *X. fastidiosa* genomic DNA by PCR with the specific oligonucleotides *Xf*1808F (5'-CCCAACATATGCCCGATCATTCTCATAGG-3′) and *Xf*1808R (5'-AAACTCGAGTCCCGGATCGTTGGCAAC-3'), which contained *Nde*I and *Xho*I restriction sites, respectively. The PCR amplification product was cloned into the pET-29a(+) (Novagen, Madison, WI, USA) expression vector, which added a C-terminal six-histidine tag to the coding sequence. Clones containing the *Xf5′-Nt* insert were sequenced and transformed into the expression strain *E. coli* BL21(DE3). For *Xf*5'-Nt overexpression, BL21(DE3) cells were grown at 37°C in 1 L LB containing kanamycin (30 µg $mL^{-1}$) until an $OD_{600}$ of 0.8 was achieved. The expression of the recombinant protein was induced with 5.6 mM lactose followed by cultivation for 3 h at 37°C and 300 rpm. The culture was harvested by centrifugation (3000 *g* for 15 min at 4°C), and the cell pellets were resuspended in 50 mL buffer A (50 mM Tris-HCl, pH 8.0, and 300 mM NaCl) plus 1 mg $ml^{-1}$ lysozyme and incubated on ice for 30 min. The cells were disrupted by sonication, and the unbroken cells and debris were removed by centrifugation

(27,000 *g* for 40 min at 4°C). The *Xf*5'-Nt protein was purified in a single chromatographic step on a Ni-NTA column (Qiagen; Hilden, Germany) equilibrated with buffer A. The purified *Xf*5'-Nt protein was eluted with six column volumes of buffer A containing 250 mM imidazole, and the purity was estimated using SDS-PAGE. The protein concentration was determined spectrophotometrically and calculated from the absorbance at 280 nm with a calculated molar absorption coefficient ($\varepsilon_{280}$) of 18450 $M^{-1}$ $cm^{-1}$.

2.2. *Identification of the recombinant protein by LC-MS/MS*

The identity of recombinant *Xf*5'-Nt was confirmed by mass spectrometry analysis. Prior to protein sequence analysis, the SDS-PAGE gel band of purified *Xf*5'-Nt was excised and prepared according to the methods of Shevchenko et al. [17]. The peptide mixtures were separated by reverse-phase liquid chromatography (LC) using a nanoACQUITY UPLC System (Waters, UK) in line with an electrospray MS-QTOF (Waters, UK). Four microliters of sample was loaded onto a trapping column (Symmetry C18 Trap, 5 µm, 180 µm x 20 mm; Waters, UK) for preconcentration using a flow with a rate of 0.6 µL $min^{-1}$ and containing 5% acetonitrile and 0.1% formic acid, which was followed by the separation of the peptides using an LC column (Symmetry BEH300 C18 Column, 1.7 µm, 100 µm x 100 mm). Peptides were eluted using a 50-min linear gradient of solvent B (95% acetonitrile and 0.1% formic acid in water) at a flow rate of 0.6 µL $min^{-1}$. Solvent A consisted of 0.1% formic acid in water. The entire analysis was performed using the positive-ion mode with a needle voltage of 3 kV. The mass range used was *m/z* 200 to 2000, and tandem mass spectrometry (MS/MS) spectra were acquired for the most intense peaks (≥10 counts). Multiple charged precursor ions were selected for fragmentation and peptide sequencing using automated data-dependent acquisition (DDA) MassLynx software (Waters) by switching from the MS mode to the MS/MS mode and then returning to the MS

mode. The resulting fragmented spectra were processed using the ProteinLynx v4.0 software (Waters). MASCOT MS/MS Ion Search (Matrix Science) was used to blast the sequences against the NCBInr database. Combined MS-MS/MS searches were conducted with a parent ion mass tolerance of 0.3 Da, an MS/MS mass tolerance of ±0.1 Da, carbamidomethylation of cysteine (fixed modification) and methionine oxidation (variable modification) and were compared against the NCBInr bacteria databank. According to MASCOT probability analysis, only significant ($P < 0.05$) hits were accepted.

2.3. *Circular dichroism measurements*

The far-UV circular dichroism (CD) spectra of the recombinant *Xf*5'-Nt were collected on a JASCO J-810 Spectropolarimeter dichrograph (Japan Spectroscopic; Japan). The assays were performed in a quartz cuvette with a path length of 1 mm, and 10 accumulations within the range of 260-180 nm at a rate of 50 nm $min^{-1}$ at 24°C were recorded with *Xf*5'-Nt at an approximate concentration of 5 µM in 10 mM sodium phosphate buffer at pH 7. The deconvolution and statistical analysis of the CD spectra were performed using the DichroWeb server [18].

2.4. *Size-exclusion chromatography*

Gel filtration chromatography was performed with an ÄKTA-FPLC system using a Superdex 200 HR 10⁄30 column (GE Healthcare; Sweden). Purified *Xf*5'-Nt (200 µg) was loaded onto the column, and the chromatography was performed at a flow rate of 0.5 ml $min^{-1}$ using buffer B (50 mM Tris-HCl, pH 8.0, and 150 mM NaCl). The HMW and LMW calibration kits (GE Healthcare; Sweden) were used as standard molecular weight markers for column calibration.

2.5. *Biochemical characterization*

The phosphatase activity of the recombinant *Xf*5'-Nt was evaluated *in vitro* using the artificial substrate *p*-nitrophenyl phosphate (*p*NPP; Sigma, USA). Assays to determine the pH and cofactor dependence and kinetic parameters were performed at room temperature, and the data were obtained spectrophotometrically at 410 nm. For pH-dependence assays, the buffers MES (pH range of 5-6.5), HEPES (pH range of 7-8) and Tris-HCl (pH range of 8.5-10) were used. The presence or absence of divalent metal ions, including $Mg^{2+}$, $Mn^{2+}$, $Cu^{2+}$, $Ni^{2+}$, $Ca^{2+}$, $Zn^{2+}$ and $Co^{2+}$, were evaluated as cofactors. Subsequent to the determination of the pH optimum and dependence of cofactors, kinetic experiments were performed in 50 mM HEPES buffer (pH 7.0) with 1 mM $Mg^{2+}$. All the reactions were performed in triplicate and repeated three times using approximately 4 µg of freshly purified protein. Kinetic parameters were obtained using GraphPad Prism (Graph–Pad Software, San Diego, CA, USA).

*2.6. Western blot analysis*

The *X. fastidiosa* subsp. *pauca* 9a5c [19] was used to obtain the different phases of bacterial biofilm formation and planktonic cells using a protocol established by De Souza et al. [20]. Polyclonal antibodies against *Xf*5'-Nt were produced by Rheabiotech (Campinas, Brazil) and used in the *Xf*5'-Nt immunodetection during *X. fastidiosa* planktonic and biofilm growth. For western blot analysis, the total amount of *X. fastidiosa* proteins from different developmental phases of biofilm formation and planktonic growth were extracted, normalized and analyzed as described by Santos *et al*. [21].

## 3. Results and discussion

### *3.1. Purification and initial Characterization of Xf5'-Nt*

Functional genomics studies focusing on the characterization of proteins presumably involved in the pathogenicity, adaption and survival of a pathogen provide an interesting approach to better understand the biology and genetics of an organism. Particularly with regard to the plant pathogen *X. fastidiosa*, numerous protein targets that are associated with pathogenesis were annotated during its genome analysis [22]; however, only functional studies can clarify the involvement of these targets in bacterial virulence and pathogenicity.

The 5'-nucleotidase activity has previously been associated with bacterial pathogenicity, including such important pathogens as *Staphylococcus aureus, Bacillus anthracis, Streptococcus sanguinis* and *Haemophilus influenzae* [23-25]. Within this context, Fan et al. [24] have reported that, as a virulence factor, a nucleotidase could act in ATP hydrolysis and still generate adenosine, an immunosuppressive molecule. Thus, in addition to regulating the intracellular nucleotide pools, the nucleotidase activity is involved in bacterial survival, allowing the pathogen to escape host defense responses.

In the present study, the *X. fastidiosa* 9a5c ORF that encodes *Xf*5'-Nt was successfully cloned. DNA sequencing confirmed the correct oligonucleotide sequence in the *Xf5'-Nt*:pET-29a(+) construct. The recombinant protein was purified by affinity chromatography (Fig. 1A). *Xf*5'-Nt has a molecular mass of 35.9 kDa, which corresponds to the 320-amino acid sequence encoded by ORF *Xf*1808 plus the C-terminal $His_6$-Tag added by the pET-29a(+) vector. Approximately 22 mg of soluble *Xf*5'-Nt protein was obtained per liter of bacterial culture. Mass spectroscopic analysis of the recombinant purified protein indicated a sequence coverage of 77%

with the *Xf*5'-Nt amino acid sequence of the *X. fastidiosa* 9a5c strain obtained from GenBank (**AAF84888.1**), which confirmed the identity of the target protein.

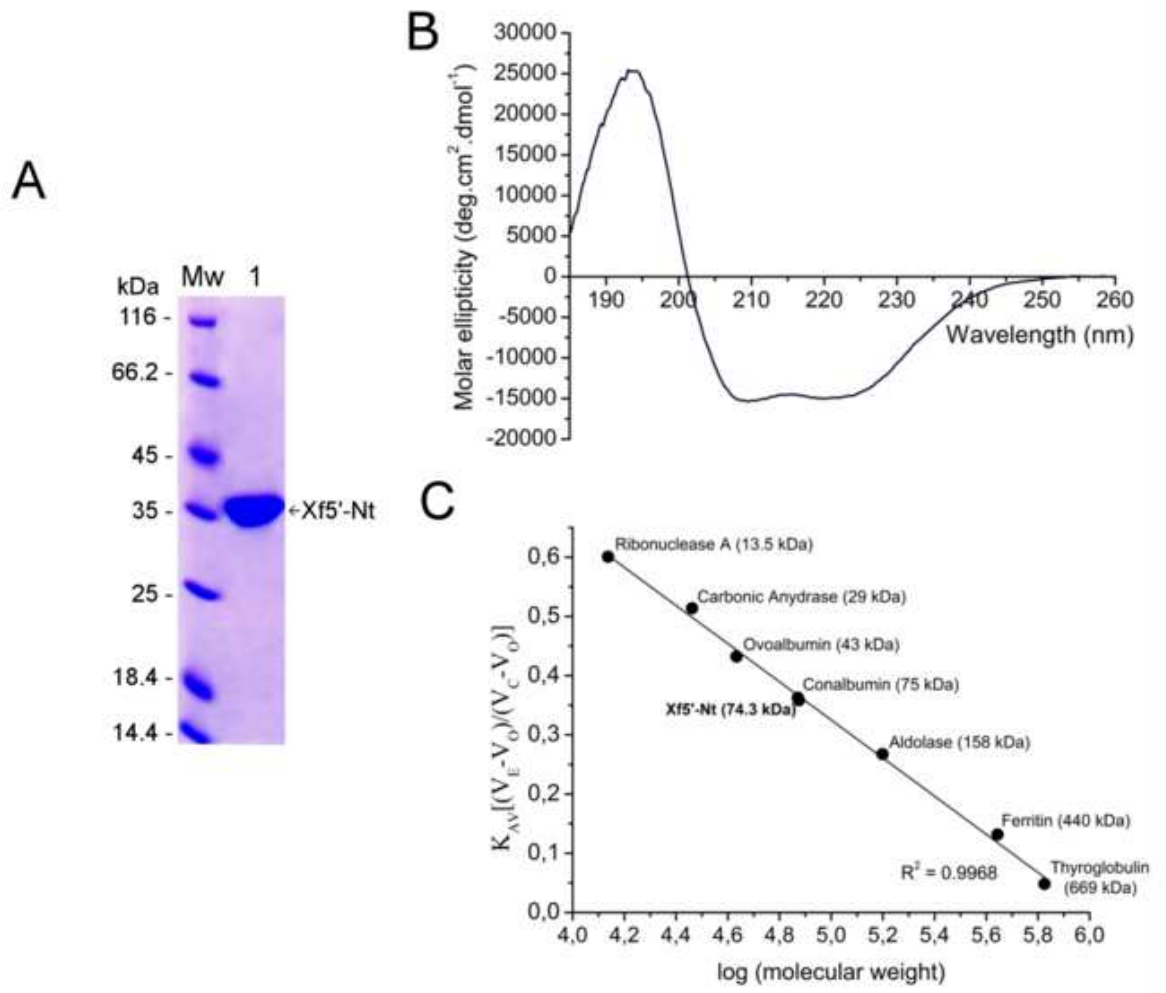


**Figure 1.** Characterization of *Xf*5'-Nt from *X. fastidiosa.* (A) 12 % SDS-PAGE of *Xf*5'-Nt purification. The purified *Xf*5'-Nt (lane 1) was eluted with six column volumes of buffer A containing 250 mM imidazole. Molecular weight markers (Mw) are indicated on the right. (B) Circular dichroism spectrum obtained for purified *Xf*5'-Nt. (C) Calibration curve of *Xf*5'-Nt size-exclusion chromatography analysis. The expected molecular mass for recombinant *Xf*5'-Nt is 35.9 kDa; the estimated molecular weight for *Xf*5'-Nt by size-exclusion chromatography is 74.3 kDa. *Xf*5'-Nt likely exists as a dimer in solution.

Hunsucker et al. [26] analyzed a human cytosolic 5'-nucleotidase I (cN-I) and, after scanning the human cN-I sequence against the GenBank database, observed that in addition to pigeon cN-I [10], cN-I was significantly related to the *X. fastidiosa Xf*5'-Nt, which is reported herein. A comparative alignment of the amino acid sequences of human and pigeon cN-I and *X. fastidiosa Xf*5'-Nt, previously reported [26] (Supplemental Fig. S1) indicated that all three sequences contain a conserved classical Walker B motif, (R/K)$X_{1\text{-}4}$G$X_{2\text{-}4}$ϕ$X$ϕ(D/E) (*X* is any amino acid and ϕ is a hydrophobic amino acid residue), associated with the nucleotide binding pocket and also share a conserved kinase-2 motif (IFFDD) near the C-terminus. Note that the kinase-2 domain is often composed of four hydrophobic amino acid residues followed by an aspartate that may interact with divalent metal ions that act as cofactors for enzymatic activity [27]. This important amino acid residue is conserved in *Xf*5'-Nt and strongly suggests the requirement of divalent metals for proper enzymatic catalysis.

*3.2. Secondary structure and size-exclusion chromatography analysis*

The CD analysis of the *Xf*5'-Nt revealed a typical spectrum of a protein with a predominance of α-helical structure (Fig. 1B), and analysis using the DichroWeb server [18] indicated that *Xf*5'-Nt is composed of 37% α-helices and 14% β-sheets. The experimental results obtained by CD are consistent with the *Xf*5'-Nt secondary structure prediction (35% α-helices and 14% β-sheets) obtained *in silico* using the PSIPRED server [28].

Analytical size-exclusion chromatography indicated that the recombinant purified *Xf*5'-Nt was eluted with a retention time corresponding to a calculated molecular mass of 74.3 kDa (Fig. 1C), indicating that *Xf*5'-Nt likely exists as a dimer in solution because the observed mass represents approximately twice the mass of the monomer (35.9 kDa). The oligomeric state of other 5'-nucleotidases described previously suggests that this class of enzyme may exist in

solution as monomers, dimers and tetramers [7]. The oligomeric assembly of these proteins is directly involved in their function and may modulate substrate recognition and specificity [29]. Therefore, the different oligomeric forms observed among the 5'-nucleotidases may be one explanation for the wide range of substrate specificities and various biological roles of these enzymes [5].

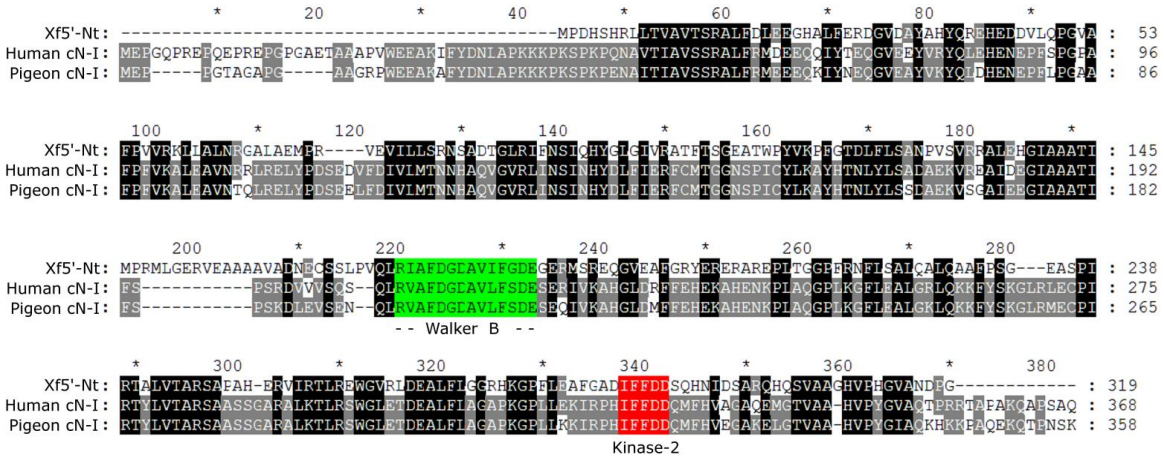


**Supplemental Figure S1.** Multiple sequence alignment of *Xylella fastidiosa Xf*5'-Nt (accession number **NP_299368.1**), human cN-I (accession number **AAK01294.1**) and pigeon cN-I (accession number **CAB43554.1**). The regions fully conserved in the three sequences (black) and the residues that are strongly similar between the sequences (gray) are highlighted. The Walker B and kinase-2 motifs are indicated in green and red, respectively, in all sequences.

*3.3. Enzymatic assays*

For the initial *Xf*5'-Nt biochemical characterization, we used the general artificial substrate for phosphatase activity, pNPP. Prior to evaluating the enzymatic kinetic parameters,

we investigated the optimal pH and the dependence of cofactors for enzyme activity. *Xf*5'-Nt demonstrates the highest activity at pH 7 (Fig. 2A), and this pH value is consistent with the pH optimum described for human cN-I [7], which is related to *Xf*5'-Nt. Regarding cofactor dependence, *Xf*5'-Nt exhibited the highest affinity for $Mg^{2+}$, followed by $Mn^{2+}>Co^{2+}>Cu^{2+}>Ni^{2+}>Ca^{2+}>Zn^{2+}$ (Fig. 2B). Considerable phosphatase activity was also observed in assays in which no metal ions were added to the enzymatic reaction; however, this finding can be explained by the presence of nickel ions in the resin used to purify the recombinant protein, whereas in the presence of EDTA, low activity was observed (Fig. 2B). These results were expected because *Xf*5'-Nt contains a key aspartate (at position 291 in the amino acid sequence) in the conserved structural kinase-2 motif that is responsible for metal ion binding (Supplemental Fig. S1). $Mg^{2+}$ is described as the best metal ion for optimal 5'-nucleotidase activity and can partially be replaced by other divalent cations, including $Mn^{2+}$ and $Co^{2+}$ [5], which is similar to the results observed in the present study.

The kinetic parameters obtained using pNPP as the substrate revealed that *Xf*5'-Nt demonstrated typical Michaelis-Menten behavior, with a $K_m$ value of 0.2241 mM. These results indicate that *Xf*5'-Nt possesses high affinity for pNPP. Biochemical characterization of other 5'-nucleotidases revealed that enzymes in this family demonstrate $K_m$ values ranging from micromolar for pyrimidine deoxyribonucleotide monophosphates to millimolar-submillimolar for purine substrates and pyrimidine ribonucleoside monophosphates [26, 30]. However, additional enzymatic assays using natural substrates are required to evaluate more accurate biochemical features of *Xf*5'-Nt.

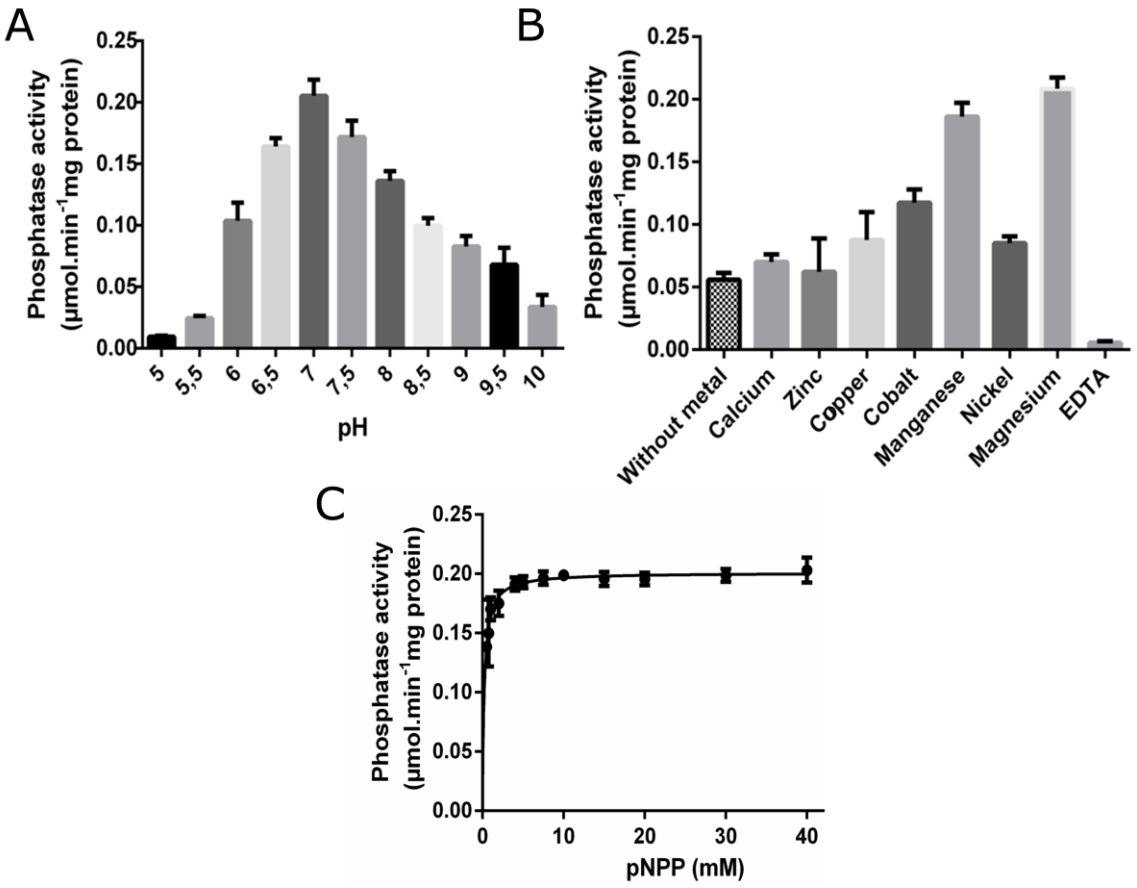


**Figure 2.** Initial enzymatic characterization of purified recombinant *Xf*5'-Nt using pNPP as a substrate. (A) pH dependence of *Xf*5'-Nt in different buffers, including MES (pH 5–6.5), HEPES (pH 7.0–8.0) and Tris–HCl (pH 8.5–10). (B) Divalent metal ion dependence of *Xf*5'-Nt in HEPES (pH 7). Each metal was added at a concentration of 0.1 mM, except for $Mg^{2+}$ (added at 1 mM). A test reaction without metal and another with EDTA were also analyzed. (C) Kinetics curve of *Xf*5'-Nt using pNPP (0.1–40 mM) as the substrate. The reaction mixture contained 50 mM HEPES, pH 7 and 1 mM $Mg^{2+}$.

*3.4. Xf5'-Nt immunodetection during X. fastidiosa biofilm and planktonic growth*

We investigated the presence and the differential expression pattern of *Xf*5'-Nt during *X. fastidiosa* biofilm formation and planktonic cell growth (Fig. 3). Studies focusing on the

differential gene expression between the biofilm and planktonic lifestyles of bacterial growth commonly use techniques such as RT-PCR and DNA microarray technology [20, 31, 32]; however, such techniques only provide an indication of the presence of mRNA and do not confirm the presence of expressed protein. In contrast, experimental approaches based on direct protein detection may lead to more accurate results concerning the presence and biological role played by a certain protein. Our findings indicate that *Xf*5'-Nt was differentially expressed between the *X. fastidiosa* biofilm formation and planktonic growth phases (Fig. 3A). We investigated the presence of *Xf*5'-Nt in biofilms at 3, 5, 10, 15, 20 and 30 days of formation because these days match the different stages of *X. fastidiosa* biofilm formation [20]. Specifically, days 3-5 correspond to the phase in which the initial adhesion of cells to the substrate occurs; microcolonies are formed within 10 days; the maturation of the biofilm begins at day 15; the biofilm is fully mature at day 20; and the biofilm dispersal phase occurs 30 days after the initial adhesion. The statistical analysis of the ratio of the intensity and area (pixels) of the protein bands visualized on nitrocellulose membranes demonstrated statistically significant differences ($P < 0.05$; Student's *t*-test) in the *Xf*5'-Nt expression pattern during the different phases of *X. fastidiosa* biofilm formation and planktonic growth (Fig. 3B). *Xf*5'-Nt expression was greater in biofilms than in planktonic phases, especially during the initial phase (3-5 days) in which the differences were significantly higher.

During the initial steps of bacterial biofilm formation, effector molecules of quorum sensing are responsible for regulating the cellular metabolism and coordinate the microbial growth rate and virulence [33-37]. Thus, such molecules are responsible for ensuring the adhesion of cells on the substrate to be colonized as well as the subsequent maintenance and development of the biofilm [38]. Therefore, enzymes with 5'-nucleotidase activity may be important for the dephosphorylation/phosphorylation-dependent activation of molecules

involved in the cellular signals that stimulate bacterial biofilm formation and development. However, such signaling molecules and regulatory mechanisms remain unknown.

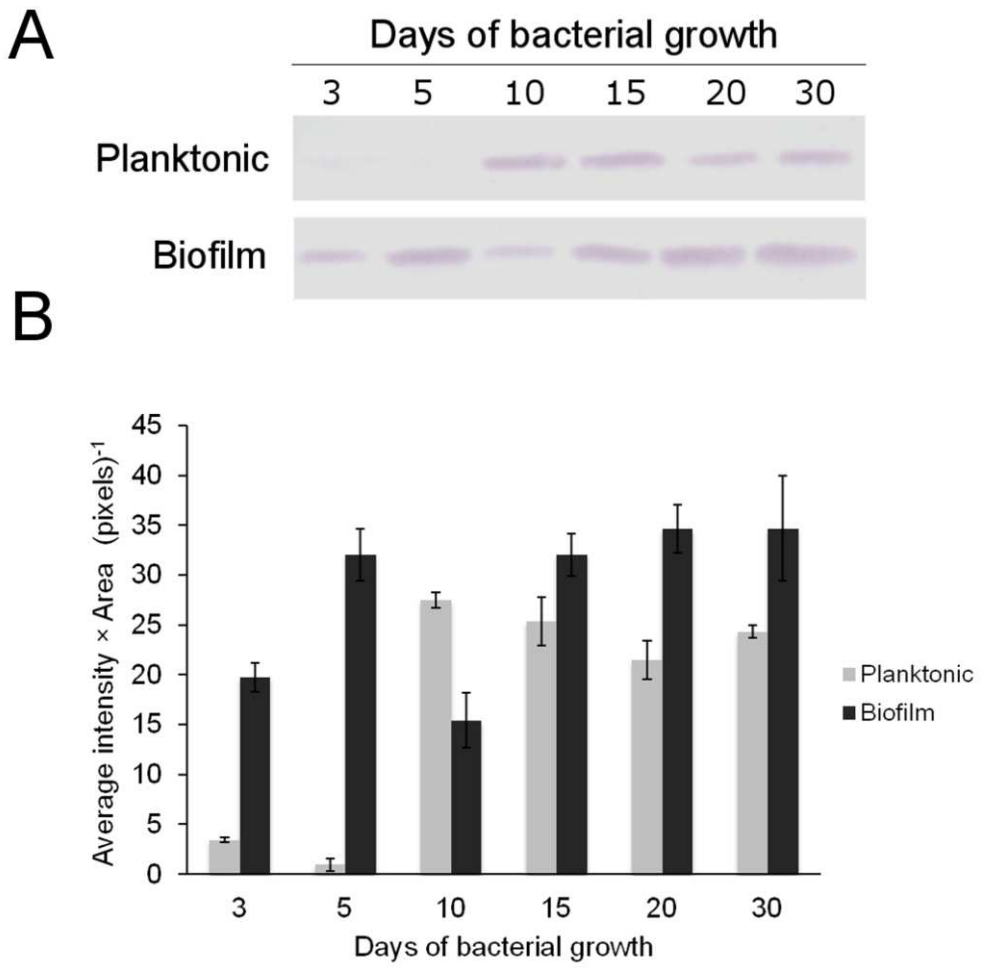


**Figure 3.** *Xf*5'-Nt immunodetection during *X. fastidiosa* biofilm formation and planktonic growth. (A) Total protein samples were isolated from the different biofilm growth phases and from planktonic cells, normalized using BCA quantification, and evaluated by western blot using polyclonal antibodies against *Xf*5'-Nt. (B) *Xf*5'-Nt expression profiles of biofilm (black bars) and planktonic cells (gray bars) were quantified using EDAS software. The bars represent the average of three independent experiments. The error bars indicate the standard errors from experiments performed in triplicate.

## 4. Conclusion

The 5'-nucleotidases are known as multifunctional enzymes that possess a wide range of biological functions ranging from maintaining cellular nucleotide pools to the control of cellular homeostasis. However, this is the first time that the role of these enzymes in the formation and development of bacterial biofilms has been investigated.

In this study, we characterized a protein that is overexpressed during *X. fastidiosa* biofilm formation, particularly in the early stages of its formation, and found that the expression levels in the biofilm were significantly higher than those in the planktonic phase. Biofilm formation by *X. fastidiosa* is considered its primary mechanism of pathogenicity; therefore, understanding the dynamics of the formation of this structure can aid in a better understanding of the biology of this phytopathogenic bacterium and enable the development of new approaches to control this pathogen.

Future research on the complete biochemical and biophysical characterization of 5'-nucleotidases may shed more light on these fascinating enzymes that clearly possess functions beyond the regulation of nucleotide metabolism.

## Acknowledgments

This study was supported by grants from the Fundação de Amparo à Pesquisa do Estado de São Paulo (FAPESP, Process 01/07533-7). C.A.S. was the recipient of a Ph.D. fellowship from FAPESP (Process 08/55690-3). We gratefully acknowledge the Laboratório Nacional de Biociências (LNBio, Campinas, Brazil) for support with the spectroscopic studies. The authors declare no conflicts of interest.

## References

[1] Koerner JF. Enzymes of nucleic acid metabolism. Annual Review of Biochemistry. 1970;39:291-322.

[2] Reichard P. Interactions between deoxyribonucleotide and DNA synthesis. Annual Review of Biochemistry. 1988;57:349-74.

[3] Bogan KL, Brenner C. 5'-Nucleotidases and their new roles in NAD+ and phosphate metabolism. New Journal of Chemistry. 2010;34:845-53.

[4] Hunsucker SA, Mitchell BS, Spychala J. The 5'-nucleotidases as regulators of nucleotide and drug metabolism. Pharmacology & Therapeutics. 2005;107:1-30.

[5] Zimmermann H. 5'-Nucleotidase: molecular structure and functional aspects. Biochemical Journal. 1992;285:345-65.

[6] Kohn J, Reis JL. Bacterial nucleotidases. Journal of bacteriology. 1963;86:713-6.

[7] Bianchi V, Spychala J. Mammalian 5'-nucleotidases. Journal of Biological Chemistry. 2003;278:46195-8.

[8] Misumi Y, Ogata S, Ohkubo K, Hirose S, Ikehara Y. Primary structure of human placental 5′-nucleotidase and identification of the glycolipid anchor in the mature form. European Journal of Biochemistry. 1990;191:563-9.

[9] Oka J, Matsumoto A, Hosokawa Y, Inoue S. Molecular cloning of human cytosolic purine 5'-nucleotidase. Biochemical and Biophysical Research Communications. 1994;205:917-22.

[10] Sala-Newby GB, Skladanowski AC, Newby AC. The mechanism of adenosine formation in cells: Cloning of cytosolic 5'-nucleotidase. Journal of Biological Chemistry. 1999;274:17789-93.

[11] Amici A, Emanuelli M, Raffaelli N, Ruggieri S, Saccucci F, Magni G. Human erythrocyte pyrimidine 5'-nucleotidase, PN-I, is identical to p36, a protein associated to lupus inclusion formation in response to α-interferon. Blood. 2000;96:1596-8.

[12] Rampazzo C, Gallinaro L, Milanesi E, Frigimelica E, Reichard P, Bianchi V. A deoxyribonucleotidase in mitochondria: Involvement in regulation of dNTP pools and possible link to genetic disease. Proceedings of the National Academy of Sciences. 2000;97:8239-44.

[13] Rampazzo C, Johansson M, Gallinaro L, Ferraro P, Hellman U, Karlsson A, et al. Mammalian 5'(3')-deoxyribonucleotidase, cDNA cloning, and overexpression of the enzyme in *Escherichia coli* and mammalian cells. Journal of Biological Chemistry. 2000;275:5409-15.

[14] Sala-Newby GB, Newby AC. Cloning of a mouse cytosolic 5'-nucleotidase-I identifies a new gene related to human autoimmune infertility-related protein. Biochimica et Biophysica Acta (BBA) - Gene Structure and Expression. 2001;1521:12-8.

[15] Mansfield J, Genin S, Magori S, Citovsky V, Sriariyanum M, Ronald P, et al. Top 10 plant pathogenic bacteria in molecular plant pathology. Molecular Plant Pathology. 2012;13:614-29.

[16] Marques LLR, Ceri H, Manfio GP, Reid DM, Olson ME. Characterization of biofilm formation by *Xylella fastidiosa in vitro*. Plant Disease. 2002;86:633-8.

[17] Shevchenko A, Wilm M, Vorm O, Mann M. Mass spectrometric sequencing of proteins from silver-stained polyacrylamide gels. Analytical Chemistry. 1996;68:850-8.

[18] Whitmore L, Wallace BA. DICHROWEB, an online server for protein secondary structure analyses from circular dichroism spectroscopic data. Nucleic Acids Research. 2004;32:W668-W73.

[19] Schaad NW, Postnikova E, Lacy G, Fatmi MB, Chang C-J. *Xylella fastidiosa* subspecies: *X. fastidiosa* subsp [correction] *fastidiosa* [correction], subsp. nov., *X. fastidiosa* subsp. *multiplex* subsp. nov., and *X. fastidiosa* subsp. *pauca* subsp. nov. Systematic and Applied Microbiology. 2004;27:290-300.

[20] de Souza AA, Takita MA, Coletta-Filho HcD, Caldana C, Yanai GM, Muto NH, et al. Gene expression profile of the plant pathogen *Xylella fastidiosa* during biofilm formation *in vitro*. FEMS Microbiology Letters. 2004;237:341-53.

[21] Santos CA, Toledo MAS, Trivella DBB, Beloti LL, Schneider DRS, Saraiva AM, et al. Functional and structural studies of the disulfide isomerase DsbC from the plant pathogen *Xylella fastidiosa* reveals a redox-dependent oligomeric modulation *in vitro*. FEBS Journal. 2012;279:3828-43.

[22] Simpson AJ, Reinach FC, Arruda P, Abreu FA, Acencio M, Alvarenga R, et al. The genome sequence of the plant pathogen *Xylella fastidiosa*. Nature. 2000;406:151-9.

[23] Thammavongsa V, Kern JW, Missiakas DM, Schneewind O. *Staphylococcus aureus* synthesizes adenosine to escape host immune responses. Journal of Experimental Medicine. 2009;206:2417-27

[24] Fan J, Zhang Y, Chuang-Smith ON, Frank KL, Guenther BD, Kern M, et al. Ecto-5′-nucleotidase: A candidate virulence factor in *Streptococcus sanguinis* experimental endocarditis. PLoS ONE. 2012;7:e38059.

[25] Zagursky RJ, Ooi P, Jones KF, Fiske MJ, Smith RP, Green BA. Identification of a *Haemophilus influenzae* 5′-nucleotidase protein: cloning of the *nucA* gene and immunogenicity and characterization of the NucA protein. Infection and Immunity. 2000;68:2525-34.

[26] Hunsucker SA, Spychala J, Mitchell BS. Human cytosolic 5'-nucleotidase I: characterization and role in nucleoside analog resistance. Journal of Biological Chemistry. 2001;276:10498-504.

[27] Traut TW. The functions and consensus motifs of nine types of peptide segments that form different types of nucleotide-binding sites. European Journal of Biochemistry. 1994;222:9-19.

[28] Buchan DWA, Ward SM, Lobley AE, Nugent TCO, Bryson K, Jones DT. Protein annotation and modelling servers at University College London. Nucleic Acids Research. 2010;38:W563-W8.

[29] Matthews JM, Sunde M. Dimers, oligomers, everywhere. In: Matthews JM, editor. Protein dimerization and oligomerization in biology: Springer New York; 2012. p. 1-18.

[30] Garvey EP, Lowen GT, Almond MR. Nucleotide and nucleoside analogues as inhibitors of cytosolic 5'-nucleotidase I from heart. Biochemistry. 1998;37:9043-51.

[31] Schembri MA, Kjærgaard K, Klemm P. Global gene expression in *Escherichia coli* biofilms. Molecular Microbiology. 2003;48:253-67.

[32] Yadav MK, Kwon SK, Cho CG, Park S-W, Chae S-W, Song J-J. Gene expression profile of early in vitro biofilms of *Streptococcus pneumoniae*. Microbiology and Immunology. 2012;56:621-9.

[33] Lazar V. Quorum sensing in biofilms - how to destroy the bacterial citadels or their cohesion/power? Anaerobe. 2011;17:280-5.

[34] Li Y-H, Tian X. Quorum sensing and bacterial social interactions in biofilms. Sensors. 2012;12:2519-38.

[35] Hammer BK, Bassler BL. Quorum sensing controls biofilm formation in *Vibrio cholerae*. Molecular Microbiology. 2003;50:101-4.

[36] Davies DG, Parsek MR, Pearson JP, Iglewski BH, Costerton JW, Greenberg EP. The involvement of cell-to-cell signals in the development of a bacterial biofilm. Science. 1998;280:295-8.

[37] Zhao Y, Qian G, Yin F, Fan J, Zhai Z, Liu C, et al. Proteomic analysis of the regulatory function of DSF-dependent quorum sensing in *Xanthomonas oryzae* pv. *oryzicola*. Microbial Pathogenesis. 2011;50:48-55.

[38] Dunne WM. Bacterial adhesion: Seen Any good biofilms lately? Clinical Microbiology Reviews. 2002;15:155-66.

# 4. CAPÍTULO 3

## 4.1 ARTIGO 1

**"A novel protein refolding protocol for the solubilization and purification of recombinant peptidoglycan-associated lipoprotein from *Xylella fastidiosa* overexpressed in *Escherichia coli*"**

**Autores**: Clelton A. Santos, Lilian L. Beloti, Marcelo A.S. Toledo, Aline Crucello, Marianna T.P. Favaro, Juliano S. Mendes, André S. Santiago, Adriano R. Azzoni, Anete P. Souza

**Publicado na Revista *Protein Expression and Purification***

**Volume 82 (2), páginas 284–289, Abril 2012**

Protein Expression and Purification 82 (2012) 284–289

Contents lists available at SciVerse ScienceDirect

Protein Expression and Purification

journal homepage: www.elsevier.com/locate/yprep

# A novel protein refolding protocol for the solubilization and purification of recombinant peptidoglycan-associated lipoprotein from *Xylella fastidiosa* overexpressed in *Escherichia coli*

Clelton A. Santos [a], Lilian L. Beloti [a], Marcelo A.S. Toledo [a], Aline Crucello [a], Marianna T.P. Favaro [a], Juliano S. Mendes [a], André S. Santiago [a], Adriano R. Azzoni [a,b], Anete P. Souza [a,c,*]

[a] Centro de Biologia Molecular e Engenharia Genética (CBMEG), Universidade Estadual de Campinas, Campinas, SP, Brazil
[b] Departamento de Engenharia Química, Escola Politécnica, Universidade de São Paulo, São Paulo, SP, Brazil
[c] Departamento de Biologia Vegetal, Instituto de Biologia (IB), Universidade Estadual de Campinas, Campinas, SP, Brazil

ARTICLE INFO

*Article history:*
Received 24 December 2011
and in revised form 17 January 2012
Available online 28 January 2012

*Keywords:*
Protein refolding
Pal
Outer membrane protein
Peptidoglycan
*Xylella fastidiosa*

ABSTRACT

*Xylella fastidiosa* is a Gram-negative xylem-limited plant pathogenic bacterium responsible for several economically important crop diseases. Here, we present a novel and efficient protein refolding protocol for the solubilization and purification of recombinant *X. fastidiosa* peptidoglycan-associated lipoprotein (XfPal). Pal is an outer membrane protein that plays important roles in maintaining the integrity of the cell envelope and in bacterial pathogenicity. Because Pal has a highly hydrophobic N-terminal domain, the heterologous expression studies necessary for structural and functional protein characterization are laborious once the recombinant protein is present in inclusion bodies. Our protocol based on the denaturation of the XfPal-enriched inclusion bodies with 8 M urea followed by buffer-exchange steps via dialysis proved effective for the solubilization and subsequent purification of XfPal, allowing us to obtain a large amount of relatively pure and folded protein. In addition, XfPal was biochemically and functionally characterized. The method for purification reported herein is valuable for further research on the three-dimensional structure and function of Pal and other outer membrane proteins and can contribute to a better understanding of the role of these proteins in bacterial pathogenicity, especially with regard to the plant pathogen *X. fastidiosa*.



## Introduction

The peptidoglycan-associated lipoprotein (Pal[1]) is an outer membrane (OM) protein found in Gram-negative bacteria [1,2]. It is anchored to the OM by an N-terminal lipid moiety and interacts strongly with the peptidoglycan layer through its C-terminal region [3], playing an important role in maintaining the integrity of the cell envelope [3,4].

Several studies indicate a significant role for Pal in the survival and pathogenesis of certain bacteria, including *Escherichia coli* [5,6], *Aggregatibacter actinomycetemcomitans* [7], *Haemophilus ducreyi* [8], *Erwinia chrysanthemi* [9], *Vibrio cholerae* [10], and *Caulobacter crescentus* [11]; however, its role in virulence is poorly understood. In addition to its structural functions, Pal is highly immunogenic and is considered a perfect antigen for the production of vaccines [12,13].

Pal is a component of the Tol–Pal system [1] and interacts with several factors involved in this system, including TolB and TolA, and with cell envelope proteins, such as OmpA (outer membrane protein A) and Lpp (lipoprotein) [1,14–16]. However, due to the fact that Pal has a highly hydrophobic N-terminal domain and is incorporated into inclusion bodies, the heterologous expression studies necessary for structural and functional protein characterization are challenging. The principal protocol that is widely used for the solubilization and purification of native bacterial Pal is based on the protocol described for the purification of Pal from *Haemophilus influenzae* (HiPal), also known as P6 [17]. However, this protocol employs several steps involving ultracentrifugation, the use of anionic detergents, and heat treatment with a final low yield of purified protein (approximately 0.5 mg per liter of bacterial culture [18]), which hinders the characterization of this protein.

In the present work, we developed a novel and efficient protocol for the solubilization and purification of recombinant Pal from

* Corresponding author at: Centro de Biologia Molecular e Engenharia Genética (CBMEG), Universidade Estadual de Campinas, CP 6010, 13083-875 Campinas, SP, Brazil. Fax: +55 19 3521 1089.
*E-mail address:* anete@unicamp.br (A.P. Souza).

[1] *Abbreviations used:* Pal, peptidoglycan-associated lipoprotein; OM, outer membrane; OmpA, outer membrane protein A; Lpp, lipoprotein; HiPal, Pal from *Haemophilus influenzae*; XfPal, Pal from *Xylella fastidiosa*; PMSF, phenylmethanesulfonyl fluoride; CD, circular dichroism; SDS, sodium dodecyl sulfate.

1046-5928/$ - see front matter © 2012 Elsevier Inc. All rights reserved.
doi:10.1016/j.pep.2012.01.010

*Xylella fastidiosa* (XfPal) overexpressed in *E. coli*. *X. fastidiosa* is a Gram-negative xylem-limited plant pathogenic bacterium that is responsible for several economically important plant diseases, including citrus variegated chlorosis, phony peach disease, plum leaf scald, Pierce's disease of grapes, and leaf scorch of almond, coffee, elm, oak, oleander, pear and sycamore [19,20]. The protocol is based on the treatment of the XfPal-enriched inclusion bodies with 8 M urea followed by buffer-exchange steps via dialysis, a method that proved effective for the solubilization and subsequent purification of XfPal. We achieved a relatively pure protein yield of greater than 17 mg per liter of bacterial culture. In addition, XfPal was biochemically and functionally characterized. The goals of our work are to encourage new studies focused on the structure and function of this protein to provide further information about of the relationship between Pal and bacterial pathogenesis.

## Materials and methods

### Materials

The *E. coli* DH5-α strain was used as the host strain for cloning, and the *E. coli* BL21 (DE3) strain (Novagen; USA) was the host strain for the heterologous protein expression. The *E. coli* JW0731 strain [21] was used for the peptidoglycan extraction. The oligonucleotides primers were synthesized by Sinapse Technologies (Brazil). The pET29a(+) expression vector was obtained from Novagen (USA). The *Nde*I and *Xho*I restriction enzymes were purchased from New England Biolabs (UK). The protease inhibitor phenylmethanesulfonyl fluoride (PMSF) and lysozyme were obtained from Sigma Chemical (USA). The urea reagent used for protein refolding was acquired from GE Healthcare (Sweden). The Ni–NTA affinity resin was obtained from Qiagen (Germany). The molecular mass marker (LMW and HMW) and the Superdex 75 10/300 GL chromatography column were purchased from GE Healthcare (Sweden). The total protein concentration was determined using a micro BCA™ protein assay kit (Thermo Scientific; USA). All other chemicals used were of biochemical research grade.

### Alignment of XfPal with H. influenzae (HiPal)

The HiPal (GenBank accession number: AAX87436.1) and XfPal (GenBank accession number: AAF84702.1) precursor amino acid sequences were obtained from the NCBI databank (www.ncbi.nih.gov) and aligned using ClustalW2 (http://www.ebi.ac.uk/Tools/clustalw2/index.html). Further editing was performed using GENEDOC software [22].

### XfPal cloning and overexpression

The sequence of the mature XfPal protein was obtained from the *X. fastidiosa* comparative database (http://www.xylella.lncc.br/). The coding sequence of the *xfpal* gene (ORF *Xf*1624; 432 bp) was amplified by PCR from *X. fastidiosa* (9a5c strain) genomic DNA using the specific oligonucleotides Xf1624F (5′-CTAATCATATGGCACCAACTGTTTCTAC-3′) and Xf1624R (5′-AAACTCGAGCTTCGCTGTATAGACG-3′), which contained *Nde*I and *Xho*I restriction sites, respectively. The PCR amplification product was cloned into the pET29a(+) (Novagen; USA) expression vector, which added a C-terminal six-histidine tag to the coding sequence. The presence of base substitutions in the recombinant plasmid was assessed by DNA sequencing. XfPal was overexpressed in the *E. coli* BL21 (DE3) strain. The cells were grown at 37 °C with shaking at 300 rpm in 1 L of LB broth containing kanamycin (30 μg/mL) until an $OD_{600}$ of 0.6–0.8 was reached. The expression of the recombinant protein was induced by the addition of 5.6 mM lactose, followed by cultivation for 4 h at 37 °C and 300 rpm. The culture was harvested by centrifugation (3000*g* for 15 min at 4 °C), and the cell pellets (approximately 3 g wet weight) were resuspended in 50 mL of buffer A (50 mM Tris–HCl pH 8 and 300 mM NaCl) plus 1 mg/mL lysozyme and 1 mM PMSF and were incubated for 30 min on ice. The cells were disrupted by sonication, and the insoluble fraction was collected by centrifugation (27,000*g* for 40 min at 4 °C).

### Protein refolding and XfPal purification

The XfPal-enriched inclusion bodies obtained after XfPal overexpression were used in a protein refolding procedure. The first step of the protein refolding process consisted of washing the inclusion bodies. The inclusion bodies were resuspended in 20 mL of buffer A containing 1 M urea and sonicated four times for 50 s at 70% of the maximum power in an ultrasonic homogenizer 4710 (Cole-Parmer Instrument Co.; Chicago, IL, USA), followed by centrifugation (27,000*g* for 40 min at 4 °C). The inclusion body wash step was repeated three times. Subsequently, the material collected by centrifugation after the last washing step was resuspended in 10 mL of buffer A. The total washed inclusion bodies were divided into two 100 mL beakers and shaken on an orbital shaker at 30 rpm at room temperature. Each fraction of the washed inclusion bodies was denatured by adding a freshly prepared 8 M urea solution dropwise with the aid of a Pasteur pipette until a transparent and homogeneous solution was obtained (approximately 40 mL of 8 M urea was added to each beaker). The denatured protein samples were initially dialyzed at a 1:10 ratio against buffer A containing 10% v/v glycerol and 0.1 mM EDTA (refolding buffer) at 4 °C for 4 h. Afterward, another dialysis step was performed at a 1:100 ratio against the same buffer at 4 °C for 16 h. The solubilized protein sample was recovered by centrifugation (27,000*g* for 40 min at 4 °C). The XfPal protein purification was performed in a single gravity flow chromatography step using a column packed with 1 mL of Ni–NTA resin (Qiagen; Germany) equilibrated with buffer A. The purified XfPal protein was eluted using a three-step gradient of imidazole (100, 250 and 500 mM) in buffer A, each step containing 7 mL of the respective buffer. The purity of the protein samples was estimated by SDS–PAGE and staining with Coomassie brilliant blue R-250. The total protein concentration was determined using a micro BCA™ protein assay kit or by spectroscopy using a calculated molar absorption coefficient at 280 nm ($\varepsilon_{280}$) of 16,180 $M^{-1}$/cm for the purified protein sample.

### Circular dichroism measurements

Circular dichroism (CD) spectra of recombinant XfPal were collected using a Jasco J-810 Spectropolarimeter dichrograph (Japan Spectroscopic; Tokyo, Japan). The far-UV CD spectra were generated at 24 °C using the XfPal protein at a concentration of approximately 6 μM in 10 mM sodium phosphate buffer at pH 8. The assays were performed using a quartz cuvette with a path length of 1 mm, and 10 determinations within the range of 270–190 nm, at a rate of 50 nm/min, were recorded for each sample and averaged. The deconvolution and statistical analysis of the CD spectra were performed using the Dichroweb server [23].

### Analytical size-exclusion chromatography

For the analytical gel filtration experiments, approximately 1 mg protein samples were loaded into a Superdex 75 10/300 GL column. After equilibration of the column with buffer A, the protein sample was loaded at a flow rate of 0.5 mL/min. The Superdex column was calibrated using HMW and LMW calibration kits as standard molecular weight markers.

*In vitro XfPal-peptidoglycan associated assay*

The *E. coli* JW0731 strain, a *pal*-null mutant kindly provided by the National BioResource Project (NIG Japan), was used for the peptidoglycan preparation according to the protocol established by Leduc et al. [24] with minor modifications. Briefly, cells corresponding to 1 L of culture with an $OD_{600}$ of 0.8 were suspended in 10 mL of 9% w/v NaCl and then mixed with an equal volume of 8% w/v sodium dodecyl sulfate (SDS). The suspension was boiled for 30 min at 98 °C and, after standing at room temperature overnight, the sample was centrifuged (27,000*g* for 1 h at 25 °C). The pelleted material was resuspended in 1 mL of water, washed with five cycles of resuspension and recentrifugation in water, and then resuspended in 0.5 mL of 10 mM sodium phosphate buffer, pH 8.

For the *in vitro* XfPal-peptidoglycan binding assay [18], 4 μg of the purified XfPal or a control protein, which has no affinity for peptidoglycan were centrifuged (27,000*g* for 1 h at 25 °C), and then the samples were individually incubated with 50 μL of purified peptidoglycan (final volume, 100 μL) in 10 mM sodium phosphate buffer (pH 8) containing 150 mM NaCl for 1 h at room temperature. The mixture was then centrifuged (27,000*g* for 1 h at 25 °C). The supernatant was collected, and the pellet was washed in 100 μL of 10 mM sodium phosphate buffer (pH 8) containing 500 mM NaCl; the wash fraction was collected after centrifugation (as above). The pellet was resuspended in 40 μL of Laemmli buffer. The supernatant (S), wash (W), and pellet (P) fractions were separated on 13.5% SDS–PAGE. After electrophoresis, the proteins were transferred to nitrocellulose membranes (Immobilon™-Nc; Sigma) using a Trans-Blot Semi-Dry Transfer Cell (Bio-Rad; USA) according to the manufacturer's instructions. Polyclonal antibodies against XfPal (or against the control protein) were produced by Rheabiotech (Campinas, Brazil) and used in the XfPal-peptidoglycan associated assay. The detection of XfPal (or the control protein) was performed using a 1:8000 dilution of anti-XfPal (or anti-control protein) and a 1:8000 dilution of anti-rabbit IgG with conjugated alkaline phosphatase (Santa Cruz Biotechnology Inc.; USA). The membranes were developed using the NBT/BCIP chromogenic substrates (Promega; USA).

## Results and discussion

*Alignment of XfPal with HiPal*

The alignment of the XfPal and HiPal precursor amino acid sequences showed that XfPal is 33 amino acid residues longer than HiPal (Fig. 1). XfPal and HiPal exhibited a high degree of conservation, with approximately 41% identity. A signal sequence typical of lipoprotein precursors, which includes the LVACS motif [1] cleaved by signal peptidase II during the translocation through the cytoplasmic membrane, is present in both sequences. Following the LVACS motif, XfPal contains 17 amino acid residues that are not found in the HiPal precursor sequence. However, the mature XfPal was annotated in the *X. fastidiosa* 9a5c strain genome database as starting with a methionine residue that is 12 amino acid residues at the C-terminal of the LVACS motif. The N-terminal

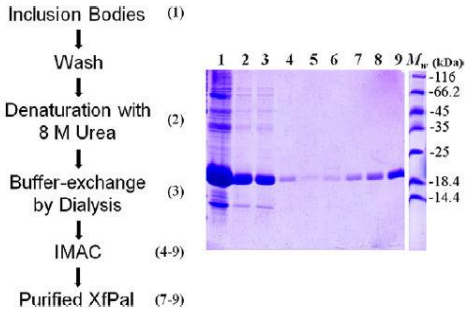


**Fig. 2.** Steps of the protein refolding protocol and XfPal purification. For details on the refolding protocol, see the 'Materials and methods' section. The numbers inside the parentheses show the protein samples used for the 13.5% SDS–PAGE. XfPal purification was performed using immobilized metal ion affinity chromatography (IMAC). The purified XfPal was eluted with seven column volumes of buffer A containing 100, 250 and 500 mM imidazole. Molecular mass markers ($M_w$) are indicated on the right. The predicted weight of recombinant XfPal is 16.8 kDa.

hydrophobic amino acid residues described as being responsible for anchoring the outer membrane-like protein in the membrane [1,2,15,16] are present in the structure of the mature XfPal. In addition, a high degree of conservation in the C-terminal region, which is responsible for Pal-peptidoglycan binding [1,3], was observed.

*XfPal overexpression and protein refolding*

The DNA sequence encoding the mature XfPal was successfully cloned into the pET29a(+) vector. DNA sequencing confirmed that there was no alteration or base substitution in the sequence of the positive clone used for the protein overexpression.

In contrast to other studies in which only the soluble periplasmic domain of Pal was used for heterologous expression [25,26], in this study, we also included the N-terminal hydrophobic domain of XfPal in the expressed protein. Being incorporated into the inclusion bodies, XfPal was found almost entirely in the insoluble fraction. Although, some studies show the solubilization of Pal with the use of detergents such as SDS, Triton X-100 and deoxycholate (DOC) [24,27], these detergents were not effective for the solubilization of XfPal. Thus, we developed a new and efficient protein refolding protocol for XfPal solubilization (Fig. 2). This protocol, which consisted of an initial step of washing of the XfPal-rich inclusion bodies with 1 M urea followed by denaturation with 8 M urea (according to a described methodology), allowed the recovery of approximately 17 mg of purified XfPal per liter of bacterial culture. Two steps appear to be crucial for the high efficiency of the protein refolding protocol developed: (1) the denaturation of the inclusion bodies with 8 M urea and (2) the protein renaturation, consisting of the dialysis steps for removing the urea.

We observed that when the urea solution was added rapidly to the inclusion bodies, the yield of purified protein was compromised; with quantities of less than 50% being recovered in comparison to

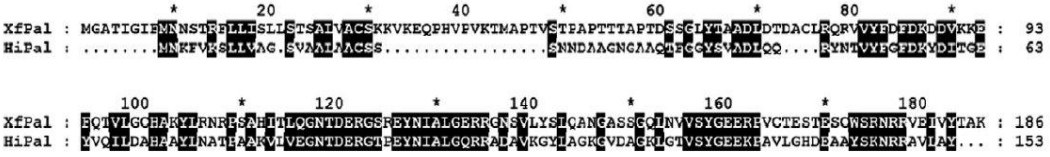


**Fig. 1.** ClustalW2 alignment of the amino acid precursor sequences of Pal proteins from *Xylella fastidiosa* 9a5c strain (XfPal) and *Haemophilus influenzae* (HiPal). XfPal and HiPal showed a high degree of conservation, with approximately 41% identity. The regions conserved in the two sequences are shown in black.

**Table 1**
Summary of the yields of the individual steps in the refolding and purification of recombinant XfPal from inclusion bodies produced per liter of bacterial culture.

| Step | Volume (mL) | Total protein[c] (mg/mL) | XfPal[d] (mg) | XfPal (%) | XfPal purity (%) |
|---|---|---|---|---|---|
| *Refolding*[a] | | | | | |
| Inclusion bodies, washed | 10 | 11.25 | – | 100 | 80 |
| Refolded protein | 85 | 1.47 | – | – | 85 |
| Soluble protein recovered | 70 | 1.46 | – | – | 90 |
| *Purification by IMAC*[b] | | | | | |
| Flow-through | 65 | 0.05 | 0 | 0 | – |
| Eluate | 20 | 0.87 | 17.9 | 22 | 98 |

[a] For details on the protein refolding procedure, see the 'Materials and methods' section.
[b] Immobilized metal ion affinity chromatography.
[c] Determined using a micro BCA™ protein assay kit.
[d] Determined spectrophotometrically using a calculated molar absorption coefficient at 280 nm ($\varepsilon_{280}$) of 16,180 $M^{-1}$/cm.

the amount obtained when urea was added dropwise. This fact seems to be related to the kinetics of protein denaturation performed by urea [28] in which the constant dripping allows better protein denaturation. Another critical step was the protein renaturation procedure. We found that glycerol was essential for the stabilization of the hydrophobic regions of XfPal. The dialysis steps in which this compound was added in quantities less than 10% in the refolding buffer also compromised the final yield of the protein.

It should be noted that despite the fact that mature XfPal contain four cysteine residues no reducing agents were added at any step of the refolding procedure. Some of these cysteine residues, especially the cysteines in the N-terminal region, can be modified with lipids [1], so that the intrinsic properties of the protein were not influenced. More details regarding the yield of XfPal protein refolding are presented in Table 1.

### *XfPal purification*

After protein solubilization, XfPal was purified by affinity chromatography, resulting in approximately 17 mg of purified XfPal per liter of bacterial culture (Table 1). The purified protein has a predicted mass of 16.8 kDa, corresponding to the 144-amino acid sequence encoded by ORF *Xf*1624 plus the C-terminal $His_6$-Tag added by the pET29a(+) vector. The purity of the protein was assessed by 13.5% SDS–PAGE (Fig. 2). An interesting feature of the purification step was that XfPal appeared on the stained SDS–PAGE gel with a mass exceeding 18 kDa, higher than predicted. This fact can be explained by the presence of covalently linked fatty acids or other components associated with the protein [29] or simply by the hydrophobic characteristics of XfPal as analysis by mass spectrometry confirmed the identity of the recombinant protein (data not shown).

### *Secondary structure and size-exclusion chromatography analysis*

The CD spectrum of purified XfPal showed that the refolded recombinant protein has secondary folding. The CD analysis yielded spectra characteristic of a protein containing a mixture of α-helix and β-sheet structures (Fig. 3). The prediction of the secondary structure for XfPal using the PSIPRED server [30] produced results similar to those obtained by the deconvolution of the experimental data obtained by CD, which indicated approximately 30% α-helices and 15% β-sheets. These results are in accordance with known elements of secondary structure for XfPal homologs [26].

The oligomeric state of purified XfPal was analyzed using size-exclusion chromatography (Fig. 4). Previous studies have shown that Pal can be found in two distinct forms in the cell envelope: bound to peptidoglycan or complexed with TolB [18]. A monomer is often observed for both forms. Samples of refolded XfPal were eluted in two peaks during gel filtration chromatography assays

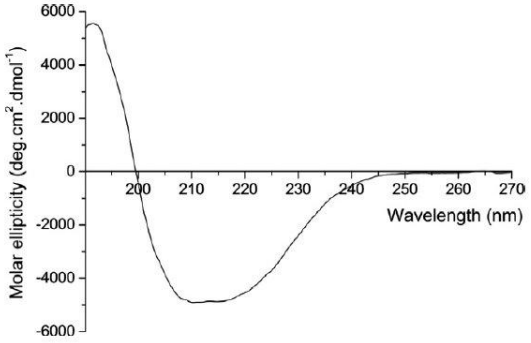


**Fig. 3.** Circular dichroism spectrum obtained for purified XfPal. The deconvolution of the experimental data obtained with the Dichroweb server shows the presence of approximately 30% α-helices and 15% β-sheets, results similar to those obtained using the PSIPRED server.

(Fig. 4A), one with a retention time that corresponds to an apparent molecular weight of 20.8 kDa for (peak 2, Fig. 4B) and the other with an elution profile typical of a larger oligomer (peak 1). This pattern, which shows the presence of protein aggregates, has been observed for other proteins during a refolding protocol [31]. However, using the protocol presented here, a large amount (approximately 67%) of the protein obtained was in the monomeric state, an indication of correct folding.

### *XfPal interacts in vitro with purified peptidoglycan*

We assessed the ability of the purified XfPal to interact *in vitro* with peptidoglycan. According to methodology described by Bouveret et al. [18] when purified peptidoglycan is incubated with soluble and purified Pal protein, they can interact *in vitro*. After the interaction assay, the protein and peptidoglycan are mostly observed in the insoluble fraction (pellet) and no protein is observed in the supernatant. Thus, the interaction is confirmed as the soluble protein is "dragged" into the pellet fraction by peptidoglycan. Following this protocol, our experiments show that purified XfPal was able to interact with peptidoglycan under the evaluated conditions, because the protein was no longer observed in the soluble fraction (S) after incubation with the peptidoglycan and was only detected in the pellet fraction containing the peptidoglycan (P) (Fig. 5A). We also used a control protein in this experiment, with no described affinity for peptidoglycan. In contrast to the results obtained by Bouveret et al. [18] in which the control protein was observed only in the soluble fraction (i.e., not interacting with

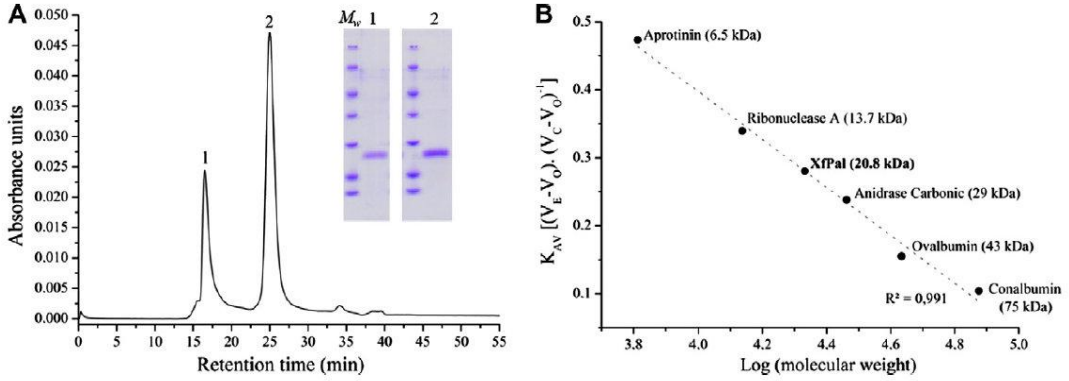


**Fig. 4.** Refolded XfPal size-exclusion chromatography analysis. (A) Gel filtration chromatogram of refolded XfPal shows the presence of the XfPal monomer (peak 2) and other oligomers (peak 1). Protein samples collected for each peak were analyzed by SDS–PAGE and are shown above on the chromatogram. (B) Calibration curve for purified XfPal. The expected molecular mass for recombinant XfPal is 16.8 kDa; the estimated molecular weight for XfPal is 20.8 kDa.

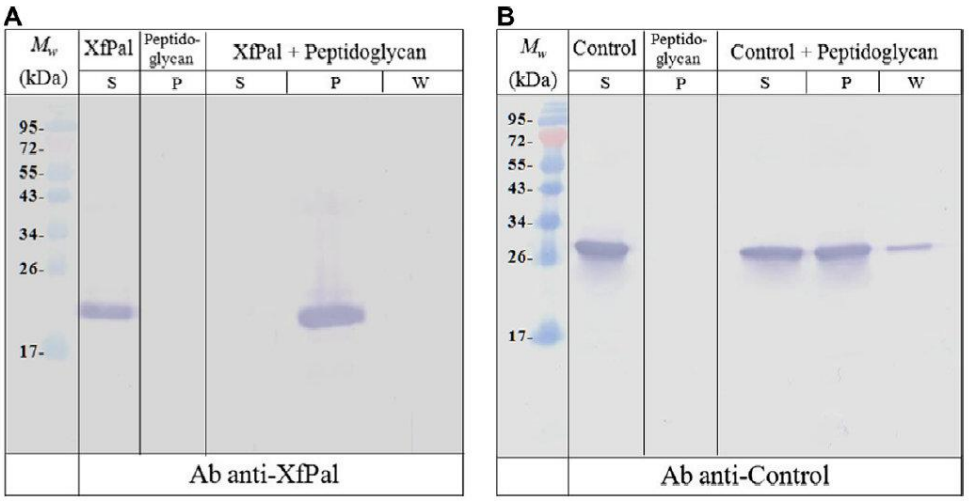


**Fig. 5.** *In vitro* XfPal-peptidoglycan association assay. Purified XfPal or control protein was incubated with peptidoglycan as described in the 'Materials and methods' section. After 1 h at room temperature, the samples were centrifuged, and the supernatant (S), wash (W) and pellet (P) fractions were resolved by 13.5% SDS–PAGE. After electrophoresis, the proteins were transferred to nitrocellulose membranes, and proteins were immunodetected using antibodies against XfPal or the control protein (Ab anti-XfPal or Ab anti-control). Molecular mass markers ($M_w$) are indicated on the left.

the peptidoglycan), we observed that the control protein used in the present work was observed in the soluble fraction (S), the pellet containing the peptidoglycan (P) and the wash fraction (W) (Fig. 5B). This result may be explained by the experimental conditions, as the control protein used in this work may have precipitated when incubated with the peptidoglycan. This fact was confirmed by the result of the wash fraction because the control protein was also detected. In addition, we must also consider the fact that non-specific interactions can occur, if the hydrophobic regions of the control protein interact with the peptidoglycan, which could lead to the observed results. However, we observed a markedly greater affinity of XfPal protein for the peptidoglycan (when compared to our control protein), because XfPal was completely absent from the soluble fraction and was only detected in the fraction containing peptidoglycan, even after the complex XfPal-peptidoglycan had been subjected to a wash step with 500 mM NaCl.

## Conclusion

In this work, we developed a new and efficient protein refolding protocol for the solubilization of recombinant XfPal, which enabled us to perform an initial characterization of this protein. XfPal was produced in a large quantity, with the presence of secondary structure and correct folding, and was able to interact *in vitro* with peptidoglycan. In addition, based on our results, we were able to confirm the prediction of ORF *Xf*1624 as a peptidoglycan-associated lipoprotein, as established in the *X. fastidiosa* genome database.

Bacterial outer membrane proteins, such as Pal, play an important role in pathogen-host interactions. Although the study of these proteins is limited because of the difficulties associated with protein separation and purification, such studies have been facilitated by improvement of existing techniques and development of new ones. It is, therefore, of great importance to both refine the

existing methods and develop new techniques that will allow the study of challenging proteins, particularly membrane proteins.

In this regard, the purification protocol reported here is valuable for further research on the three-dimensional structure and functions of Pal and can contribute to the better understanding of the role of this protein in bacterial pathogenicity, especially within the context of the plant pathogen *X. fastidiosa*.

## Acknowledgments

This study was supported by grants from the Fundação de Amparo à Pesquisa do Estado de São Paulo (FAPESP, Process 2001/07533-7). C.A.S. is recipient of a graduate fellowship from FAPESP (Process 2008/55690-3). L.L.B., M.A.S.T., A.C., and M.T.P.F. received graduate fellowships from FAPESP. A.P.S. is recipient of a research fellowship from the Conselho Nacional de Desenvolvimento Científico e Tecnológico (CNPq). We gratefully acknowledge the Laboratório de Espectroscopia e Calorimetria (LEC), Laboratório Nacional de Biociências – LNBio (Campinas, Brazil), for the support on the circular dichroism studies.

## References

[1] R. Godlewska, K. Wiśniewska, Z. Pietras, E.K. Jagusztyn-Krynicka, Peptidoglycan-associated lipoprotein (Pal) of Gram-negative bacteria: function, structure, role in pathogenesis and potential application in immunoprophylaxis, FEMS Microbiol. Lett. 298 (2009) 1–11.
[2] L.M. Parsons, F. Lin, J. Orban, Peptidoglycan recognition by Pal, an outer membrane lipoprotein, Biochemistry 45 (2006) 2122–2128.
[3] J.C. Lazzaroni, R. Portalier, The *excC* gene of *Escherichia coli* K-12 required for cell envelope integrity encodes the peptidoglycan-associated lipoprotein (PAL), Mol. Microbiol. 6 (1992) 735–742.
[4] E. Cascales, A. Bernadac, M. Gavioli, J.C. Lazzaroni, R. Lloubes, Pal lipoprotein of *Escherichia coli* plays a major role in outer membrane integrity, J. Bacteriol. 184 (2002) 754–759.
[5] J. Hellman, J.D. Roberts Jr., M.M. Tehan, J.E. Allaire, H.S. Warren, Bacterial peptidoglycan-associated lipoprotein is released into the bloodstream in gram-negative sepsis and causes inflammation and death in mice, J. Biol. Chem. 277 (2002) 14274–14280.
[6] M.D. Liang, A. Bagchi, H.S. Warren, M.M. Tehan, J.A. Trigilio, L.K. Beasley-Topliffe, B.L. Tesini, J.C. Lazzaroni, M.J. Fenton, J. Hellman, Bacterial peptidoglycan-associated lipoprotein: a naturally occurring toll-like receptor 2 agonist that is shed into serum and has synergy with lipopolysaccharide, J. Infect. Dis. 191 (2005) 939–948.
[7] R. Ihalin, M. Karched, K. Eneslatt, S. Asikainen, Characterization of immunoaffinity purified peptidoglycan-associated lipoprotein of *Actinobacillus actinomycetemcomitans*, J. Chromatogr. B Analyt. Technol. Biomed. Life Sci. 831 (2006) 116–125.
[8] K.R. Fortney, R.S. Young, M.E. Bauer, B.P. Katz, A.F. Hood, R.S. Munson Jr., S.M. Spinola, Expression of peptidoglycan-associated lipoprotein is required for virulence in the human model of *Haemophilus ducreyi* infection, Infect. Immun. 68 (2000) 6441–6448.
[9] J.F. Dubuisson, A. Vianney, N. Hugouvieux-Cotte-Pattat, J.C. Lazzaroni, Tol–Pal proteins are critical cell envelope components of *Erwinia chrysanthemi* affecting cell morphology and virulence, Microbiology 151 (2005) 3337–3347.
[10] A.J. Heilpern, M.K. Waldor, CTXphi infection of *Vibrio cholerae* requires the *tolQRA* gene products, J. Bacteriol. 182 (2000) 1739–1747.
[11] Y.C. Yeh, L.R. Comolli, K.H. Downing, L. Shapiro, H.H. McAdams, The *Caulobacter* Tol–Pal complex is essential for outer membrane integrity and the positioning of a polar localization factor, J. Bacteriol. 192 (2010) 4847–4858.
[12] M. McMahon, T.F. Murphy, J. Kyd, Y. Thanavala, Role of an immunodominant T cell epitope of the P6 protein of nontypeable *Haemophilus influenzae* in murine protective immunity, Vaccine 23 (2005) 3590–3596.
[13] T.F. Murphy, C. Kirkham, A.J. Lesse, Construction of a mutant and characterization of the role of the vaccine antigen P6 in outer membrane integrity of nontypeable *Haemophilus influenzae*, Infect. Immun. 74 (2006) 5169–5176.
[14] M.C. Ray, P. Germon, A. Vianney, R. Portalier, J.C. Lazzaroni, Identification by genetic suppression of *Escherichia coli* TolB residues important for TolB–Pal interaction, J. Bacteriol. 182 (2000) 821–824.
[15] E. Cascales, R. Lloubes, Deletion analyses of the peptidoglycan-associated lipoprotein Pal reveals three independent binding sequences including a TolA box, Mol. Microbiol. 51 (2004) 873–885.
[16] T. Clavel, P. Germon, A. Vianney, R. Portalier, J.C. Lazzaroni, TolB protein of *Escherichia coli* K-12 interacts with the outer membrane peptidoglycan-associated proteins Pal, Lpp and OmpA, Mol. Microbiol. 29 (1998) 359–367.
[17] G.W. Zlotnick, V.T. Sanfilippo, J.A. Mattler, D.H. Kirkley, R.A. Boykins, R.C. Seid Jr., Purification and characterization of a peptidoglycan-associated lipoprotein from *Haemophilus influenzae*, J. Biol. Chem. 263 (1988) 9790–9794.
[18] E. Bouveret, H. Bénédetti, A. Rigal, E. Loret, C. Lazdunski, *In vitro* characterization of peptidoglycan-associated lipoprotein (PAL)-peptidoglycan and PAL–TolB interactions, J. Bacteriol. 181 (1999) 6306–6311.
[19] C.J. Chang, M. Garnier, L. Zreik, V. Rossetti, J.M. Bové, Culture and serological detection of xylem-limited bacterium causing citrus variegated chlorosis and its identification as a strain of *Xylella fastidiosa*, Curr. Microbiol. 27 (1993) 137–142.
[20] S. Chatterjee, R.P. Almeida, S. Lindow, Living in two worlds: the plant and insect lifestyles of *Xylella fastidiosa*, Annu. Rev. Phytopathol. 46 (2008) 243–271.
[21] T. Baba, T. Ara, M. Hasegawa, Y. Takai, Y. Okumura, M. Baba, K.A. Datsenko, M. Tomita, B.L. Wanner, H. Mori, Construction of *Escherichia coli* K-12 in-frame, single-gene knockout mutants: the Keio collection, Mol. Syst. Biol. 2 (2006) 2006.0008.
[22] H.B. Nicholas, K.B. Jr. Nicholas, D.W. Deerfield, Genedoc: analysis and visualization of genetic variation, EMBnet.news 4 (1997) 1–4.
[23] L. Whitmore, B.A. Wallace, DICHROWEB, an online server for protein secondary structure analyses from circular dichroism spectroscopic data, Nucleic Acids Res. 32 (2004) W668–W673.
[24] M. Leduc, D. Joseleau-Petit, L.I. Rothfield, Interactions of membrane lipoproteins with the murein sacculus of *Escherichia coli* as shown by chemical cross-linking studies of intact cells, FEMS Microbiol. Lett. 51 (1989) 11–14.
[25] S.R. Loftus, D. Walker, M.J. Maté, D.A. Bonsor, R. James, G.R. Moore, C. Kleanthous, Competitive recruitment of the periplasmic translocation portal TolB by a natively disordered domain of colicin E9, Proc. Natl. Acad. Sci. USA 103 (2006) 12353–12358.
[26] D.A. Bonsor, I. Grishkovskaya, E.J. Dodson, C. Kleanthous, Molecular mimicry enables competitive recruitment by a natively disordered protein, J. Am. Chem. Soc. 129 (2007) 4800–4807.
[27] T. Mizuno, A novel peptidoglycan-associated lipoprotein found in the cell envelope of *Pseudomonas aeruginosa* and *Escherichia coli*, J. Biochem. 86 (1979) 991–1000.
[28] O.D. Monera, C.M. Kay, R.S. Hodges, Protein denaturation with guanidine hydrochloride or urea provides a different estimate of stability depending on the contributions of electrostatic interactions, Protein Sci. 3 (1994) 1984–1991.
[29] T. Mizuno, A novel peptidoglycan-associated lipoprotein (PAL) found in the outer membrane of *Proteus mirabilis* and other Gram-negative bacteria, J. Biochem. 89 (1981) 1039–1049.
[30] L.J. McGuffin, K. Bryson, D.T. Jones, The PSIPRED protein structure prediction server, Bioinformatics 16 (2000) 404–405.
[31] H. Lilie, E. Schwarz, R. Rudolph, Advances in refolding of proteins produced in *E. coli*, Curr. Opin. Biotechnol. 9 (1998) 497–501.

## 4.2 ARTIGO 2

# "Initial characterization of the trans-envelope TolB-Pal complex of the plant pathogen *Xylella fastidiosa*"

**Autores:** Clelton A. Santos, Marcelo A.S. Toledo, Richard Janissen, Lilian L. Beloti1, Aline Crucello, Maria A.C. Horta, André S. Santiago, Juliano S. Mendes, Monica A. Cotta, Alessandra A. Souza, Anete P. Souza

**Manuscrito em Preparação**

## Introdução

O sistema Tol-Pal é ubíquo em bactérias Gram-negativas, sendo organizado tipicamente na forma de dois *operons*: um contem os genes *tolQ*, *tolR* e *tolA* que codificam proteínas que se localizam na membrana interna, e o outro contem os genes *tolB* e *pal* (Sturgis, 2001). A proteína Pal (lipoproteína associada ao peptidoglicano), produto da expressão do gene *pal*, reside na interfase entre a membrana externa e interna e se associa fortemente a camada de peptidoglicano. TolB (proteína de translocação B), produto da expressão do gene *tolB*, atua no periplasma bacteriano e pode interagir com a proteína Pal (Bouveret et al. 1999).

A deleção de qualquer um dos genes *tol* leva a formação de vesículas na membrana externa, redução da quantidade de EPS da superfície celular, defeitos na divisão celular e aumento da sensibilidade a antibióticos e detergentes (Lazzaroni et al. 1999; Llamas et al. 2000; Vines et al. 2005). Desta forma, acredita-se que as proteínas do sistema Tol-Pal desempenhem grande papel na manutenção e integridade do envelope bacteriano.

Adicionalmente, os genes *tol* já foram descritos como estando envolvidos na patogenicidade de *Pseudomonas aeruginosa*, *Salmonella typhimurium* e *Vibrio cholerae* (Heilpern & Waldor, 2000; Whiteley et al. 2001; Tamayo et al. 2002; Cameron et al. 2008). Contudo, Gerding et al. (2007) propuseram que o sistema Tol-Pal faz parte da maquinaria de divisão celular de bactérias Gram-negativas, sendo requerido para a correta invaginação do envelope celular durante a constrição celular em *Escherichia coli.* Entretanto, o papel exato das proteínas codificas pelos operons *tol-pal* permanecem não completamente conhecido.

Neste trabalho, efetuou-se a caracterização inicial das proteínas *Xf*TolB e *Xf*Pal, pertencentes ao sistema Tol-Pal de *Xylella fastidiosa*. Utilizando-se ferramentas para a caracterização proteica, confirmou-se a interação *in vitro* entre *Xf*TolB e *Xf*Pal e avaliou-se o

perfil de expressão de ambas proteínas durante a formação e desenvolvimento do biofilme de *X. fastidiosa.* Em adição, utilizando imunofluorescência foi analisada a localização de *Xf*TolB e *Xf*Pal durante o crescimento de *X. fastidiosa*. Os resultados demonstram que *Xf*TolB e *Xf*Pal são importantes para a formação e desenvolvimento do biofilme bacteriano. Observou-se também que durante o crescimento de *X. fastidiosa,* as proteínas *Xf*TolB e *Xf*Pal parecem ocupar a mesma localização na célula, evidenciando uma possível interação *in vivo*.

## Material e Métodos

*Clonagem, expressão e purificação*

A clonagem, expressão e purificação de *Xf*Pal foi realizada como descrito por Santos et al. (2012a).

A sequência codificante do gene *XftolB* (ORF *Xf*1625; 1468 pb) foi amplificada por PCR a partir do DNA genômico de *X. fastidiosa* (linhagem 9a5c) utilizando os oligonucleótidos específicos *Xf*1625D (5'-CCAAACATATGACGAAATTTCCACGCTGG-3') e *Xf*1625R (5'-AAACTCGAGATGTACGCTCCGGTAAGGCCC-3'), contendo sítios de restrição para as enzimas *Nde*I e *Xho*I, respectivamente. O produto de amplificação por PCR foi clonado no vetor de expressão pET29a (+) (Novagen; EUA), que acrescenta, na região C-terminal da sequência codificante, uma cauda contendo seis resíduos de histidina. A presença de substituições de bases no plasmídeo recombinante foi avaliada por sequenciamento de DNA. *Xf*TolB foi super-expressa em *E. coli* BL21 (DE3). As células foram cultivadas a 37 °C com agitação a 300 rpm, em 1 L de LB contendo canamicina (30 µg/mL) até que a $DO_{600nm}$ de 0,6-0,8 foi alcançada. A expressão da proteína recombinante foi induzida pela adição de 5,6 mM de lactose, seguido por cultivo durante 16 h a 25 °C e 200 rpm. A cultura foi então centrifugada (3000 g, 15 min, 4 °C), e as

células foram ressuspendidas em 50 mL de tampão A (50 mM Tris-HCl pH 8 e NaCl 300 mM) contendo 1 mg/mL de lisozima e 2 mM PMSF. As células foram rompidas por sonicação e a fração solúvel foi recolhida por centrifugação (27000 g, 40 min, 4 °C). A purificação de *Xf*TolB foi realizada empregando cromatografia de afinidade ao níquel utilizando a resina Ni-NTA (Qiagen, Alemanha) equilibrada com tampão A. A proteína purificada foi eluída utilizando um gradiente de imidazol (0 a 500 mM) e a pureza das amostras foi estimada por SDS-PAGE.

**Dicroísmo circular**

Análises de dicroísmo circular (CD) foram realizadas utilizando um espectropolarímetro JASCO J-810 (Tokio, Japão). As cubetas de quartzo utilizadas possuíam caminho ótico de 0,1 mm e as medidas foram realizadas a 24 °C usando amostras de proteína a 4 µM em 10 mM tampão fosfato de sódio pH 8.0. A análise estatística e a deconvolução do espectro de CD obtido foram realizadas utilizando o servidor DICRHOWEB (Whitmore & Wallace, 2004).

**Cromatografia de exclusão molecular analítica**

A interação entre as proteínas recombinantes *Xf*TolB e *Xf*Pal foi avaliada *in vitro* utilizando cromatografia de exclusão molecular (SEC) empregando uma coluna Superdex 75 10/300 (GE Healthcare; Uppsala, Suécia), como descritor em Zhang et al. (2010). Amostras das proteínas purificadas foram misturadas em igual concentração (~50 µM) e incubadas por 15 h a 4 °C. Em seguida, amostras individuais e da mistura de *Xf*TolB e *Xf*Pal foram separadas na coluna utilizando um fluxo de 0,5 mL/min com o tampão A. As frações da eluição de cada corrida cromatográfica foram coletas e analisadas por SDS-PAGE.

**Análises de *western blot***

*X. fastidiosa* subsp. *pauca* 9a5c (Schaad et al. 2004) foi utilizada para a obtenção das diferentes fases de formação de biofilme bacteriano e células planctônicas utilizando um protocolo estabelecido por Souza et al. (2004). Os anticorpos policlonais anti-*Xf*TolB e anti-*Xf*Pal foram produzidos por Rheabiotech Ltda (São Paulo/SP, Brasil), e utilizados na imunodetecção de *Xf*TolB e *Xf*Pal durante o crescimento em biofilme e planctônico de *X. fastidiosa*. Para as análises de *western blot*, a quantidade total de proteínas de *X. fastidiosa* das diferentes fases do biofilme e das células planctônicas, foi extraída, normalizada e os resultados analisados como descrito por Santos et al. (2012b).

**Análises de imunofluorescência**

Para as análises de imunofluorescência, culturas de *X. fastidiosa* subsp. *pauca* 9a5c ($OD_{600\ nm}$ 0,1) foram inoculadas em lamínulas de vidros e incubadas estaticamente por 15 h a 28 °C. Para aumentar a eficiência de adsorção dos anticorpos ao material biológico, as lamínulas contendo as células foram tratadas com lisozima (5 mg/mL) durante 15 min. Para reduzir a adsorção inespecífica dos anticorpos utilizou-se 500 µL de BSA (2%)-PBS. A imunodetecção de *Xf*TolB e *Xf*Pal foi realizada utilizando-se anticorpos específicos para *Xf*TolB e para *Xf*Pal (RheaBiotech Ltda; São Paulo/ SP, Brasil). Após a incubação com os anticorpos específicos as lamínulas passaram por etapas de lavagem com PBS-Tween 20 (0,05%) e em seguida foram incubadas com o anticorpo IgG conjugado com Cy5 (Santa Cruz Biotechnology, EUA).

Para a detecção das proteínas alvo utilizando-se imunofluorescência as lamínulas preparadas, foram subsequentemente analisadas usando um microscópio de epi-fluorescência (Nikon TE2000U, EUA) com sistema interno de controle de temperatura EMCCD (Andor IXON3, 1024×1024 pixels, Irlanda). A excitação do Cy5-fluoróforo e a autofluorescência

bacteriana foram obtidas utilizando-se uma de lâmpada de Xenon (150 W) com conjuntos específicos de filtro (AHF; Tübingen, Alemanha). Para cada amostra, a autofluorescência das bactérias no comprimento de onda verde foi analisada seguida de medições no comprimento de onda vermelho para a localização do anticorpo conjugado com Cy5. Finalmente, as imagens obtidas foram sobrepostas e a localização das proteínas *Xf*TolB e *Xf*Pal na célula foi analisada.

## Resultados e Discussão

*Clonagem, expressão e purificação*

A proteína *Xf*Pal foi produzida em grande quantidades (aproximadamente 15 mg de proteína purificada por litro de cultura bacteriana) como descrita por Santos et al. (2012a). *Xf*TolB foi clonada, expressa e purificada neste trabalho. Análises de sequenciamento de DNA revelaram a ausência de substituições de bases na construção pET29:*XftolB* utilizada para os experimentos de expressão heteróloga. *Xf*TolB foi expressa e em seguida purificada utilizando cromatografia de afinidade ao níquel. Grande quantidade de proteína recombinante purificada foi obtida (aproximadamente 14 mg de proteína purificada por litro de cultura bacteriana). A Figura 4.1A, apresenta o gel de SDS-PAGE da purificação de *Xf*TolB.

Análises iniciais do conteúdo de estruturas secundárias da proteína recombinante purificada revelaram o predomínio de estruturas tipo folha β (Figura 4.1B). A deconvolução do espectro de CD obtido confirmaram a presença de 39% de folha β e 8% de α-hélice, resultados similares aos observados para TolB de *E. coli* (Carr et al. 2000). O conteúdo de estruturas secundárias de *Xf*Pal foi novamente avaliado e os resultados foram idênticos aos descritos anteriormente (Santos et al. 2012a).

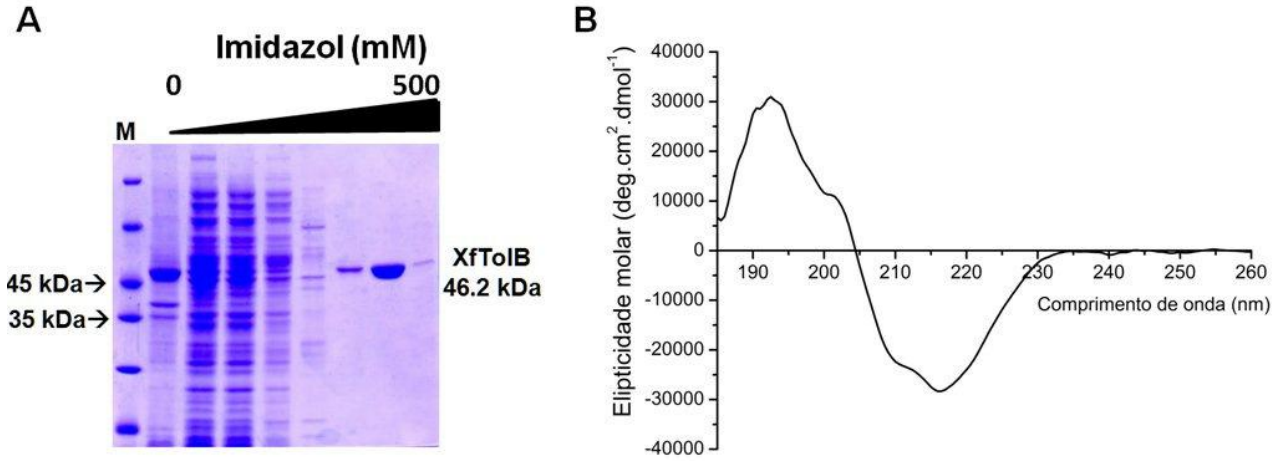


**Figura 4.1.** Purificação de *Xf*TolB. (A) SDS-PAGE (12 %) das frações da cromatografia de afinidade obtidas durante a eluição de *Xf*TolB. (B) Análises de CD de *Xf*TolB, revelando predominância de estruturas secundárias do tipo folha β.

*XfTolB e XfPal interagem in vitro*

Foi utilizada cromatografia de exclusão molecular para avaliar *in vitro* a interação entre *Xf*TolB e *Xf*Pal. Inicialmente, amostras individuais das proteínas *Xf*Pal e *Xf*TolB foram analisadas individualmente. O perfil cromatográfico de *Xf*Pal foi idêntico ao descrito por Santos et al. (2012a) (Figura 4.2). *Xf*TolB foi eluída como um único pico durante as análises de SEC (Figura 2), apresentando tempo de retenção que corresponde a massa molecular de 29 kDa. Este resultado é contrastante com a massa molecular estimada para o monômero de *Xf*TolB que é 46,2 kDa. Contudo, Zhang et al. (2010), descrevem resultados similares para a proteína tolB de *E. coli*. Assim uma explicação provável para tal fato reside nos aspectos estruturais da proteína TolB. O princípio da técnica de SEC é baseado no formato molecular das proteínas, sendo uma técnica desenvolvida principalmente para proteínas globulares, o que não é o caso da proteína TolB.

Após as análises individuais das proteínas *Xf*TolB e *Xf*Pal, foram avaliadas por SEC amostras nas quais ambas as proteínas haviam sido misturadas e incubadas por 15 h a 4 °C. Os resultados dessa análise revelarou que a mistura entre *Xf*TolB e *Xf*Pal apresentou um perfil cromatográfico diferente das amostras individuais, apresentando um pico de eluição adicional (Figura 4.2). Análises de SDS-PAGE mostraram que o pico adicional representava amostras das proteínas *Xf*TolB e *Xf*Pal, confirmando a interação *in vitro* de *Xf*TolB-*Xf*Pal. Além disso, nota-se o total desaparecimento dos picos correspondentes à proteína *Xf*Pal. É provável que a interação com *Xf*TolB estabilize *Xf*Pal e, devido a isto, houve o desaparecimento do pico correspondente à porção agregada de *Xf*Pal. Contudo, análises adicionais ainda são necessárias para investigar mais detalhes da interação entre *Xf*TolB e *Xf*Pal.

*Expressão durante a formação de biofilme e imunofluorescência*

Avaliou-se o perfil de expressão de *Xf*TolB e *Xf*Pal durante as diferentes fases de formação do biofilme e durante o crescimento planctônico de *X. fastidiosa*. Os resultados obtidos demonstram que tanto *Xf*TolB quanto *Xf*Pal são expressas diferencialmente durante as diferentes fases de formação do biofilme e, de acordo com o tipo de crescimento de *X. fastidiosa* (planctônico versus biofilme) (Figura 4.3). *Xf*Pal foi expressa em maiores quantidade que *Xf*TolB (Figura 4.3A; B). Tal observação é condizente com o fato da proteína Pal estar presente em quantidades bem maiores que *Xf*TolB no envelope celular bacteriano (Gerding et al. 2007). Análises estatísticas da razão entre a intensidade média e a área em *pixels* das bandas visualizadas nas membranas de nitrocelulose utilizadas nos experimentos de *western blot* revelaram diferenças estatísticas significantes ($P < 0.05$) no perfil de expressão de *Xf*TolB e *Xf*Pal (Figura 4.3C;D). Contudo, nota-se uma diferença acentuada nas fases iniciais (3-5 dias) de

formação do biofilme, além de se observar perfil de expressão correspondente entre *Xf*TolB e *Xf*Pal.

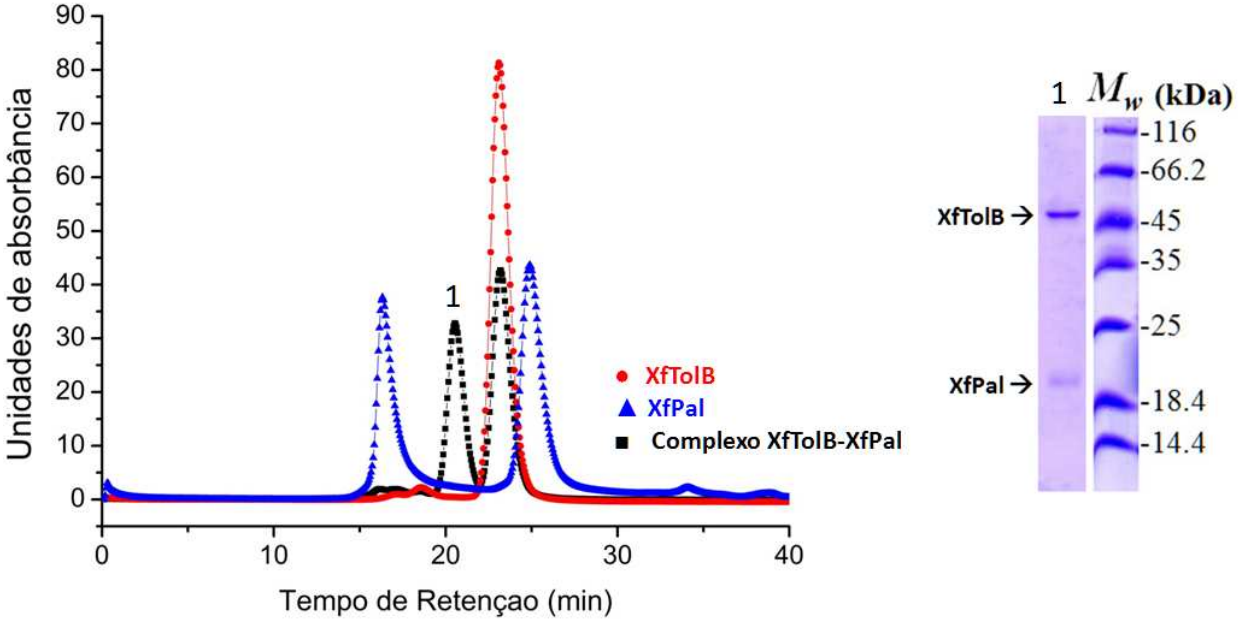


**Figura 4.2.** Cromatografia de exclusão molecular analítica. O perfil cromatográfico de *Xf*TolB, *Xf*Pal e do complexo *Xf*TolB-*Xf*Pal é mostrado, respectivamente, em vermelho, azul e preto. Em detalhe (lado direito) é apresentado o gel de SDS-PAGE (12%) da fração (1) correspondente a interação entre *Xf*TolB e *Xf*Pal.

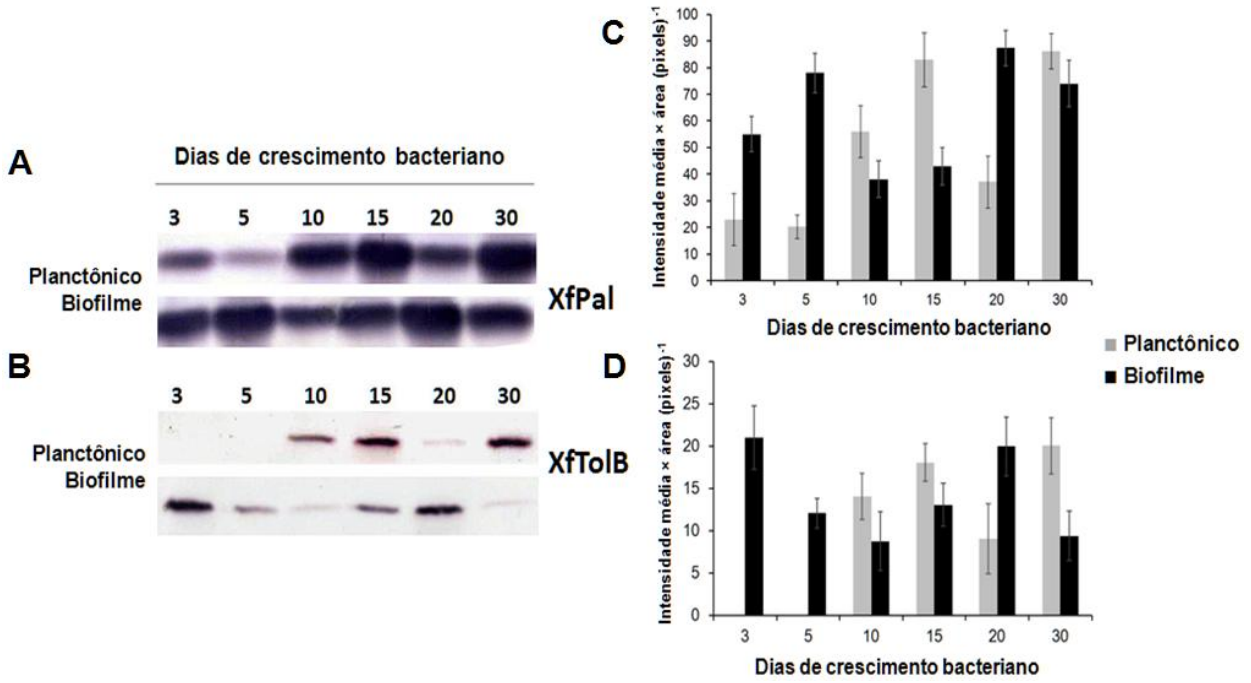


**Figura 4.3.** Detecção de *Xf*TolB e *Xf*Pal durante o crescimento planctônico e em biofilme de *X. fastidiosa*. (A) Análises de *western blot Xf*Pal; (B) Análises de *western blot* de *Xf*TolB; (C) Quantificação do nível de expressão de *Xf*Pal; (D) quantificação do nível de expressão de *Xf*TolB.

As proteínas TolB e Pal já foram descritas como estando envolvidas no processo de divisão celular, assim, caso *Xf*TolB e *Xf*Pal desempenhem o mesmo papel em *X. fastidiosa*, tais proteínas podem ser alvos importantes para a compreensão da regulação e desenvolvimento do biofilme formado por esta bactéria, requerendo estudos adicionais para investigar tais hipóteses. Neste sentido, avaliou-se também a localização de *Xf*TolB e *Xf*Pal utilizando-se técnicas de imunofluorescência. Os resultados preliminares desta análise, revelaram que *Xf*TolB e *Xf*Pal ora se localizam nas extremidades polares da célula, ora se concentram no centro da célula (Figura 4.4). O processo de divisão celular culmina com a formação de duas células filhas após o evento de fissão binária, propriamente dita, que ocorre no centro da célula parental, dando origem a

duas células filhas. Assim tais resultados evidenciam que: i) *Xf*TolB e *Xf*Pal parecem interagir *in vivo*; ii) Devido ao fato de, em determinados momentos do ciclo celular, ambas as proteínas serem observadas no centro da célula, supõe-se que elas possam estar envolvidas na maquinaria de divisão celular de *X. fastidiosa*. Apesar das evidências, ainda são necessárias novas análises de imunoflourescência, nas quais a taxa de crescimento bacteriana seja investigada mais criteriosamente, para que se possa confirmar o envolvimento de *Xf*TolB e *Xf*Pal no processo de divisão celular de *X. fastidiosa*.

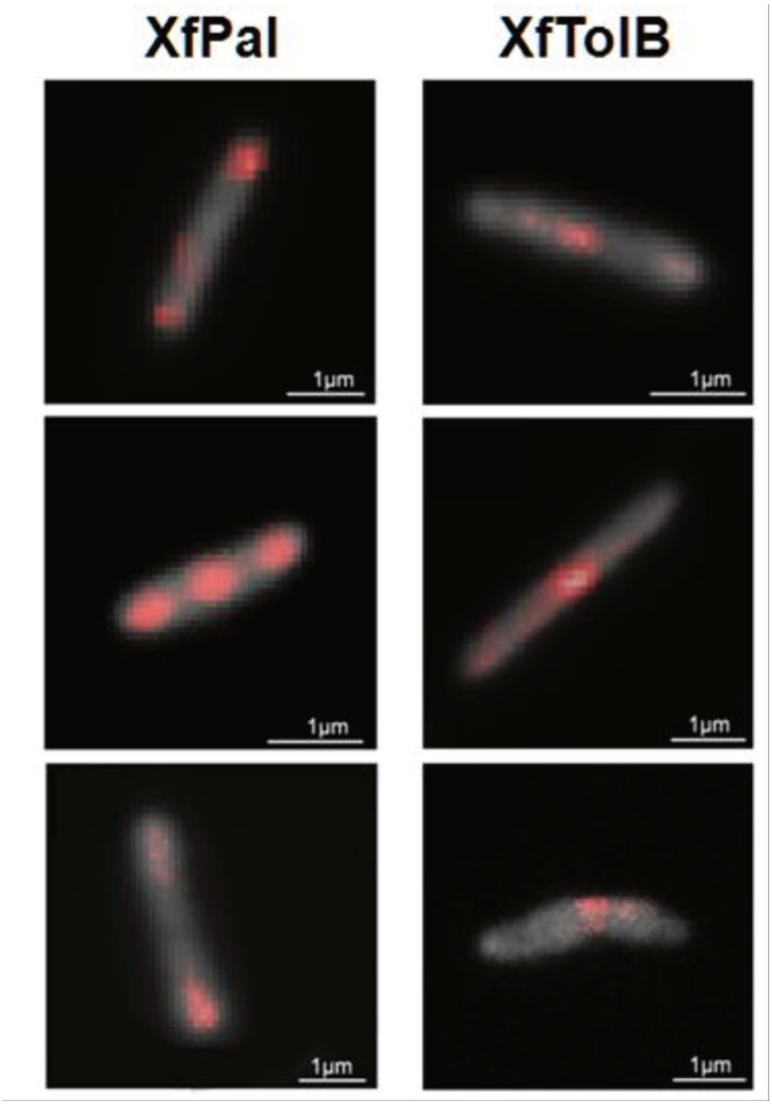


**Figura 4.4.** Imunolocalização de *Xf*Pal e *Xf*TolB (vermelho) durante o crescimento de *X. fastidiosa*.

## Referências

Bouveret E, Benedetti H, Rigal A, Loret E, Lazdunski C. *In vitro* characterization of peptidoglycan-associated lipoprotein (PAL)–peptidoglycan and PAL–TolB interactions. Journal of Bacteriology. 1999;181:6306-11.

Cameron DE, Urbach JM, Mekalanos JJ. A defined transposon mutant library and its use in identifying motility genes in *Vibrio cholerae*. Proceedings of the National Academy of Sciences 2008;105: 8736-41.

Carr S, Penfold CN, Bamford V, James R, Hemmings AM. The structure of TolB, an essential component of the *tol*-dependent translocation system, and its protein-protein interaction with the translocation domain of colicin E9. Structure. 2000;15:57-66.

Gerding MA, Ogata Y, Pecora ND, Niki H, de Boer PA. The trans-envelope Tol-Pal complex is part of the cell division machinery and required for proper outer-membrane invagination during cell constriction in *E. coli*. Molecular Microbiology. 2007;63:1008-25.

Heilpern AJ, Waldor MK CTXphi infection of *Vibrio cholerae* requires the *tolQRA* gene products. Journal of Bacteriology. 2000;182:1739-47.

Lazzaroni JC, Germon P, Ray MC, Vianney A. The Tol proteins of *Escherichia coli* and their involvement in the uptake of biomolecules and outer membrane stability. FEMS Microbiology Letters 1999;177:191-7.

Llamas MA, Ramos JL, Rodriguez-Herva JJ. Mutations in each of the *tol* genes of *Pseudomonas putida* reveal that they are critical for maintenance of outer membrane stability. Journal of Bacteriology. 2000;182: 4764-72.

Santos CA, Beloti LL, Toledo MAS, Crucello A, Favaro MTP, Mendes JS, et al. A novel protein refolding protocol for the solubilization and purification of recombinant peptidoglycan-associated lipoprotein from *Xylella fastidiosa* overexpressed in *Escherichia coli*. Protein Expression and Purification. 2012a; 82:284-9.

Santos CA, Toledo MAS, Trivella DBB, Beloti LL, Schneider DRS, Saraiva AM, et al. Functional and structural studies of the disulfide isomerase DsbC from the plant pathogen *Xylella fastidiosa* reveals a redox-dependent oligomeric modulation *in vitro*. FEBS Journal. 2012b;279:3828-43.

Schaad NW, Postnikova E, Lacy G, Fatmi MB, Chang C-J. *Xylella fastidiosa* subspecies: *X. fastidiosa* subsp [correction] *fastidiosa* [correction], subsp. nov., *X. fastidiosa* subsp. *multiplex* subsp. nov., and *X. fastidiosa* subsp. *pauca* subsp. nov. Systematic and Applied Microbiology. 2004;27:290-300.

Souza AA, Takita MA, Coletta-Filho HcD, Caldana C, Yanai GM, Muto NH, et al. Gene expression profile of the plant pathogen *Xylella fastidiosa* during biofilm formation *in vitro*. FEMS Microbiology Letters. 2004;237:341-53.

Sturgis JN. Organisation and evolution of the *tol-pal* gene cluster. Journal of Molecular Microbiology Biotechnology. 2001;3:113-22.

Tamayo R, Ryan SS, McCoy AJ, Gunn JS. Identification and genetic characterization of *PmrA*-regulated genes and genes involved in polymyxin B resistance in *Salmonella enterica* Serovar *typhimurium*. Infection and Immunity. 2002;70:6770-8.

Vines ED, Marolda CL, Balachandran A, Valvano MA. Defective O-antigen polymerization in *tolA* and *pal* mutants of *Escherichia coli* in response to extracytoplasmic stress. Journal of Bacteriology. 2005;187:3359-68.

Whiteley M, Gangera MG, Bumgarner RE, Parsek MR, Teitzel GM, Lory S, et al. Gene expression in *Pseudomonas aeruginosa* biofilms. Nature. 2001;413:860-4.

Whitmore L, Wallace BA. DICHROWEB, an online server for protein secondary structure analyses from circular dichroism spectroscopic data. Nucleic Acids Research. 2004;32:W668-73.

Zhang Y, Li C, Vankemmelbeke MN, Bardelang P, Paoli M, Penfold CN, James R.The crystal structure of the TolB box of colicin A in complex with TolB reveals important differences in the recruitment of the common TolB translocation portal used by group A colicins. Molecular Microbiology. 2010;75:623-36.

# 5. RESULTADOS COMPLEMENTARES

## 5.1. Caracterização estrutural das proteínas Alvo (SAXS – Cristalização)

Grandes esforços foram feitos para a caracterização estrutural das proteínas alvo deste projeto.

Com relação á cristalografia, quatro testes de *screening* inicial foram inicialmente realizados no Laboratório Automatizado de Cristalização de Proteínas (RobLab, LNBio, Campinas, SP), compreendendo amostras das proteínas *Xf*5´-Nt, *Xf*TolB e *Xf*DsbC na presença de 3 mM do agente redutor TCEP (tris-2-carboxietil fosfina) e *Xf*DsbC sem a presença do referido agente redutor.

Dentre as quatro amostras de proteínas ensaiadas para cristalização, foram observados sinais de cristais apenas para as amostras da proteína *Xf*TolB e *Xf*DsbC (tanto na presença quanto na ausência de TCEP). Testes de refinamento dos cristais da proteína chegaram a ser realizados para a proteina *Xf*DsbC no laboratório de Biologia Estrutural e Cristalografia do IQ/UNICAMP. Contudo, os padrões de difração coletados para tais cristais mostraram padrão de difração de sal ou outras moléculas muito pequenas, indicando que estes não eram cristais de proteína.

Ao contrário dos resultados obtidos com a cristalografia, os resultados da análise estrutural empregando espalhamento de raios-X a baixos ângulos (SAXS – *Small Angle X-ray Scattering*) conduziram a dados de alta qualidade, principalmente para a proteína *Xf*DsbC (Capítulo 1). Além da proteína *Xf*DsbC, as proteínas *Xf*Pal, *Xf*TolB e *Xf*5'-Nt também foram submetidas a coleta de SAXS. Os dados destas análises foram tratados de acordo com a metodologia descrita para a proteína *Xf*DsbC (Capítulo 1).

Para a proteína *Xf*5'-Nt os resultados de SAXS (Figura 5.1) evidenciaram que a região de Guinier (Figura 5.1B) encontra-se no limite de validade, sendo esta uma característica de um

grande oligômero ou uma amostra com tendências a agregação. Além disso, o Krakty plot evidenciou certo grau de desenovelamento (Figura 5.1C).

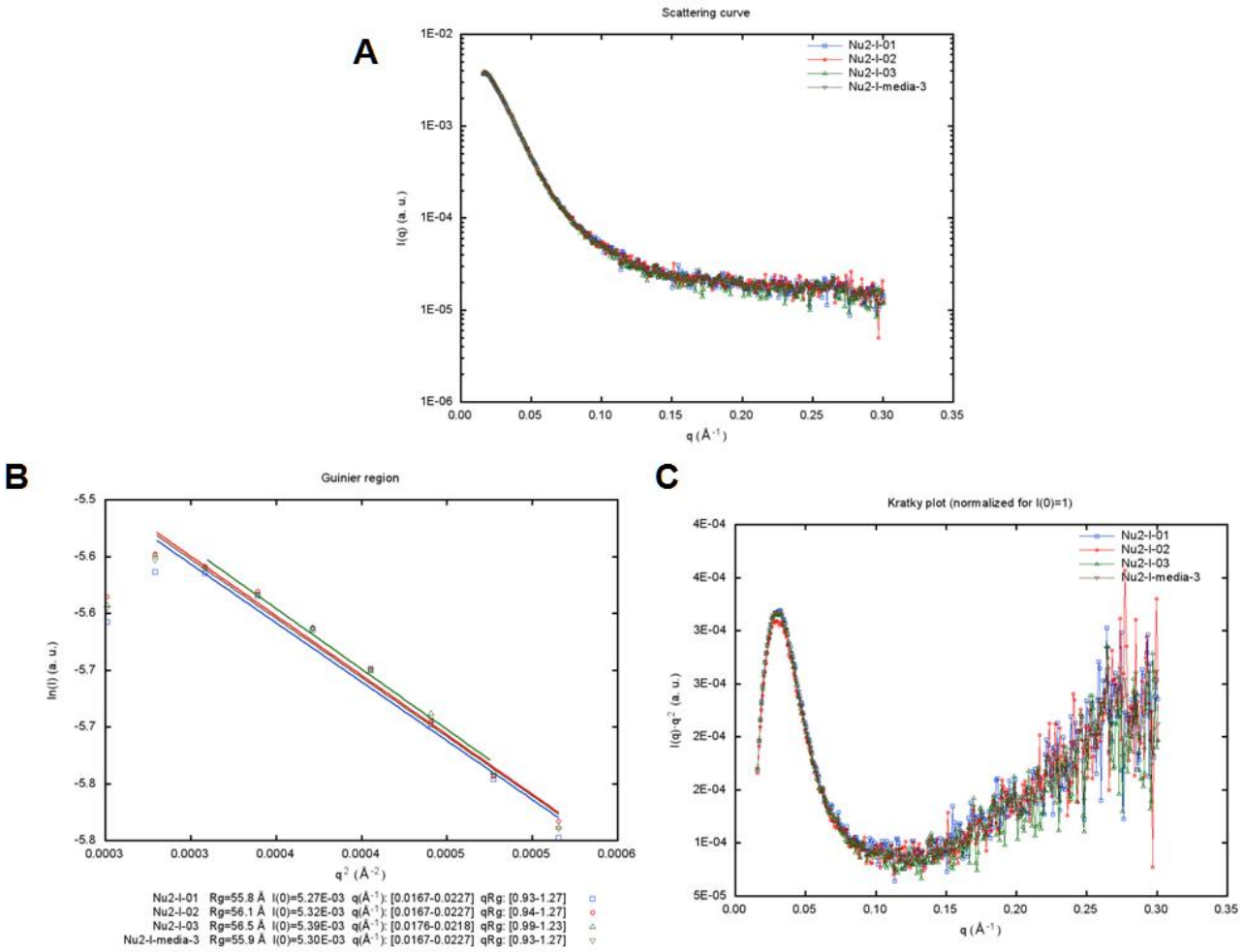


**Figura 5.1.** Análise por SAXS da proteína *Xf*5'-Nt. A) Curva de espalhamento; B) Região de Guinier; C) Kratky Plot.

Os resultados de SAXS obtidos para *Xf*5'-Nt, evidenciaram uma possível explicação para o resultado negativo observado no *screening* inicial de cristalização desta proteína. Nas condições avaliadas *Xf*5'-Nt se apresenta, em solução, com massa de centenas de kDa (tanto empregando um padrão quanto pelo método SAX MoW), desta forma a presença de oligômeros

inespecíficos poderia impedir a formação dos cristais. Para a proteína *Xf*5'-Nt como a *P*(r) não é confiável devido aos resultados obtidos, não há como prosseguir com confiabilidade como amostras desta proteína nas condições avaliadas.

Para a proteína *Xf*Pal (que foi obtida empregando um protocolo de re-enovelamento protéico descrito no Capítulo 3), o resultado de SAXS indicou, de maneira inequívoca a presença de agregados (Figura 5.2). Este resultado é típico para proteínas que passam por etapas de re-enovelamento proteico, o que inviabiliza análises pela referida técnica.

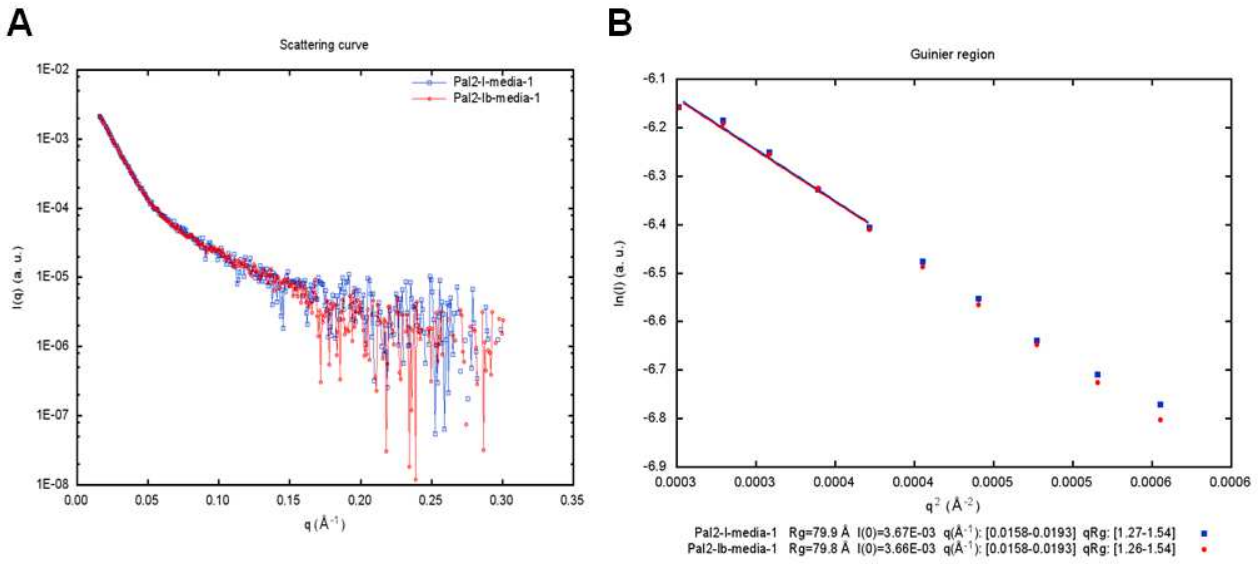


**Figura 5.2.** Análise por SAXS da proteína *Xf*Pal. A) Curva de espalhamento; B) Região de Guinier.

Para a proteína *Xf*TolB, duas condições foram avaliadas empregando SAXS: em uma destas condições a amostra de proteína foi anteriormente submetidas a separação por cromatografia de exclusão molecular (TolBGF), a outra amostra não foi submetida a esta etapa

adicional de separação. Curiosamente, os resultados obtidos para amostras de *Xf*TolB nestas duas condições foram diferentes. Para a amostra não submetida à etapa cromatográfica adicional, os resultados apontaram para uma estrutura prolata com $D_{max}$ de 133 Å e Rg de 43 Å, em acordo com o predito pela análise de Guinier (Figura 5.3). Contudo, para esta amostra foi observado uma mudança nítida no $I_0$ (Figura 5.3B) de acordo com a sequência de curvas, indicando uma possível alteração conformacional ao longo do tempo. Para a amostra de *Xf*TolB submetida a SEC os resultados apontaram para uma proteína prolata com $D_{max}$ de 91 Å e Rg 29 Å, coerente com o a análise de Guinier (Figura 5.3B ). Desta forma, a análise de amostras da mesma proteína avaliada em condições diferentes revelou resultados contrastantes, o que requer uma nova coleta de dados explorando condições experimentais adicionais, bem como novas informações sobre a estrutura de proteínas homólogas a *Xf*TolB para a interpretação dos dados.

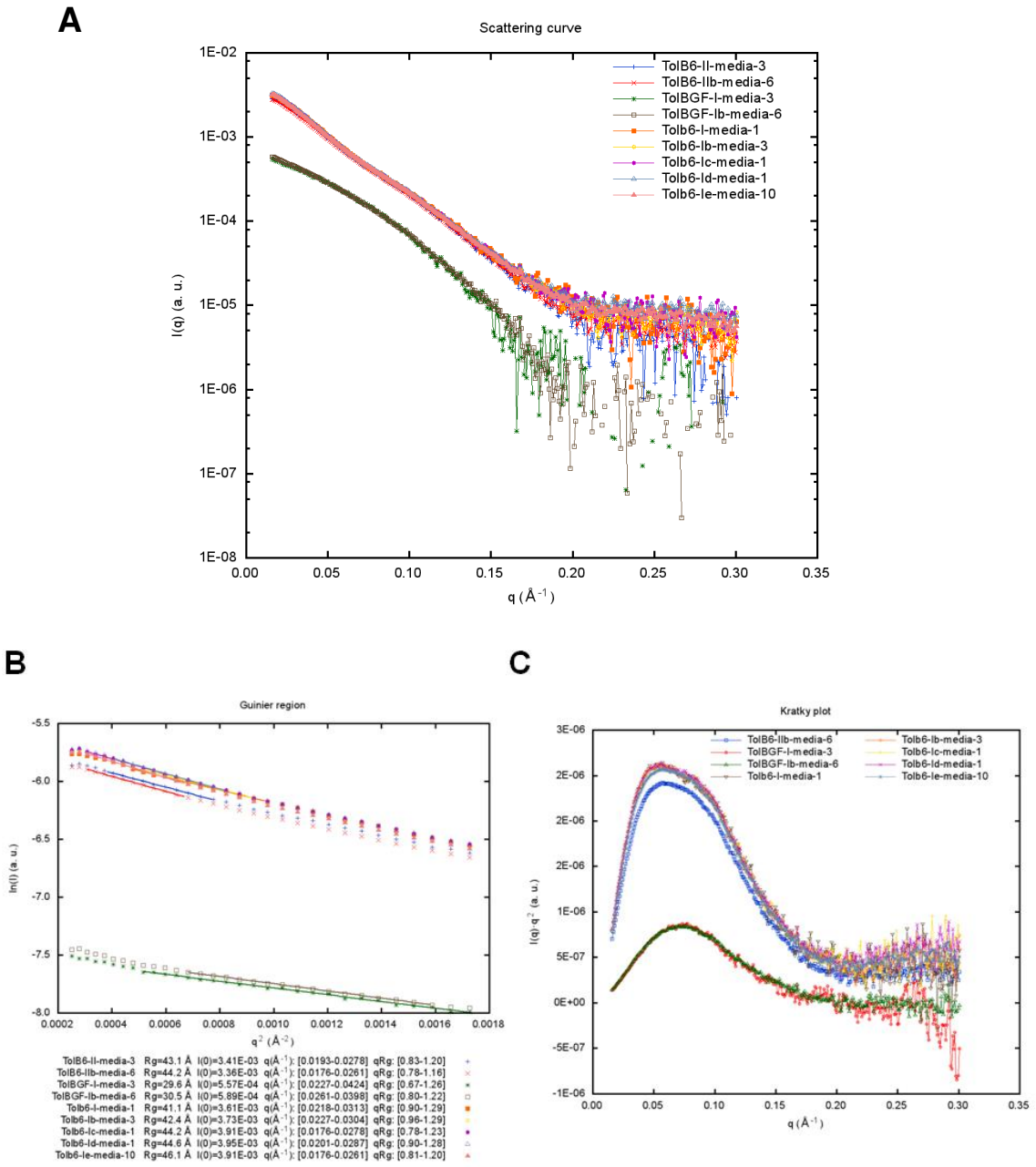


**Figura 5.3.** Análise por SAXS da proteína *Xf*TolB e *Xf*TolB-GF (amostra submetida a cromatografia de exclusão molecular). A) Curva de espalhamento; B) Região de Guinier; C) Kratky Plot.

# 6. CONCLUSÕES E PERSPECTIVAS

Estudos estruturais e funcionais de proteínas supostamente relacionadas à patogenicidade, adaptação e sobrevivência de um patógeno reúnem interessantes abordagens que podem permitir a melhor compreensão da biologia e genética deste organismo. Especialmente com relação à bactéria fitopatogênica *X. fastidiosa*, numerosas proteínas alvo associadas com patogenicidade foram anotadas durante a análise de seu genoma, entretanto, somente os estudos funcionais podem, de fato, esclarecer o envolvimento destas proteínas com a virulência e patogenicidade bacteriana.

Neste estudo, utilizando-se de ferramentas para a caracterização de proteínas, quatro proteínas alvos (*Xf*DsbC, *Xf*5'-Nt, *Xf*TolB e *Xf*Pal) foram escolhidas para análise. Resultados obtidos baseado-se em análises *in silico*, haviam associado estas quatro proteínas à patogenicidade, adaptação e sobrevivência.

Dentre os resultados obtidos ressalta-se:

i) *Xf*DsbC está envolvida na formação e desenvolvimento do biofilme de *X. fastidiosa* não tendo ela sido detectada durante o crescimento planctônico de *X. fastidiosa* nas condições avaliadas. Adicionalmente observou-se a super-expressão de *Xf*DsbC após a administração de um choque subletal com cobre, o que indica o envolvimento de tal proteína na resposta ao estresse oxidativo. Dados estruturais revelaram ainda que o estado oligomérico de *Xf*DsbC responde as condições redox do ambiente; *Xf*DsbC se apresentou como um dímero em condição reduzida e uma forma tetramérica foi observada em condição oxidante,

em solução. Assim a modulação redox dependente observada *in vitro* para *Xf*DsbC pode estar envolvida com o reconhecimento e especificidade de substrato, e este constitui um papel que ainda não havia sido descrito para proteínas homólogas de DsbC.

ii) Ensaios bioquímicos revelaram a atividade de fosfatase de *Xf*5'-Nt e evidenciaram a dependência de co-fatores (metais divalentes) para a completa atividade enzimática. *Xf*5'-Nt foi detectada durante a formação do biofilme de *X. fastidiosa*, especialmente durante a fases inicias de sua formação. Assim, é possível que a rede de desfosforilação/fosforilação catalisada pelas enzimas pertencentes a família das 5'-nucleotidases possa ter papel importante na formação do biofilme bacteriano, adicionando novos conhecimentos na área de metabolismo de nucleotídeos e patogenicidade bacteriana.

iii) A caracterização de *Xf*Pal e *Xf*TolB permitiu a associação destas proteínas com a formação do biofilme de *X. fastidiosa*. Inicialmente, um novo protocolo para a solubilização e purificação da lipoproteína *Xf*Pal de *X. fastidiosa* foi desenvolvido, permitindo a caracterização funcional de *Xf*Pal. Subsequentemente, demonstrou-se que a proteína recombinante *Xf*TolB pode interagir *in vitro* com *Xf*Pal. Além disso, utilizando-se de técnicas de imunofluorescência a localização de *Xf*TolB e *Xf*Pal foi analisada durante o crescimento de *X. fastidiosa*. Os resultados de tais análises, mostraram que *Xf*TolB e *Xf*Pal se acumulam ora nas extremidades polares da célula, ora no centro da célula, indicando que ambas

proteínas parecem interagir *in vivo* e podem estar relacionadas com o processo de divisão celular.

Apesar das dificuldades encontradas na caracterização estrutural, utilizando-se de ensaios funcionais foi possível confirmar o envolvimento das quatro proteínas alvos na formação e desenvolvimento do biofilme de *X. fastidiosa*, o qual é aceito como sendo o principal mecanismo de patogenicidade desta bactéria.

Ao final de tais análises, nota-se que além de conhecer as proteínas que compõem o biofilme bacteriano é necessário também determinar seus mecanismos de ação e regulação. Provavelmente, valendo-se desses conhecimentos será possível modular a formação desta estrutura (biofilme). Além disso, para a completa compreensão do papel de uma proteína alvo é necessário ainda associar os ensaios obtidos *in vitro* com as proteínas recombinantes, com estudos de campo *in vivo*, analisando a proteína selvagem durante o crescimento do patógeno.

Para a linhagem de *X. fastidiosa* 9a5c abordagens utilizando-se de mutantes com genes interrompidos ainda não são possíveis devido as limitações técnicas associadas a tais experimentos. Contudo, estudos focando na caracterização de proteínas recombinantes têm permitido a definição de alvos importantes para a patogenicidade de *X. fastidiosa* e poderão, em um futuro próximo, conduzir a novos e eficientes métodos de controle deste fitopatógeno.

## 7. REFERÊNCIAS

Almeida, R.P.P.; Nascimento, F.E.; Chau, J.; Prado, S.S.; Tsai, C-W.; Lopes, S.A.; Lopes, J.R.S. 2008. Genetic structure and biology of *Xylella fastidiosa* strains causing disease in citrus and coffee in Brazil. *Appl. Environ. Microbiol.* 74: 3690–3701.

Alves, E.; Leite, B.; Marucci, R.C.; Pascholati, S.F.; Lopes, J.R.S.; Andersen, P.C. 2008. Retention sites for *Xylella fastidiosa* in four sharpshooter vectors (Hemiptera: Cicadellidae) analyzed by scanning electron microscopy. *Curr. Microbiol.* 56: 531–538.

Azzoni, A.R.; Tada, S.F.S.; Rosselli, L.K.; Paula, D.P.; Catani, C.F.; Sabino, A.A.; Eberlin, M.N.; Barbosa, J.A.R.G.; Guimarães, B.G.; Medrano, F.J.; Souza, A.P. 2004. Expression and purification of a small heat shock protein from the plant pathogen *Xylella fastidiosa*. *Protein Expr. Purif.* 33: 297–303.

Berkmen, M.; Boyd, D.; Beckwith, J. 2005. The nonconsecutive disulfide bond of *Escherichia coli* phytase (AppA) renders it dependent on the protein-disulfide isomerase, DsbC. *J. Biol. Chem.* 280: 11387–11394.

Bessette, P.H.; Cotto, J.J.; Gilbert, H.F.; Georgiou, G. 1999. *In vivo* and *in vitro* function of the *Escherichia coli* periplasmic cysteine oxido reductase DsbG. *J Biol. Chem.* 274: 7784–7792.

Bonsor, D.A.; Mireille, O.H.; Sharma, V.A.; Krachler, A.M.; Housden, N.G.; Lilly, K.J.; James, R.; Moore, G.R.; Kleanthous, C. 2009 Allosteric β-propeller signalling in TolB and its manipulation by translocating colicin. *EMBO J.* 28: 2846–2857.

Cascales, E.; Bernadac, A.; Gavioli, M.; Lazzaroni, J.C.; Lloubes, R. 2002. Pal lipoprotein of *Escherichia coli* plays a major role in outer membrane integrity. *J. Bacteriol.* 184: 754–759.

Caserta, R.; Takita, M.A.; Targon, M.L.; Rosselli-Murai, L.K.; de Souza A.P.; Peroni, L.; Stach-Machado, D.R.; Andrade, A.; Labate, C.A.; Kitajima, E.W.; Machado, M.A.; de Souza, A.A. 2010**.** Expression of *Xylella fastidiosa* fimbrial and afimbrial proteins during biofilm formation. *Appl Environ. Microbiol.* 76: 4250–4259

Chang, C.J.; Garnier, M.; Zreik, L.; Rossetti, V.; Bové, J.M. 1993. Culture and serological detection of the xylem-limited bacterium causing citrus variegated chlorosis and its identification as a strain of *Xylella fastidiosa*. *Curr. Microbiol*. 27: 137–142.

Click, E.M.; Webster, R.E. 1997. Filamentous phage infection: required interactions with the TolA protein. *J. Bacteriol*. 179: 6464–6471.

Collmer, A. 1998. Determinants of pathogenicity and avirulence in plant pathogenic bacteria. *Curr. Opin. Plant. Biol.* 1: 329–335.

da Silva, A.C.R.; *et al*. 2002. Comparison of the genomes of two *Xanthomonas* pathogens with differing host specificities. *Nature.* 417: 459–463.

Dubuisson, J. F.; Vianney, A.; Lazzaroni, J. C. 2002. Mutational analysis of the TolA C-terminal domain of *Escherichia coli* and genetic evidence for an interaction between TolA and TolB. *J. Bacteriol.* 184: 4620–4625.

Gerding, M.A.; Ogata, Y.; Pecora,N.D.; Niki, H.; de Boer, P.A.J. 2007. The trans–envelope Tol–Pal complex is part of the cell division machinery and required for proper outer-membrane invagination during cell constriction in *E. coli*. *Mol. Microbiol.* 63: 1008–1025.

Hiniker, A.; Bardwell, J.C. 2004. *In vivo* substrate specificity of periplasmic disulfide oxidoreductases. *J Biol. Chem.* 279: 12967–12973.

Hiniker, A.; Collet, J.F.; Bardwell, J.C. 2005. Copper stress causes an *in vivo* requirement for the *Escherichia coli* disulfide isomerase DsbC. *J Biol. Chem.* 280: 33785–33791.

Hopkins, D.L. 1989. *Xylella fastidiosa*: a xylem-limited bacterial pathogen of plants. *Annu. Rev. Phytophatol.* 27: 271–290.

Kadokura, H.; Beckwith, J. 2010. Mechanisms of oxidative protein folding in the bacterial cell envelope. *Antioxid. Redox Signal.* 8: 1231–1246.

Kadokura, H.; Katzen, F.; Beckwith, J. 2003. Protein disulfide bond formation in prokaryotes. *Annu. Rev. Biochem.* 72: 111–135.

Kohn, J.; Reis, J.L. 1963. Bacterial nucleotidases. *J Bacteriol*. 86:713–716.

Lazzaroni, J.C.; Dubuisson, J.F.; Vianney, A. 2002. The Tol proteins of *Escherichia coli* and their involvement in the translocation of group A colicins. *Biochimie.* 84: 391–397.

Lee, R.F.; Derrick, K.S.; Beretta, M.J.G.; Chagas, C.M.; Rosetti, V. 1991. Citros variegated chlorosis: a new destructive disease of citrus in Brazil. *Citros Industry* Oct: 12–15.

Liu, X.; Wang, C.C. 2001. Disulfide-dependent folding and export of *Escherichia coli* DsbC. *J Biol. Chem.* 276: 1146–1151.

McCarthy, A.A.; Haebel, P.W.; Törrönen, A.; Rybin, V.; Baker, E.N.; Metcalf, P. 2000. Crystal structure of the protein disulfide bond isomerase, DsbC, from *Escherichia coli*. *Nat. Struct. Biol.* 7: 196–199.

Messens, J.; Collet, J.F.; Van Belle, K.; Brosens, E.; Loris, R.; Wyns, L. 2007. The oxidase DsbA folds a protein with a nonconsecutive disulfide. *J. Biol. Chem.* 282: 31302–31307.

Ponniah, K.; Loo, T.S.; Edwards, P.J.B.; Pascal, S.M.; Jameson, G.B.; Norris, G.E. 2010. The production of soluble and correctly folded recombinant bovine β-lactoglobulin variants A and B in *Escherichia coli* for NMR studies. *Protein Expres. Purif*. 70: 283–289.

Purcell, A.H.; Hopkins, D.L. 1996. Fastidious xylem-limited bacterial plant pathogens. *Annu. Rev. Phytopathol*. 34: 131–151.

Rietsch, A.; Bessette, P.; Georgiou, G.; Beckwith, J. 1997. Reduction of the periplasmic disulfide bond isomerase, DsbC, occurs by passage of electrons from cytoplasmic thioredoxin. *J Bacteriol.* 179: 6602–6608.

Roberto, S.R.; Coutinho, A.; De Lima, J.E.O.; Miranda, V.S.; Carlos, E.F. 1996. Transmissão de *Xylella fastidiosa* pelas cigarrinhas *Dilobopterus costalimai*, *Acrogonia terminalis* e *Oncometopia facialis* em citros. *Fitopatol. Bras.* 21: 517–518.

Rosselli, L.K.; Oliveira, C.L.P.; Azzoni, A.R.; Tada, S.F.S.; Catani, C.F.; Saraiva, A.M.; Soares, J.S.M.; Medrano, F.J.; Torriani, I.L.; Souza, A.P. 2006. A new member of the aldo-keto reductase family from the plant pathogen *Xylella fastidiosa*. *Arch. Biochem. Biophy.* 453: 143–150.

Rosselli-Murai, L.K.; Sforça, M.L.; Sassonia, R.C.; Azzoni, A.R.; Murai, M.J.; de Souza, A.P.; Zeri, A.C. 2012. Structural characterization of the H-NS protein from *Xylella fastidiosa* and its interaction with DNA. *Arch. Biochem. Biophys*. 526: 22–28.

Saraiva, A.M.; Reis, M.A.; Tada, S.F.; Rosselli-Murai, L.K.; Schneider, D.R.; Pelloso, A.C.; Toledo, M.A.; Giles, C.; Aparicio, R.; de Souza, A.P. 2009. Functional and small-angle X-ray scattering studies of a new stationary phase survival protein E (SurE) from *Xylella fastidiosa* – evidence of allosteric behaviour. *FEBS J.* 276: 6751–6762.

Sauer, K.; Camper, A. K.; Ehrlich, G. D.; Costerton, J. W.; Davies, D. G. 2002. *Pseudomonas aeruginosa* displays multiple phenotypes during development as a biofilm. *J. Bacteriol*. 184: 1140–1154.

Shouldice, S.R.; Cho, S-H.; Boyd, D.; Heras, B.; Eser, M.; Beckwith, J.; Riggs, P.; Martin, J.M.; Berkmen, M. 2010. *In vivo* oxidative protein folding can be facilitated by oxidation–reduction cycling. *Mol. Microbiol.* 75: 13–28.

Silva, M.S., De Souza, A.A., Takita, M.A., Labate, C.A., Machado, M.A. 2011. Analysis of the biofilm proteome of *Xylella fastidiosa*. *Proteome Sci*. 9: 58.

Simpson, A.J.G. *et al*. 2000. The genome sequence of the plant pathogen *Xylella fastidiosa. Nature.* 406: 151–157.

Souza, A.A.; Takita, M.A.; Coletta-Filho, H.D.; Caldana, C.; Yanai, G.M.; Muto, N.H.;Oliveira, R.C.; Nunes, L.R.; Machado, M.A. 2004. Gene expression profile of the plant pathogen *Xylella fastidiosa* during biofilm formation *in vitro*. *FEMS Microbiol Lett*. 237: 341-353.

Stoodley, P.; Sauer, K.; Davies, D. G.; Costerton, J. W. 2002. Biofilms as complex differentiated communities. *Annu. Rev. Microbiol*. 56:187–209.

Sturgis, J.N. 2001. Organisation and evolution of the *tol-pal* gene cluster. *J. Mol. Microbiol. Biotechnol.* 3: 113–122.

Toledo, M.A.S.; Schneider, D.R.; Azzoni, A.R.; Favaro, M.T.P.; Pelloso, A.C.; Santos, C.A.; Saraiva, A.M.; Souza, A.P. 2011. Characterization of an oxidative stress response regulator, homologous to *Escherichia coli* OxyR, from the phytopathogen *Xylella fastidiosa*. *Protein Expres. Purif*. 75: 204–210.

Travensolo, R.F.; Garcia, W.; Muniz, J.R.C.; Caruso, C.S.; Lemos, E.G.M.; Carrilho, E.; Araujo, A.P.U. 2008. Cloning, expression, purification and characterization of recombinant glutathione-S-transferase from *Xylella fastidiosa*. *Protein Expres. Purif*. 59: 153–160.

Vertommen, D.; Depuydt, M.; Pan, J.; Leverrier, P.; Knoops, L.; Szikora, J.P.; Messens, J.; Bardwell, J.C.; Collet, J.F. 2008. The disulphide isomerase DsbC cooperates with the oxidase DsbA in a DsbD-independent manner. *Mol Microbiol.* 67: 336–349.

Vianney, A.; Muller, M.M.; Clavel, T.; Lazzaroni, J.C.; Portalier, R.; Webster, R.E. 1996. Characterization of the *tol-pal* region of *Escherichia coli* K-12: translational control of *tolR* expression by TolQ and identification of a new open reading frame downstream of *pal* encoding a periplasmic protein. *J. Bacteriol,* 07: 4031–4038.

Vojnov, A.A.; do Amaral, A.M.; Dow, J.M.; Castagnaro, A.P.; Marano, M.R. 2010. Bacteria causing important diseases of citrus utilise distinct modes of pathogenesis to attack a common host. *Appl. Microbiol. Biotechnol*. 87: 467–477.

Walburger, A.; Claude Lazdunski, C.; Corda, Y. 2002. The Tol/Pal system function requires an interaction between the C-terminal domain of TolA and the N-terminal domain of TolB. *Mol. Microbiol.* 44: 695–708.

Webster, R. 1991. The *tol* gene products and the import of macromolecules into *E. coli*. *Mol. Microbiol*. 5: 1005–1011.

Wells, J.M.; Raju, B.C.; Hung, H.Y.; Weisberg, W.G.; Mandelco-Paul, L.; Brenner, D.J. 1987. *Xylella fastidiosa,* new-genus, new-species gram-negative, xylem-limited fastidious plant bacteria related to *Xanthomonas* spp. *Int. J. Syst. Bacteriol.* 37: 136–143.

## 8. ANEXO

# Small-angle X-ray scattering and *in silico* modeling approaches for the accurate functional annotation of an LysR-type transcriptional regulator

**Autores:** Marcelo A.S. Toledo, Clelton A. Santos, Juliano S. Mendes, Alexandre C. Pelloso, Lilian L. Beloti, Aline Crucello, Marianna T.P. Favaro, André S. Santiago, Dilaine R.S. Schneider, Antonio M. Saraiva, Dagmar R. Stach-Machado, Alessandra A. Souza, Daniela B.B. Trivella, Ricardo Aparicio, Ljubica Tasic, Adriano R. Azzoni, Anete P. Souza

**Publicado na Revista *Biochimica et Biophysica Acta (BBA) – Proteins and Proteomics***

**Volume 1834 (3), páginas 697-707, Março 2013**

Biochimica et Biophysica Acta 1834 (2013) 697–707

Contents lists available at SciVerse ScienceDirect

Biochimica et Biophysica Acta

journal homepage: www.elsevier.com/locate/bbapap

# Small-angle X-ray scattering and *in silico* modeling approaches for the accurate functional annotation of an LysR-type transcriptional regulator

M.A.S. Toledo [a,1], C.A. Santos [a,1], J.S. Mendes [a,1], A.C. Pelloso [a], L.L. Beloti [a], A. Crucello [a], M.T.P. Favaro [a], A.S. Santiago [a], D.R.S. Schneider [a], A.M. Saraiva [a,b], D.R. Stach-Machado [c], A.A. Souza [d], D.B.B. Trivella [e], R. Aparicio [e], L. Tasic [f], A.R. Azzoni [a,g], A.P. Souza [a,h,*]

[a] *Centro de Biologia Molecular e Engenharia Genética, Universidade Estadual de Campinas, Campinas, SP, Brazil*
[b] *Instituto Nacional de Metrologia, Qualidade e Tecnologia, Rio de Janeiro, Brazil*
[c] *Departamento de Imunologia — Instituto de Biologia — Univerisade Estadual de Campinas, Campinas, SP, Brazil*
[d] *Centro APTA Citros Sylvio Moreira/IAC, Rodovia Anhanguera Km 158, Cordeirópolis, SP, Brazil*
[e] *Laboratório de Biologia Estrutural e Cristalografia, Instituto de Química, Universidade Estadual de Campinas, Campinas, SP, Brazil*
[f] *Laboratório de Química Biológica, Instituto de Química, Universidade Estadual de Campinas, Campinas, SP, Brazil*
[g] *Departamento de Engenharia Química, Escola Politécnica, Universidade de São Paulo, São Paulo, SP, Brazil*
[h] *Instituto de Biologia, Universidade Estadual de Campinas, Departamento de Biologia Vegetal, Campinas, SP, Brazil*

ARTICLE INFO

*Article history:*
Received 23 June 2012
Received in revised form 24 December 2012
Accepted 26 December 2012
Available online 5 January 2013

*Keywords:*
LysR-like transcriptional regulator (LTTR)
Small-angle X-ray scattering (SAXS)
Benzoate
Muconate
Biofilm
Citrus variegated chlorosis (CVC)

ABSTRACT

*Xylella fastidiosa* is a xylem-limited, Gram-negative phytopathogen responsible for economically relevant crop diseases. Its genome was thus sequenced in an effort to characterize and understand its metabolism and pathogenic mechanisms. However, the assignment of the proper functions to the identified *open reading frames* (ORFs) of this pathogen was impaired due to a lack of sequence similarity in the databases. In the present work, we used small-angle X-ray scattering and *in silico* modeling approaches to characterize and assign a function to a predicted LysR-type transcriptional regulator in the *X. fastidiosa* (XfLysRL) genome. XfLysRL was predicted to be a homologue of BenM, which is a transcriptional regulator involved in the degradation pathway of aromatic compounds. Further functional assays confirmed the structural prediction because we observed that XfLysRL interacts with benzoate and *cis,cis*-muconic acid (also known as 2E,4E-hexa-2,4-dienedioic acid; hereafter named muconate), both of which are co-factors of BenM. In addition, we showed that the XfLysRL protein is differentially expressed during the different stages of *X. fastidiosa* biofilm formation and planktonic cell growth, which indicates that its expression responds to a cellular signal that is likely related to the aromatic compound degradation pathway. The assignment of the proper function to a protein is a key step toward understanding the cellular metabolic pathways and pathogenic mechanisms. In the context of *X. fastidiosa*, the characterization of the predicted ORFs may lead to a better understanding of the cellular pathways that are linked to its bacterial pathogenicity.



## 1. Introduction

*Xylella fastidiosa* is a xylem-limited, Gram-negative bacterium and the causal agent of many important crop diseases, including citrus variegated chlorosis (CVC), "phony peach" in peaches, and Pierce's disease in grapes [1–4]. Because of the economic impact of these diseases, the *X. fastidiosa* genome was sequenced [5], which allowed the identification of all of the basic genetic profiles for the survival of this bacterium, including the genes involved in metabolism, the synthesis of essential molecules (*e.g.*, amino acids, nucleotides and lipids), and mechanisms of transcription, translation and repair. However, because putative functions could be assigned to only 47% of the 2904 predicted coding regions, the functions of many *open reading frames* (ORFs) remain unknown [5–8]. Since the sequencing of the *X. fastidiosa* genome, more sophisticated experiments have been performed that have led to a better characterization and understanding of this phytopathogen and its pathogenic mechanisms [9–11]. Currently, the hypothesis for the pathogenicity of the bacterium involves the occlusion of the xylem vessels of the infected plants either through the secretion of exopolysaccharides to form biofilm structures or by mechanical occlusion, which leads to hydric stress and the appearance of disease symptoms, such as leaf marginal necrosis, leaf abscission, delayed growth, and reduced plant vigor and fruit development [12–15]. In addition, it has been reported that the gene

* Corresponding author at: Depto. de Biologia Vegetal, Universidade Estadual de Campinas, Caixa Postal 6010, CEP 13083-875, Campinas, São Paulo, Brazil. Tel.: +55 19 3521 1132.
*E-mail address:* anete@unicamp.br (A.P. Souza).
[1] These authors contributed equally to this work.

1570-9639/$ – see front matter © 2012 Published by Elsevier B.V.
http://dx.doi.org/10.1016/j.bbapap.2012.12.017

expression profile of planktonic *X. fastidiosa* cells is different from that of biofilm-forming cells. The differentially regulated ORFs are likely to be involved in the cell's ability to adhere to xylem vessels and form the biofilm structure that leads to the disease onset. Therefore, investigations of these differentially expressed ORFs have been performed to understand the biofilm formation process and thus, the pathogenicity of *X. fastidiosa* [16,17].

In this study, we characterized the protein product of Xf1448 ORF, which is predicted to be a LysR-like transcriptional regulator (LTTR; http://www.xylella.lncc.br/xf-prod-bin/annotation/final/annotation.cgi?id=&gene=XF1448). Because this ORF has little amino acid sequence similarity with other LysR-type proteins, the identification of its role in the cellular metabolism was previously impaired. The LTTR family is a well-characterized group of transcriptional regulators that is ubiquitous among bacteria, has a high degree of conservation, and has functional orthologues in *archaea* and eukaryotic organisms [18–20]. These transcriptional regulators usually control their own expression, which may occur simultaneously with the regulation of a divergently transcribed target ORF or operon [21]. Based on sequence alignments, it has been shown that LTTRs have a helix-turn-helix (HTH) DNA-binding domain located 20–90 amino acids from the N-terminus, regardless of whether the transcriptional regulator acts as an activator or repressor [21]. Generally, this DNA-binding domain interacts with the promoter region of the targeted ORF or operon through a pseudo-palindromic sequence (T-$N_{11}$-A) that is called the LTTR box [22]. However, the LTTR box may vary in both base pair composition and length [21]. The C-terminus (amino acids 95–210) of a typical LTTR contains the co-inducer binding cleft, and the interaction between the co-inducer and LTTR modulates the activating or repressing function of the protein [23–25]. The molecules that act as co-inducers are generally by-products or metabolic intermediates of the pathways that are regulated by the LTTRs [26,27]. Considering the abundance of LTTRs within the genomes of evolutionarily distant bacteria and other organisms, LTTRs have developed regulatory functions in many different pathways, including metabolism, cell division, quorum sensing, virulence, motility, nitrogen fixation, oxidative stress response, toxin production, attachment and secretion [9,28–36]. Moreover, this class of tranSmall-angle X-ray scattering and *in silico* modeling approaches for the accurate functional annotation of an LysR-type transcriptional regulatorscription factors may act in association with other regulatory pathways that induce more complex regulatory networks inside the cell. One type of interaction is the association of the LTTR with the globally expressed histone-like nucleoid-associated regulator protein (H-NS) [37].

In the present work, we identified the structure and function of the predicted LysR-type ORF Xf1448 from *X. fastidiosa* (denoted XfLysRL for LysR-like from *X. fastidiosa* in the present work). Although the XfLysRL ORF is described as a LTTR, it does not exhibit sufficient sequence similarity with well-characterized LTTRs (functionally and/or structurally), which had previously impaired a more accurate annotation of its function. However, it does contain a conserved LTTR substrate binding domain that is involved in the catabolism of aromatic compounds. Using small-angle X-ray scattering (SAXS) and *in silico* modeling, we were able to obtain a reliable protein structure envelope, which allowed us to use structural conservation to identify putative homologues with known functions. Further functional assays confirmed the role of XfLysRL in the cell, which allowed the identification of new information and knowledge of the *X. fastidiosa* metabolism.

## 2. Materials and methods

### 2.1. Cloning, expression and purification of recombinant XfLysRL

The gene corresponding with XfLysRL was amplified by PCR using genomic DNA from *X. fastidiosa* strain *9a5c* as the template. Specific primers for the target sequence were designed such that the fragments produced could be cloned into the pET28a vector with *Nde*I and *Xho*I (forward primer: 5′ — TAATCATATGCACGACGCCGCCAGT — 3′; reverse primer: 5′ — ATCTCGAGTCACCTTGCACCAGCAC — 3′). The PCR product was cloned into pET28a and chemically transformed into competent *Escherichia coli* DH5-α cells. The positive clones were sequenced to verify the identity and presence of the cloned fragment. The competent *E. coli* BL21(DE3) strain was used for the recombinant protein expression.

*E. coli* BL21(DE3) cells containing the gene that encodes XfLysRL were inoculated in 3 mL of LB medium containing 30 μg/mL kanamycin. The cells were then grown at 37 °C and 300 rpm overnight. The cultures were transferred into 1 L of LB medium containing the same concentration of antibiotic and grown to an $A_{600}$ of 0.6–0.8. The overexpression of the plasmid was induced through the addition of IPTG to a final concentration of 0.4 mM; the culture was then incubated at 25 °C and 200 rpm for 18 h. After the incubation period, the cells were centrifuged at 5000×g for 15 min (4 °C), and the pellet was resuspended in buffer A (50 mM Tris–HCl and 300 mM NaCl pH 7.5) supplemented with 1 mg/mL lysozyme and 1 mM phenylmethanesulfonyl fluoride (PMSF; Sigma Chemical, St. Louis, MO, USA). The cells were maintained under agitation conditions for 30 min (4 °C), sonicated and then centrifuged at 15,000×g for 45 min (4 °C) to obtain the protein extract. The XfLysRL protein was then purified through a single affinity chromatography step using a Ni-NTA resin (Qiagen, Hilden, Germany) equilibrated with buffer A. The purified protein was eluted using an imidazole gradient (20, 50, 75, 100, 200 and 500 mM) in buffer A. The protein yield and purity were analyzed by SDS-PAGE.

### 2.2. Size-exclusion chromatography

Size-exclusion chromatography was performed using a Superdex 75 10/300 GL column (GE Healthcare, USA). The column was equilibrated with 50 mM Tris–HCl pH 7.5 and 300 mM NaCl. The samples (250 μL) were injected at a flow rate of 0.6 mL/min. High molecular weight (HMW) and low molecular weight (LMW) gel filtration calibration kits (GE Healthcare) were used as the calibration standards, and the results were analyzed according to the instructions detailed in the calibration kit manuals. Conalbumin (75 kDa), ovalbumin (43 kDa), carbonic anhydrase (29 kDa), ribonuclease A (13.7 kDa), aprotinin (6.5 kDa) and blue dextran 2000 (2000 kDa) were used as the standards.

### 2.3. Small-angle X-ray scattering (SAXS)

The XfLysRL samples at a concentration of 1.5 mg/mL in 50 mM Tris–HCl pH 7.5, 300 mM NaCl and 500 mM imidazole buffer were subjected to SAXS data collection. The samples were centrifuged at 13,000×g and 4 °C prior to the measurements. The individual samples were carefully loaded into cells composed of two thin parallel mica windows and maintained at 25 °C throughout the measurements. The SAXS data collection was performed at the D02A-SAXS2 beamline of the Brazilian National Synchrotron Light Laboratory (LNLS, Campinas) [38] using a bi-dimensional MAR CCD 345 detector and a monochromatic X-ray beam at a wavelength of 1.488 Å. The sample-to-detector distance was adjusted to 1682.88 mm, which covers a momentum transfer interval of $0.0076<q<0.1928$ $Å^{-1}$, where $q=[(4\pi)/(\lambda)]\sin\theta$ and $2\theta$ is the scattering angle.

The protein samples and buffer solution (used as a blank during the data analysis) were exposed to the X-ray for 10 min. Six successive frames were recorded for the protein sample. A data reduction was performed using FIT2D [39], which involved the collection of the radial integration of the images, normalization to the intensity of the transmitted beam and subtraction of the buffer scattering. To prevent artifacts caused by protein degradation during the data

collection, only the first two frames were averaged to obtain the final curve. Guinier analysis was performed to evaluate the sample scattering linearity at very small angles [40] and estimate the radii of gyration, Rg, and the scattering at the zero angle, I(0). Further analyses were performed using the ATSAS package [41]. The indirect Fourier transform method, which was implemented in GNOM [39], was used to calculate the distance distribution function, P(r), which allowed the assessment of the maximum intramolecular distance ($D_{max}$) and molecular anisometry. GNOM was also used to estimate Rg and I(0). A Kratky plot [$q^2I(q)\times w$] [42,43] was used to evaluate the conformational state of the protein in solution. The molecular mass of XfLysRL was estimated using 3.3 mg/mL bovine serum albumin (BSA) as the standard. The I(0) values from the standard and sample were obtained as described above, and the equation $[Mc/I(0)]_{sample} = [Mc/I(0)]_{standard}$ (where M is the molecular mass, c is the concentration and I(0) is the scattering intensity at the zero angle) was used to estimate the molecular mass of the sample.

*Ab initio* dummy bead models were calculated from the experimental curves using DAMMIF [44] and imposing P2 symmetry. Forty models were averaged with DAMAVER [45]. Based on the normalized spatial discrepancy (NSD) values and a visual inspection, the 10 most similar models were selected and averaged, which resulted in the generation of the final envelope that was used in the subsequent structural comparisons. For better visualization, the envelope was presented as a mask that was built from the final averaged bead model using NCSMASK [46].

In parallel with the *ab initio* methods that were used to construct the low resolution envelope from the experimental curve, we conducted rigid-body modeling of XfLysRL based on homologous proteins. A monomeric structure of XfLysRL (model with the highest Small-angle X-ray scattering and *in silico* modeling approaches for the accurate functional annotation of an LysR-type transcriptional regulatorscore), which was predicted with I-TASSER [47–49], was utilized to compose a dimeric structure that was based on available crystallographic models using the following procedure. First, to define the most probable dimeric interface, homologous crystal structures of the LTTR family members (those automatically selected by I-TASSER) were analyzed to compose a dimer by applying different crystallographic symmetry operations and choosing the two monomers that corresponded with a known functional dimer [50–55]. The resulting models composed of two amino acid chains related by the appropriSmall-angle X-ray scattering and *in silico* modeling approaches for the accurate functional annotation of an LysR-type transcriptional regulatorate symmetry were then fitted against the experimental XfLysRL SAXS curve using CRYSOL [56]. The discrepancy (|) between the experimental data and computed theoretical scattering curve of each possible dimer was used to select the closest structural homologue. Using this model as a reference, the predicted XfLysRL monomer was superimposed onto each chain separately, and the resulting monomers were combined into a single file to represent the putative atomic model of the XfLysRL dimer, which was also assessed with CRYSOL. The structural alignments were performed with SUPCOMB [57].

### 2.4. Sequence alignment of XfLysRL with similar structurally characterized proteins

Protein sequence alignments were performed to identify putative homologues with known structure and function that would help in the characterization of the XfLysRL protein. An initial sequence similarity analysis was performed using the Basic Local Alignment Search Tool (BLAST, http://blast.ncbi.nlm.nih.gov/Blast.cgi), and subsequent alignments were performed using the CLUSTALW server (http://www.ebi.ac.uk/Tools/msa/clustalw2/).

### 2.5. Expression profile of XfLysRL during different stages of biofilm formation and in the presence of muconate and benzoate

To analyze the expression of XfLysRL during different steps of biofilm formation, a specific antibody against the purified protein was synthesized (RheaBiotech, Brazil) and used for the detection of the native XfLysRL in bacterial lysates. A *X. fastidiosa* subsp. *pauca* strain *9a5c* suspension in phosphate-buffered saline was inoculated in periwinkle wilt (PW) medium and grown at 28 °C with shaking at 130 rpm. Separated experiments were conducted in triplicate and analyzed during each day of growth, and no additional medium supplementation or changes were performed. The biofilm and planktonic cell extracts from days 3, 5, 10, 15, 20 and 30 of growth were analyzed by Western blot. Briefly, the pelleted cells were resuspended in 50 mM Tris–Cl pH 8.0, 25 mM NaCl, 5 mM EDTA, 2% Triton X-100, 1 mM PMSF and 1 mg/mL lysozyme and incubated on ice for 20 min. The cell disruption was achieved through 5 10-s sonication cycles with an output intensity setting of 5 in an Ultrasonic Homogenizer 4710 (Cole-Parmer, USA). The homogenate was centrifuged for 10 min at 10,000 × g, and the resulting supernatant was collected. The total protein concentration was measured using a Micro BCA™ Protein Assay Kit (Thermo Scientific, USA), and all of the samples were normalized to the same protein concentration. After SDS-PAGE, the samples were transferred to a 0.45-μm Potran BA 85 nitrocellulose membrane (Whatman, Dassel, Germany) using a Semi-Dry Transfer Cell (BioRad, CA, USA). The transferred membrane was incubated with the specific antibody against XfLysRL at a dilution of 1:4000 for 2 h and then with a secondary antibody, which was linked to an alkaline phosphatase (goat anti-rabbit IgG-AP, Souza-Cruz, Brazil), at a dilution of 1:8000 for an additional 2 h. The Western blots were developed with the BCIP/NBT Color Development Substrate (Promega, Madison, Wisconsin, USA) following the manufacturer's instructions. Three independent blots for the biofilm and planktonic samples were performed to assess the variation in the protein transfer. The signal intensity was quantified using the Kodak Electrophoresis Documentation and Analysis System (EDAS) 290 software.

A similar approach was used to evaluate the expression of XfLysRL in biofilm *X. fastidiosa* cells in the presence of muconate and benzoate. Briefly, a *X. fastidiosa* subsp. *pauca* strain *9a5c* suspension in phosphate-buffered saline was inoculated in PW medium that was not supplemented with BSA and grown at 28 °C with shaking at 130 rpm. When indicated, a sterile muconate or benzoate solution was added to the medium to final concentrations of 0.168 mM and 0.392 mM muconate and 5 mM and 10 mM benzoate. *X. fastidiosa* was also cultivated in non-supplemented medium (no benzoate or muconate) as a control. Each experiment was performed in triplicate. The biofilm cells were harvested after 10 days, and the total protein extraction and Western blot procedures were performed as described above. Each sample was normalized to a final protein concentration of 197 ng/μL. We used a 1:2000 dilution of the specific anti-XfLysRL antibody and 1:4000 dilution of the secondary antibody as described previously.

### 2.6. Interaction of XfLysRL with its putative co-inducers benzoate and muconate

Based on the sequence alignments and SAXS data, we hypothesized that XfLysRL could be a transcriptional regulator induced by benzoate and muconate to activate the degradation pathway of these compounds. Clark and colleagues (2009) analyzed the interaction of benzoate and muconate with the *Acinetobacter* sp. strain ADP1 BenM, which is a LysR-type transcriptional regulator responsible for the activation of the degradation pathway of aromatic substrates [58]. Similarly, we used fluorescence emission spectroscopy to test the ability of XfLysRL to interact with benzoate and muconate

and obtained positive results that were in agreement with our SAXS and *in silico* modeling results.

Purified XfLysRL (2.5 μM) was dialyzed against 50 mM Tris–HCl, pH 7.5, and 300 mM NaCl and then incubated with 0 to 0.7 mM muconate or 0 to 10 mM benzoate (both products were purchased from Sigma-Aldrich), and the emitted fluorescence was recorded using a Carey Eclipse spectrofluorometer (Varian, USA). The samples were excited at 295 nm and 280 nm to monitor the interactions with muconate and benzoate, respectively. The measurements were performed in triplicate, and the differences in the emissions between each spectra and the initial emission of the protein were plotted against the co-factor concentration. $K_d$ values for benzoate and muconate interactions with the protein were calculated using OriginPro 8 SRO software (OriginLab Corporation, Version 8.0724 B724) through Stern–Volmer plots and Non Linear Least Square fitting. The equation: $Q = Q_{max} \times C/(K_d + C)$ was used, in which Q is the observed fluorescence quenching, $Q_{max}$ is the maximum observed fluorescence quenching, $K_d$ is the dissociation constant and C are quenchers (benzoate or muconate) concentrations.

## 3. Results

### 3.1. Sequence alignments

An initial BLAST search of the XfLysRL sequence (UniProt ID: Q9PCQ9) using the UniProt database resulted in hits that primarily included LTTR family members. The LysR transcription factors from *Xanthomonas campestris* (Q3BT83), *Acidovorax* sp. (A1W5N6), *Tolumonas auensis* (C4LAA4), *Pseudomonas aeruginosa* (B7V4X9) and *Bordetella petrii* (A9IDT1) were the top hits and exhibited a primary sequence identity that ranged from 79 to 69%. However, the structure and function of these and other hits with ~30% identity were poorly characterized at the protein level. Conversely, the hits with <30% identity, such as the LysR family members BenM and CatM from *Acinetobacter baylyi*, CbnR from *Cupriavidus necator*, CbL and CysR from *E. coli* and CysB from *Klebsiella pneumoniae*, are well characterized [48–53], and their atomic crystal structures are available in the Protein Data Bank. An alignment of the full length XfLysRL sequence deposited in the UniProt database with those of the LTTR family members is shown in Fig. 1 and colored by amino acid conservation. The alignment and structural homology parameters are displayed in Table 1 (Supplementary data). It is noteworthy that XfLysRL does not appear to have an N-terminal DNA-binding domain, which is observed in the other LysR-type transcriptional regulators.

### 3.2. Recombinant XfLysRL protein expression, purification and initial characterization

Recombinant XfLysRL was successfully produced in the *E. coli* BL21(DE3) strain under the conditions described in the Materials and methods section and satisfactorily purified in a single affinity chromatography step. Polyacrylamide gel electrophoresis showed a high purity level, and size exclusion chromatography revealed that the protein was found as a dimer in solution under both reducing and non-reducing conditions (Fig. 2). In addition, the oligomeric state of the protein did not change when incubated with the theoretical co-inducers muconate

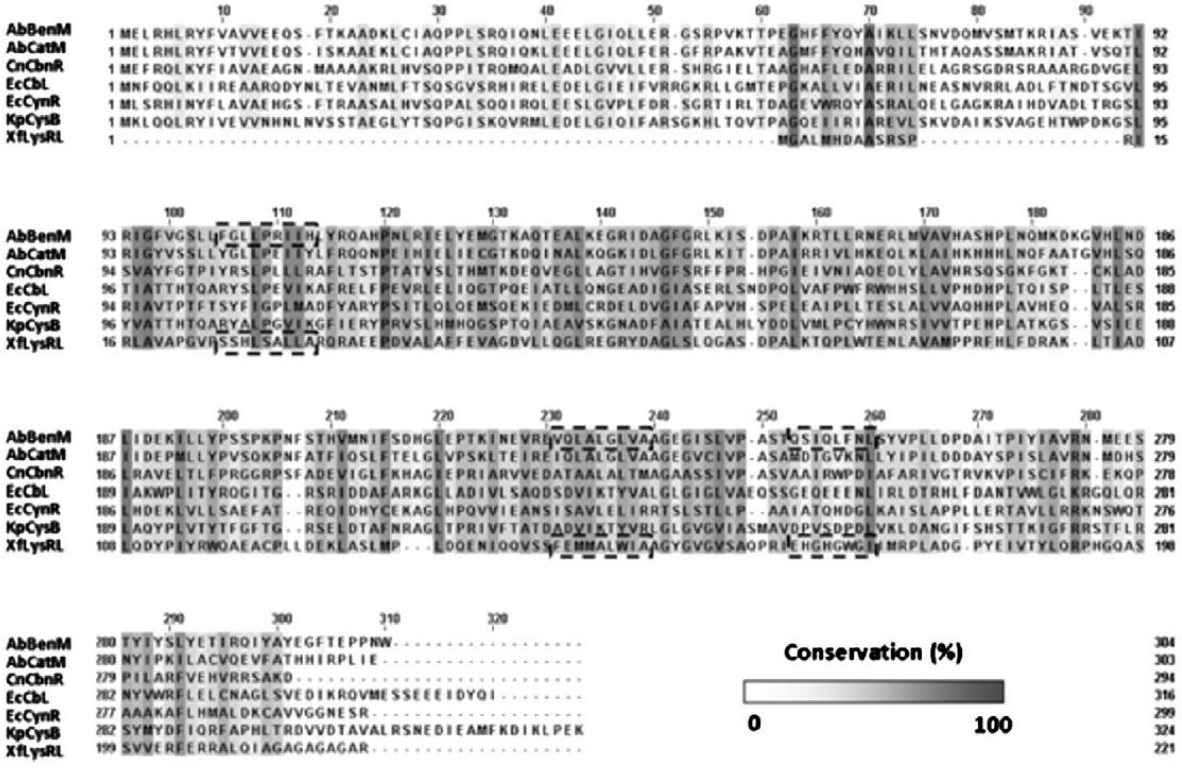


**Fig. 1.** Primary sequence alignment of LTTR family members. The amino acid sequences of *Acinetobacter baylyi* BenM (AbBenM) and CatM (AbCatM), *Cupriavidus necator* CbnR (CnCbnR), *Escherichia coli* CbL (EcCbL) and CynR (EcCynR), *Klebsiella pneumoniae* (KpCysB) and *Xylella fastidiosa* LysRL (XfLysRL) were aligned using multiple alignment algorithms in the ClustalW [20] software. The alignment is colored according to the conservation of the chosen LTTR sequences, which ranged from 0% (white) to 100% (dark gray). The reported AbBenM [14,15] and proposed XfLysRL dimerization interfaces are highlighted with dashed lines.

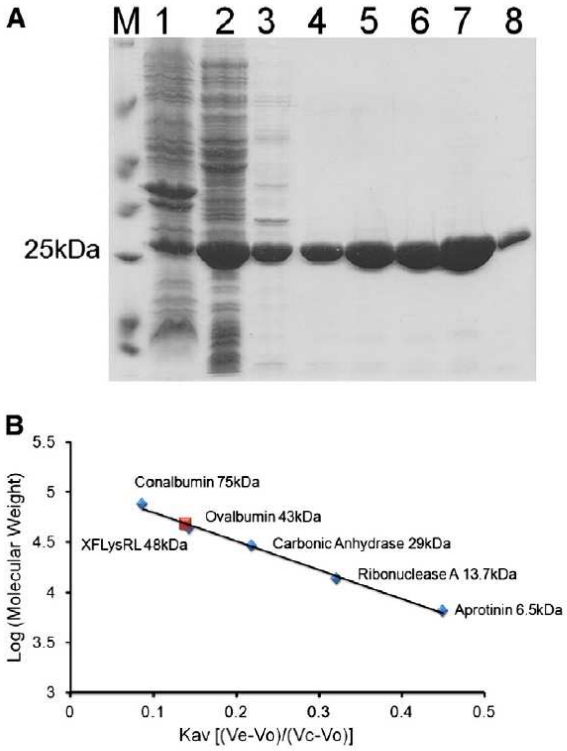


**Fig. 2.** Initial characterization of XfLysRL. (A) SDS-PAGE analysis of purified XfLysRL, in which M is the Fermentas Molecular Weight Marker, 1 is the insoluble fraction, 2 is the soluble fraction, and 3 through 8 are the elution imidazole gradient (20, 50, 75, 100, 200 and 500 mM). (B) Size exclusion chromatography of XfLysRL. Based on our calibration curve, XfLysRL is a dimer in solution with a molecular weight of 48 kDa.

and benzoate (data not shown). The secondary structure of the purified recombinant protein was analyzed by circular dichroism (CD) and determined to contain regular β-sheets and α-helixes (data not shown).

### 3.3. SAXS data analysis and modeling

Small-angle X-ray scattering (SAXS) is a technique that allows the study of the structure and interactions of a macromolecule in solution. Despite its low resolution, SAXS is considered a powerful tool for the elucidation of protein behavior in solution (which may be near physiological conditions or in the presence of different compounds, such as protein ligands or denaturing agents) and provides some key parameters, such as the molecular weight (MW), radius of gyration (Rg), and maximum intramolecular distance ($D_{max}$), that aid in the identification of the molecular envelope of the studied protein. In this study, it was possible to correlate the SAXS data on the XfLysRL protein (coupled with the *in silico* modeling results) to previously characterized proteins and hence speculate on the possible function of XfLysRL. The experimental SAXS curves were analyzed individually and revealed variation during the data collection process that is possibly related to radiation damage or protein degradation. Thus, the first two frames, which were essentially identical, were used to build the average scattering curve that was used in the additional analyses (Fig. 3A). The corresponding Guinier region (Fig. 3B) exhibited a linear behavior characteristic of monodisperse samples and was used to determine the radius of gyration, which was estimated to be 28.5 Å. The Kratky plot (Fig. 3C) had a well-defined maximum, as expected for well-folded, compact proteins. The distance distribution function, P(r), was calculated with GNOM [39] and found to have a symmetrical shape, with a $D_{max}$ of 85 Å (Fig. 3D) and corresponding radius of gyration of 27.6 Å, which is similar to the less accurate value that was estimated from the Guinier analysis.

The molecular mass of XfLysRL was estimated to be 48.4 kDa based on a comparison with the scattering curve of the BSA standard. This result strongly suggests that XfLysRL is a dimer in solution, which is in agreement with available data for other members of the LTTR family that have a truncated N-terminal domain [50]. Accordingly, a P2 symmetry was imposed during the *ab initio* modeling through which the XfLysRL envelope (Fig. 4) was determined from the experimental curves.

Based on sequence and structural alignments, an atomic model for the XfLysRL monomer was predicted using I-TASSER [47–49] and the following crystal structures of homologous LTTR family members with PDB entries: 1IXC (CbnR, *C. necator*), 1IZ1 (CbnR, *C. necator*), 2F6G (BenM, *A. baylyi*), 2HXR (CynR, *E. coli*) and 2FYI (CbL, *E. coli*). For each of these known crystal structures, the respective functional dimer structures were identified and compared with the XfLysRL scattering curve. The discrepancies calculated with CRYSOL [56], which are summarized in Table 2 (supplementary data), indicate that the dimer obtained from the PDB entry 2F6G (AbBenM) exhibited the best fit to the XfLysRL experimental data, which suggests that AbBenM has the highest structural similarity to XfLysRL. Thus, a putative XfLysRL dimer was built using the XfLysRL monomer homology model generated with I-TASSER and the experimental AbBenM dimer as the template. The resulting fit of the modeled XfLysRL dimer to the experimental curve is shown in Fig. 4A. The RMSD between the residues that are structurally aligned in the predicted XfLysRL model and crystal structure of AbBenM is relatively low (1.27 Å). Not surprisingly, the | value obtained from the fit of the putative XfLysRL dimer to the experimental curve was the same as the value obtained from the AbBenM dimer (|= 3.8), even though the former corresponds with the correct protein sequence and expected electron density, which allows for a better calculation of the theoretical scattering curve.

Further attempts to improve the fit by imposing contact conditions to maintain the dimeric interface of XfLysRL were performed using SASREF [41]. However, this approach was not able to improve the fit to the experimental data. In the absence of additional information, there was no justification to modify the imposed vinculum, which allows for a greater freedom of domain movements and potentially leads to a better fit. We also note that | is a statistical parameter that is also dependent on the noise in the data. For example, because the curve tends to be nosier at higher q values, χ values as low as 1.9 could be obtained if we limit the data to a lower resolution.

An experimental envelope for XfLysRL in solution was independently obtained using the DAMMIF software [41]. This envelope was superimposed onto the putative XfLysRL dimer (Fig. 4A) and showed a remarkable fit. Altogether, these results not only support the low-resolution modeled XfLysRL dimer and demonstrate the similarity between the AbBenM and XfLysRL monomeric structures but also imply that these two proteins dimerize in a similar manner.

Finally, we analyzed whether the residues in *A. baylyi* BenM involved in muconate and benzoate binding (both molecules are well characterized co-factors of this transcription regulator) were conserved in XfLysRL. Based on the work by Ezezika and collaborators (2007) [51], sequence alignments and our XfLysRL model, we mapped the residues in our protein sequence that might be involved in co-factor binding (Supplementary data: Fig. 1 and Table 3). *A. baylyi* BenM has two binding sites for benzoate and one for muconate [51]. We observed similarities among the residues of the second benzoate binding site, which are mainly amino acids that form a hydrophobic pocket in the structure.

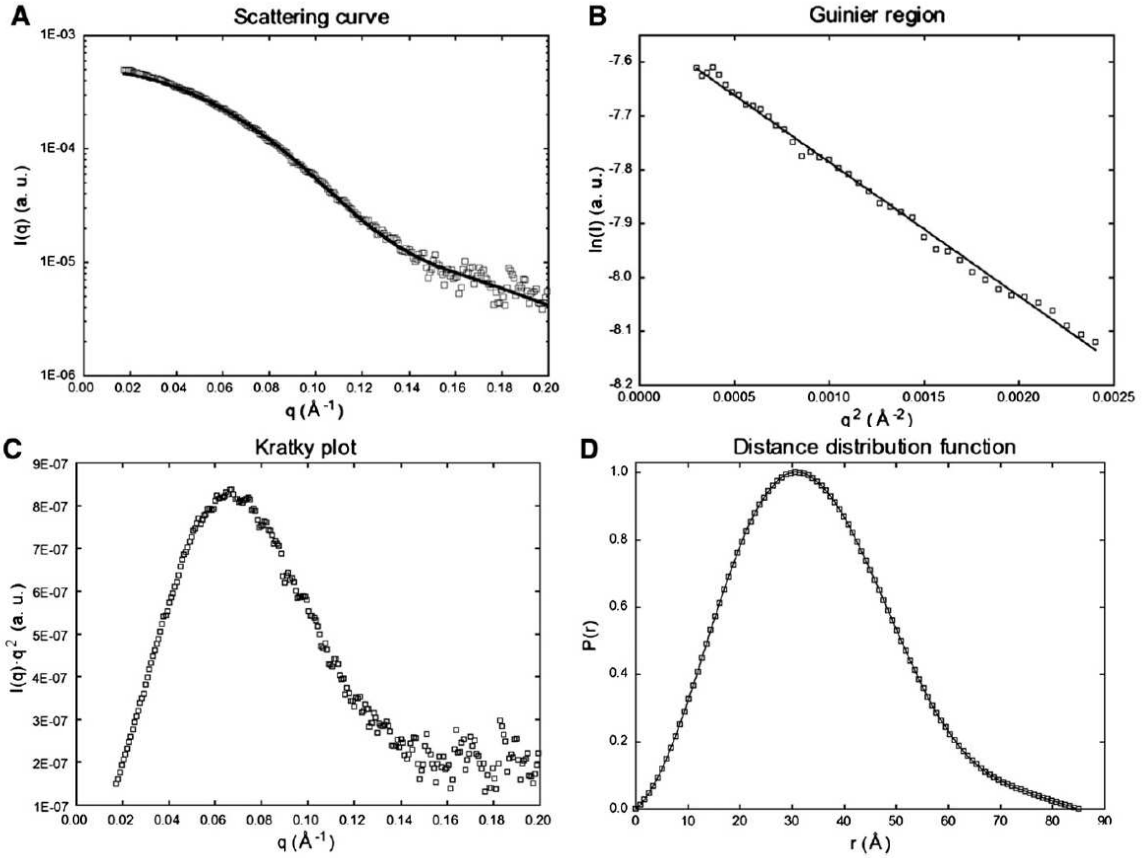


**Fig. 3.** XfLysRL SAXS data analysis. (A) Experimental solution scattering curve (open squares) and the resulting fitted model (solid line). (B) Guinier plot. (C) Kratky plot. (D) The distance distribution function P(r).

Moreover, two residues in the *A. baylyi* BenM those are crucial for benzoate binding (R160 and Y293) are not conserved in the XfLysRL sequence. However, we would like to stress that muconate and benzoate make 4 and 6 water mediated contacts with *A. baylyi* BenM residues respectively [51]. Additionally, it is reported that benzoate fits more loosely then muconate in the binding site and is surrounded by many more water molecules. Together, this information may suggest that despite the low conservation observed for XfLysRL co-inducer binding site residues, water mediated interactions may account for the observed interaction of the studied protein with both, muconate and benzoate.

### *3.4. Interactions of recombinant XfLysRL with the putative co-inducers benzoate and muconate*

As revealed through the amino acid sequence alignment, XfLysRL displays 21% identity with *A. baylyi* BenM, which is a LysR family transcription factor that regulates the catabolic pathway of aromatic compounds, specifically benzoate. Additionally, based on our SAXS data and *in silico* models, it was possible to determine the molecular envelope of the XfLysRL dimer, which was shown to fit well with the BenM dimer structure. BenM, a well-characterized LysR-type transcriptional regulator, interacts with both benzoate and muconate molecules, which act as co-inducers [58].

Fluorescence emission spectroscopy clearly showed that XfLysRL is also able to interact with benzoate and muconate because we observed a co-factor concentration-dependent fluorescence quenching in both cases (Fig. 5A and B). The data fitting shows hyperbolic curves that are indicative of the absence of cooperativity in the binding of muconate and benzoate to the protein subunits (Fig. 5C and D). The observed quenching of fluorescence upon the addition of benzoate and muconate resembles the quenching observed in the incubation of *A. baylyi* BenM with both co-factors, as reported by Clark and colleagues (2004) [58]. However, no shift in the fluorescence maximum was observed for XfLysRL during the co-factor titration, which indicates that the binding does not affect the environment of the four tryptophan residues (W100, W133, W168 and W189) present in the protein sequence. In contrast, *A. baylyi* BenM showed a shift in the fluorescence maximum to higher wavelengths when incubated with benzoate, which indicates that the unique tryptophan residue (W304) of this protein was exposed to a more hydrophilic environment upon co-factor binding [58]. XfLysRL has a higher affinity for muconate than benzoate (Fig. 5C and D), which is reflected by the calculated $K_d$ values of $0.40 \pm 0.11$ and $1.87 \pm 0.28$, respectively. These $K_d$ values are higher but not far from the values reported for *A. baylyi* BenM ($1.2 \pm 0.2$ for benzoate and $0.28 \pm 0.05$ for muconate) and for co-factor binding domain from BenM ($1.1 \pm 0.1$ for benzoate and $0.12 \pm 0.02$ for muconate) [58]. This may be explained by the low level of conservation observed in the

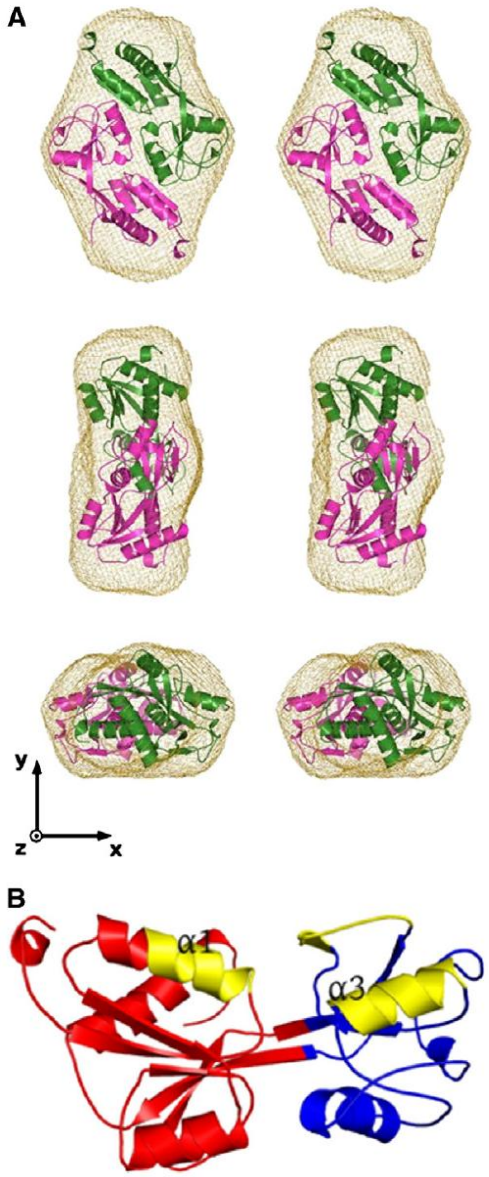


**Fig. 4.** Putative XfLysRL dimer constructed from the SAXS data. (A) Stereo view of three orthogonal orientations of an averaged SAXS envelope (gray grids), which was generated using DAMMIF and superposed with the generated XfLysRL dimer (green and magenta cartoons). The XfLysRL dimer was constructed based on the XfLysRL monomer homology models by orienting the individual subunits and comparing the resulting atomic dimeric model to the experimental scattering curve using the SASREF software. (B) The monomeric XfLysRL homology model with the two effector binding domains EBDI and EBDII, which are colored red and blue, respectively. The proposed dimerization interface is colored yellow. The figures were generated using the PyMOL software.

residues that form the co-factor binding sites in XfLysRL and *A. baylyi* BenM (Supplementary data). Additionally, these results are also in agreement with previously reported data for *A. baylyi* BenM, which showed that less amounts of muconate than benzoate were required to achieve a comparable reduction in fluorescence [58]. Taken together, these fluorescence data suggest that the recombinant XfLysRL is able to interact with both muconate and benzoate under the conditions tested.

### *3.5. XfLysRL expression oscillates between different stages of biofilm formation and is affected when cells are cultivated in the presence of muconate or benzoate*

We used Western blot analysis to evaluate the expression profile of XfLysRL during different stages of *X. fastidiosa* biofilm formation. We analyzed both planktonic and biofilm cells because it has been reported that these distinct forms of growth have different gene expression profiles that are in turn related to the ability of planktonic cells to adhere to their host surface and form biofilm structures. Therefore, the genes that are differentially regulated by planktonic and biofilm cells are likely involved in biofilm formation and in the case of *X. fastidiosa*, pathogenicity. Biofilm is a cellular aggregate that adheres to a surface and results in many adaptive advantages, such as an increased capacity of cells to take up nutrients from the environment [59], a greater resistance to antimicrobial compounds [60,61], and a higher capacity of detoxification due to the increased expression of the efflux pump genes [62]. The stages of *X. fastidiosa* biofilm formation have been well characterized and are divided into 5 phases: reversible attachment, irreversible attachment, initial maturation process, formation of mature biofilm, and dispersion [16,63]. In *X. fastidiosa* strain *9a5c*, the maturation phase occurs between days 15 and 20 *in vitro*, whereas the dispersion stage occurs between days 25 and 30. The biofilm formation in the xylem vessels is considered the primary mechanism of *X. fastidiosa* pathogenicity because it leads to hydric stress and the development of symptoms in the plant [15]. In the present work, we observed differences in the expression level of XfLysRL throughout the stages of biofilm formation and between biofilm and planktonic cells (Fig. 6A). The most significant difference was the lack of XfLysRL expression in planktonic cells at the early stages of biofilm formation (days 3 and 5) compared with its expression in biofilm cells at the same time points (Fig. 6B). In addition, we observed a decrease in the expression level of XfLysRL in the last stage of biofilm formation (day 30), which may be explained by the fact that biofilm cells dissociate from the biofilm structure and turn into planktonic cells during this stage. However, the XfLysRL protein expression is increased in planktonic cells at the same stage; this increase may be correlated with the accumulation of aromatic metabolites in the medium and the need of an additional carbon source because the depletion of the growth medium may occur at this stage. As mentioned above, proteomic investigations have shown that sessile cells present in a biofilm structure diverge from planktonic cells in their expression of central metabolism genes, including genes that are involved in amino acid metabolism, co-factor biosynthesis and carbon metabolism [64]. Therefore, because our data indicate that XfLysRL is a BenM homologue, the observed expression profile differences between planktonic and biofilm *X. fastidiosa* can be explained in light of a XfLysRL role as a transcriptional regulator that activates genes that are involved in the aromatic compound and carbon metabolism pathways. In addition, genes related to the aromatic compound metabolism pathway are directly involved in the defense against plant chemicals, which are produced through the systemic acquired resistance process [65]. In the context of *X. fastidiosa* pathogenicity, the expression of XfLysRL, which is a putative homologue of BenM, in biofilm cells could also be related to resistance to plant chemicals that are produced during the colonization process. However, further investigations are needed to draw solid conclusions regarding the role and relevance of this protein in biofilm formation and carbon metabolism.

Finally, we analyzed whether the growth of *X. fastidiosa* in the presence of muconate and benzoate would lead to an alteration in XfLysRL expression. In the presence of benzoate (10 mM), we observed a clear decrease in the expression of XfLysRL in biofilm cells compared to our control ($p = 0.048$), whereas the XfLysRL expression was increased in the presence of 0.392 mM muconate ($p = 0.033$; Fig. 7A and B). No significant differences were observed

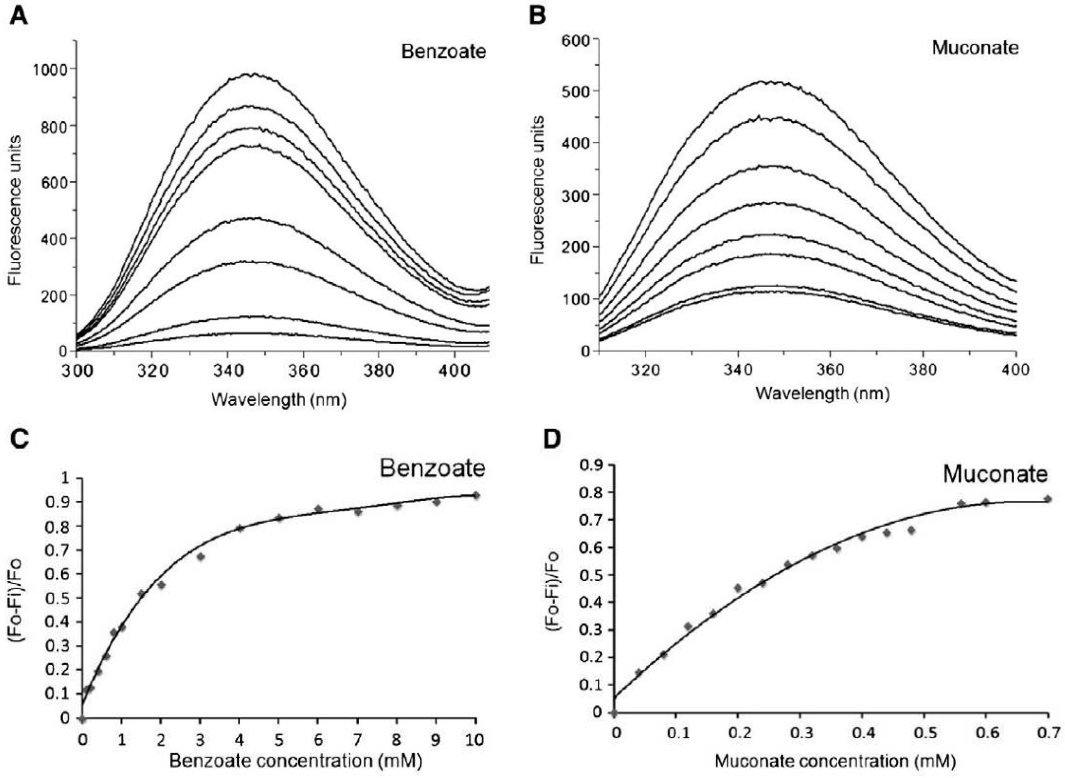


**Fig. 5.** (A) and (B) Fluorescence curves for XfLysRL in the presence of benzoate and muconate, respectively. From top to bottom, the following concentrations were used: 0, 0.1, 0.4, 0.6, 1.5, 6, and 10 mM benzoate and 0, 0.04, 0.12, 0.2, 0.32, 0.4, 0.56, and 0.7 mM muconate. (C) and (D) Change at $\Lambda_{max} = 347$ nm intensity after the addition of benzoate and muconate, respectively. This change is expressed as the initial fluorescence ($F_0$) minus the fluorescence at a specific concentration (I) of the co-factor ($F_i$) divided by the intensity of the initial fluorescence ($F_0$). Both plots were fitted to a hyperbolic curve, which indicates a lack of cooperativity in the interaction between the XfLysRL monomers and co-factors.

when the cells were cultivated in the presence of lower concentrations of muconate (0.168 mM) and benzoate (5 mM). Our data suggest that although XfLysRL exhibits structural homology with *A. baylyi* BenM, it does not have its expression induced by benzoate, which is conflicting with its speculated role as a BenM homologue.

## 4. Discussion

### *4.1. SAXS envelope and the atomic model of XfLysRL are similar to the structure of A. baylyi BenM*

We used recombinant protein expression, sequence alignments and SAXS approaches to assign a possible function to a predicted LysR-type transcriptional regulator that is present in the *X. fastidiosa* genome. Full-length LTTR family members have been identified as tetramers in solution [66,67]. However, members with a truncated N-terminal domain (containing only the effector-binding domains, EBDs) assemble as dimers in solution [50,51,53], most likely because the tetramer interface is formed through the interaction of the DNA-binding domain (DBD, N-terminal region) and the hinge that connects the EBD to the DBD [52].

In agreement with this information, size exclusion chromatography showed that the target protein XfLysRL forms a dimer in solution. An amino acid sequence alignment with other full-length LysR-type transcriptional regulators indicated that XfLysRL lacks the N-terminal binding domain. The crystal structures of diverse LTTR family members revealed similar compact dimers that are formed by their EBDs [50,53]. However, further inspection of the LTTR dimer interface showed that the residues that participate in the monomer–monomer contacts could be drastically different between the LTTR members [52]. For example, the dimer interface in the CysB EBD crystal structure is mediated by 11 β–β main chain contacts [53], whereas the dimer interfaces of the CbnR [52] and BenM [50] crystal structures are mediated by a hydrophobic cluster that is surrounded by an H-bond network.

In this work, we report a low-resolution XfLysRL EBD structure in solution. Our data strongly suggest that XfLysRL is a dimer in solution and is similar to the *A. baylyi* BenM EBD dimer [49,50]. The putative XfLysRL dimer is formed by two monomers that are oriented anti-parallel to each other to form a compact structure. The two XfLysRL EBDs are easily identified (Fig. 4B) and have the same structure topology as the LTTR members that have been previously characterized experimentally [48,50,52,53]. The suggested XfLysRL dimer interface is composed of helices α1 and α3 and a connecting loop that contains residues 21–29, 140–154, and 163–170 (highlighted as dashed lines in Fig. 1). According to the constructed XfLysRL atomic homology model, the monomer–monomer contacts are mediated mainly through hydrophobic residues, which possibly form a hydrophobic cluster that includes helix α3 and the loop from one of the monomers and helix α1 from the other monomer. Polar amino acids are also found at the putative interface and possibly surround the hydrophobic cluster, further stabilizing the XfLysRL dimer. Similar observations were made with the *A. baylyi* BenM crystal structures [49,50], which indicates that the dimer formed by XfLysRL is similar to that of its homologue, *A. baylyi* BenM.

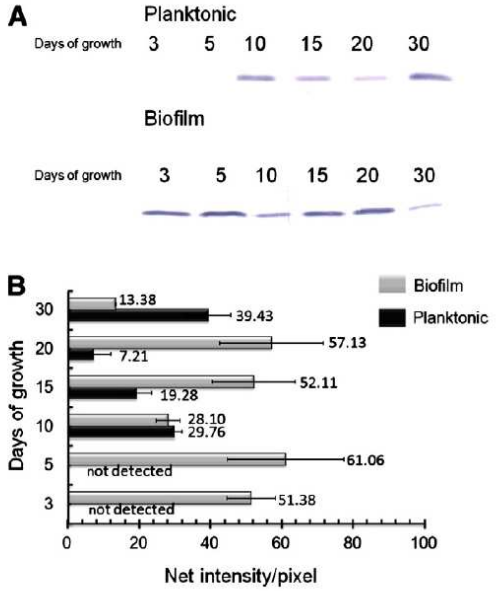


**Fig. 6.** (A) Western blot analysis of XfLysRL expression during different stages of *X. fastidiosa* biofilm formation and planktonic cell growth. (B) Total pixel intensity values of XfLysRL in biofilm and planktonic cells at each day of growth. The values represent the mean of the results obtained from three independent experiments.

### 4.2. XfLysRL interacts with benzoate and muconate, which are co-inducers of A. baylyi BenM

Although it lacks an N-terminal DNA-binding domain, we showed that the recombinant XfLysRL was able to interact with muconate and benzoate, which are both co-inducers of *A. baylyi* BenM. We observed that XfLysRL and *A. baylyi* BenM exhibited similar interaction behavior; for example, both proteins had a greater affinity for muconate than benzoate and lacked a fluorescence maximum shift upon interaction with muconate. However, benzoate caused a shift in the maximum fluorescence of *A. baylyi* BenM, which indicates that its sole tryptophan residue was exposed to a more hydrophilic environment. This shift was not observed with XfLysRL, which has four tryptophan residues in its sequence. Therefore, the observed fluorescence data for XfLysRL is a combination of the emission of four tryptophan residues, which may justify the difference from the *A. baylyi* BenM fluorescence data. Interestingly, XfLysRL exhibited reduced conservation with the *A. baylyi* BenM residues that have been found to be involved in muconate and benzoate binding. Bearing this in mind, we must consider that the observed quenching in fluorescence emission spectroscopy might be the result of unspecific binding; thus, further investigation is necessary to draw solid conclusions on the roles of muconate and benzoate as co-factors of XfLysRL.

### 4.3. XfLysRL is differentially expressed during different stages of biofilm formation and planktonic cell growth and is differentially induced by muconate and benzoate

Western blot analysis showed that XfLysRL is differentially expressed during different stages of biofilm formation and planktonic cell growth. Differences in expression were also observed between biofilm and planktonic growth, which indicates that XfLysRL is included in the pool of proteins that may contribute to the ability of *X. fastidiosa* cells to form and maintain biofilm structures. However, additional investigations are necessary to properly address this question. When *X. fastidiosa* is cultivated in the presence of benzoate and muconate, we also observed oscillations in the XfLysRL protein level in the total cellular extracts. Benzoate induced a clear reduction, whereas muconate generated a slight increase in the XfLysRL expression level that is not in agreement with the reported behavior of *A. baylyi* BenM because its expression is induced by both co-factors. Therefore, in light of our structural and functional data, we provide evidence that supports the hypothesis that XfLysRL is involved in carbon metabolism, specifically in the aromatic compound detoxification pathway.

We believe that further investigations are necessary to elucidate whether benzoate and muconate are indeed co-factors of XfLysRL, which might be achieved by the structural analysis of the XfLysRL protein in the presence of both molecules. The observed effects of muconate and benzoate on the XfLysRL expression must be confirmed by additional approaches. RT-PCR analysis of the XF1448 ORF could provide valuable information of its expression in planktonic and biofilm *X. fastidiosa* cells in the presence of muconate, benzoate or other organic compounds. Finally, the ability of XfLysRL to bind to DNA must be tested because this protein does not have an N-terminal HTH-DNA binding motif, which is common to LTTRs. Gel shift assays with promoter regions of the *X. fastidiosa* ORFs that are predicted to be involved in the carbon metabolism pathway and the promoter of XF1448 itself might indicate whether XfLysRL is able to specifically bind to DNA. Together with the presented data, these

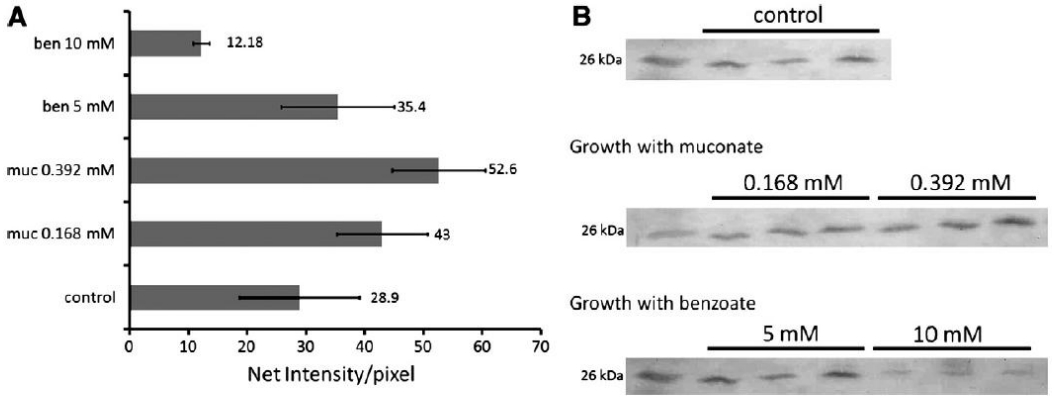


**Fig. 7.** (A) Quantification (net intensity/pixel) of XfLysRL Western blot bands obtained during *X. fastidiosa* growth in the presence of muconate and benzoate. Significant differences were obtained in the presence of 10 mM benzoate ($p = 0.048$) and 0.392 mM muconate ($p = 0.033$) compared with the control. (B) Western blots were performed for each experiment. All of the experiments with the tested concentrations of muconate and benzoate, as well as the control experiment, were performed in triplicate.

approaches might confirm the function of XfLysRL as a transcriptional regulator and determine its relevance in the *X. fastidiosa* metabolism and biofilm formation.

Supplementary data to this article can be found online at http://dx.doi.org/10.1016/j.bbapap.2012.12.017.

## Acknowledgements

This work was supported in part by the Fundação de Amparo à Pesquisa do Estado de São Paulo (FAPESP Process 01/07533-7). M.A.S. Toledo, C.A. Santos, A.C. Pelloso, L. L. Beloti, A. Crucello and M.T.P Favaro were supported by fellowships from FAPESP; D.R.S. Schneider received a PhD fellowship from the Conselho Nacional de Desenvolvimento Científico e Tecnológico (CNPq), and A.S. Santiago and J.S. Mendes received PhD fellowships from Coordenação de Aperfeiçoamento de Pessoal de Nível Superior (CAPES). The authors gratefully acknowledge the Laboratório Nacional de Luz Síncrotron (LNLS) for the beamline time and Professor Nilson Zanchin for providing CD spectropolarimeter facilities.

## References

[1] C.J. Chang, M. Garnier, L. Zreik, V. Rossetti, J.M. Bové, Culture and serological detection of the xylem limited bacterium causing citrus variegated chlorosis and its identification as a strain of *Xylella fastidiosa*, Curr. Microbiol. 27 (1993) 137–142.
[2] J.S. Hartung, J. Beretta, R.H. Brlansky, J. Spisso, R.F. Lee, Citrus variegated chlorosis bacterium: axenic culture, pathogenicity, and serological relationships with other stains of *Xylella fastidiosa*, Phytopathology 84 (1994) 591–597.
[3] M.J. Davis, A.H. Purcell, S.V. Thomson, Pierce's disease of grapevines: isolation of the causal bacterium, Science 199 (1978) 75–77.
[4] J.M. Wells, B.C. Raju, G. Nyland, Isolation, culture and pathogenicity of the bacterium causing phony peach disease, Phytopathology 73 (1983) 859–862.
[5] A.J. Simpson, F.C. Reinach, P. Arruda, F.A. Abreu, M. Acencio, R. Alvarenga, L.M. Alves, J.E. Araya, G.S. Baia, C.S. Baptista, M.H. Barros, E.D. Bonaccorsi, S. Bordin, J.M. Bové, M.R. Briones, M.R. Bueno, A.A. Camargo, L.E. Camargo, D.M. Carraro, H. Carrer, N.B. Colauto, C. Colombo, F.F. Costa, M.C. Costa, C.M. Costa-Neto, L.L. Coutinho, M. Cristofani, E. Dias-Neto, C. Docena, H. El-Dorry, A.P. Facincani, A.J. Ferreira, V.C. Ferreira, J.A. Ferro, J.S. Fraga, S.C. França, M.C. Franco, M. Frohme, L.R. Furlan, M. Garnier, G.H. Goldman, M.H. Goldman, S.L. Gomes, A. Gruber, P.L. Ho, J.D. Hoheisel, M.L. Junqueira, E.L. Kemper, J.P. Kitajima, J.E. Krieger, E.E. Kuramae, F. Laigret, M.R. Lambais, L.C. Leite, E.G. Lemos, M.V. Lemos, S.A. Lopes, C.R. Lopes, J.A. Machado, M.A. Machado, A.M. Madeira, H.M. Madeira, C.L. Marino, M.V. Marques, E.A. Martins, E.M. Martins, A.Y. Matsukuma, C.F. Menck, E.C. Miracca, C.Y. Miyaki, C.B. Monteiro-Vitorello, D.H. Moon, M.A. Nagai, A.L. Nascimento, L.E. Netto, A. Nhani Jr., F.G. Nobrega, L.R. Nunes, M.A. Oliveira, M.C. de Oliveira, R.C. de Oliveira, D.A. Palmieri, A. Paris, B.R. Peixoto, G.A. Pereira, H.A. Pereira Jr., J.B. Pesquero, R.B. Quaggio, P.G. Roberto, V. Rodrigues, A.J. de M Rosa, V.E. de Rosa Jr., R.G. de Sá, R.V. Santelli, H.E. Sawasaki, A.C. da Silva, A.M. da Silva, F.R. da Silva, W.A. da Silva Jr., J.F. da Silveira, M.L. Silvestri, W.J. Siqueira, A.A. de Souza, A.P. de Souza, M.F. Terenzi, D. Truffi, S.M. Tsai, M.H. Tsuhako, H. Vallada, M.A. van Sluys, S. Verjovski-Almeida, A.L. Vettore, M.A. Zago, M. Zatz, J. Meidanis, J.C. Setubal, The genome sequence of the plant pathogen *Xylella fastidiosa*, Nature 406 (2000) 151–159.
[6] J.M. Dow, M.J. Daniels, *Xylella* genomics and bacterial pathogenicity to plants, Yeast 17 (2000) 263–271.
[7] N.T. Keen, C.K. Dumenyo, C.H. Yang, D.A. Cooksey, From rags to riches: Insights from the first genomic sequence of a plant pathogenic bacterium, Genome Biol. 1 (2000) 10191–10194.
[8] F.R. Silva, A.L. Vettore, E.L. Kemper, A. Leite, Fastidiam gum: the *Xylella fastidiosa* exopolysaccharide possibly involved in bacterial pathogenicity, FEMS Microbiol. Lett. 203 (2001) 165–171.
[9] M.A.S. Toledo, D.R. Schneider, A.R. Azzoni, M.T.P. Favaro, A.C. Pelloso, C.A. Santos, A.M. Saraiva, A.P. Souza, Characterization of an oxidative stress response regulator, homologous to *Escherichia coli* OxyR, from the phytopathogen *Xylella fastidiosa*, Protein Expr. Purif. 75 (2011) 204–210.
[10] C.A. Santos, L.L. Beloti, M.A.S. Toledo, A. Crucello, M.T.P. Favaro, J.S. Mendes, A.S. Santiago, A.R. Azzoni, A.P. Souza, A novel protein refolding protocol for the solubilization and purification of recombinant peptidoglycan-associated lipoprotein from *Xylella fastidiosa* overexpressed in *Escherichia coli*, Protein Expr. Purif. 82 (2012) 284–289.
[11] A.M. Saraiva, M.A. Reis, S.F. Tada, L.K. Rosselli-Murai, D.R.S. Schneider, A.C. Pelloso, M.A.S. Toledo, C. Giles, R. Aparicio, A.P. Souza, Functional and small-angle X-ray scattering studies of a new stationary phase survival protein E (SurE) from *Xylella fastidiosa* — evidence of allosteric behavior, FEBS J. 276 (2009) 6751–6762.
[12] D.L. Hopkins, *Xylella fastidiosa* — xylem-limited bacterial pathogen of plants, Annu. Rev. Phytopathol. 27 (1989) 271–290.
[13] D.L. Hopkins, A.H. Purcell, *Xylella fastidiosa:* cause of Pierce's disease of grapevine and other emergent diseases, Plant Dis. 86 (2002) 1056–1066.
[14] S.M. Mircetich, S.K. Lowe, W.J. Moller, G. Nyland, Etiology of almond leaf scorch disease and transmission of causal agent, Phytopathology 66 (1976) 17–24.
[15] D. Osiro, L.A. Colnago, A.M.M.B. Otoboni, E.G.M. Lemos, A.A. de Souza, H.D.C. Filho, M.A. Machado, A kinetic model for *Xylella fastidiosa* adhesion, biofilm formation, and virulence, FEMS Microbiol. Lett. 236 (2004) 313–318.
[16] A.A. de Souza, M.A. Takita, H.D. Coletta-Filho, C. Caldana, G.M. Yanai, N.H. Muto, R.C. Oliveira, L.R. Nunes, M.A. Machado, Gene expression profile of the plant pathogen *Xylella fastidiosa* during biofilm formation *in vitro*, FEMS Microbiol. Lett. 237 (2004) 341–353.
[17] A.A. de Souza, M.A. Takita, E.O. Pereira, H.D. Coletta-Filho, M.A. Machado, Expression of pathogenicity-related genes of *Xylella fastidiosa in vitro* and in planta, Curr. Microbiol. 50 (2005) 223–228.
[18] E. Pérez-Rueda, J. Collado-Vides, Common history at the origin of the position–function correlation in transcriptional regulators in archaea and bacteria, J. Mol. Evol. 53 (2001) 172–179.
[19] J. Sun, A. Klein, A LysR-type regulator is involved in the negative regulation of genes encoding selenium-free hydrogenases in the archaeon *Methanococcus voltae*, Mol. Microbiol. 52 (2004) 563–571.
[20] E. Stec, M. Witkowska-Zimny, M.M. Hryniewicz, P. Neumann, A.J. Wilkinson, A.M. Brzozowski, C.S. Verma, J. Zaim, S. Wysocki, G.D. Bujacz, Structural basis of the sulphate starvation response in *E. coli*: crystal structure and mutational analysis of the cofactor-binding domain of the Cbl transcriptional regulator, J. Mol. Biol. 364 (2006) 309–322.
[21] S.E. Maddocks, P.C. Oyston, Structure and function of the LysR-type transcriptional regulator (LTTR) family proteins, Microbiology 154 (2008) 3609–3623.
[22] M.R. Parsek, R.W. Ye, P. Pun, A.M. Chakrabarty, Critical nucleotides in the interaction of a LysR-type regulator with its target promoter region. *catBC* promoter activation by CatR, J. Biol. Chem. 269 (1994) 11279–11284.
[23] J.E. Burn, W.D. Hamilton, J.C. Wooton, A.W. Johnston, Single and multiple mutations affecting properties of the regulatory gene *nodD* of Rhizobium, Mol. Microbiol. 3 (1989) 1567–1577.
[24] A. Cebolla, C. Sousa, V. de Lorenzo, Effector specificity mutants of the transcriptional activator NahR of naphthalene degrading *Pseudomonas* define protein sites involved in binding of aromatic inducers, J. Biol. Chem. 272 (1997) 3986–3992.
[25] C. Jørgensen, G. Dandanell, Isolation and characterization of mutations in the *Escherichia coli* regulatory protein XapR, J. Bacteriol. 181 (1999) 4397–4403.
[26] R.T. Celis, Repression and activation of arginine transport genes in *Escherichia coli* K 12 by the ArgP protein, J. Mol. Biol. 294 (1999) 1087–1095.
[27] G. van Keulen, A.N. Ridder, L. Dijkhuizen, W.G. Meijer, Analysis of DNA binding and transcriptional activation by the LysR type transcriptional regulator CbbR of *Xanthobacter flavus*, J. Bacteriol. 185 (2003) 1245–1252.
[28] G. Kovacikova, K. Skorupski, A *Vibrio cholerae* LysR homolog, AphB, cooperates with AphA at the *tcpPH* promoter to activate expression of the ToxR virulence cascade, J. Bacteriol. 181 (1999) 4250–4256.
[29] A.E. Deghmane, S. Petit, A. Topilko, Y. Pereira, D. Giorgini, M. Larribe, M.K. Taha, Intimate adhesion of *Neisseria meningitidis* to human epithelial cells is under the control of the *crag* gene, a novel LysR-type transcriptional regulator, EMBO J. 19 (2000) 1068–1078.
[30] A.E. Deghmane, D. Giorgini, M. Larribe, J.M. Alonso, M.K. Taha, Down-regulation of pili and capsule of *Neisseria meningitides* upon contact with epithelial cells is mediated by CrgA regulatory protein, Mol. Microbiol. 43 (2002) 1555–1564.
[31] H. Cao, G. Krishnan, B. Goumnerov, J. Tsongalis, R. Tompkins, L.G. Rahme, A quorum sensing-associated virulence gene of *Pseudomonas aeruginosa* encodes a LysR-like transcription regulator with a unique self-regulatory mechanism, Proc. Natl. Acad. Sci. U. S. A. 98 (2001) 14613–14618.
[32] J. Kim, J.G. Kim, Y. Kang, J.Y. Jang, G.J. Jog, J.Y. Lim, S. Kim, H. Suga, T. Nagamatsu, I. Hwang, Quorum sensing and the LysR-type transcriptional activator ToxR regulate toxoflavin biosynthesis and transport in *Burkholderia glumae*, Mol. Microbiol. 54 (2004) 921–934.
[33] D.A. Russell, G.A. Byrne, E.P. O'Connell, C.A. Boland, W.G. Meijer, The LysR-type transcriptional regulator VirR is required for expression of the virulence gene *vapA* of *Rhodococcus equi* ATCC 33701, J. Bacteriol. 186 (2004) 5576–5584.
[34] G.A. Byrne, D.A. Russell, X. Chen, W.G. Meijer, Transcriptional regulation of the *virR* operon of the intracellular pathogen *Rhodococcus equi*, J. Bacteriol. 189 (2007) 5082–5089.
[35] Z. Lu, M. Takeuchi, T. Sato, The LysR-type transcriptional regulator YofA controls cell division through the regulation of expression of ftsW in *Bacillus subtilis*, J. Bacteriol. 189 (2007) 5642–5651.
[36] V. Sperandio, C.C. Li, J.B. Kaper, Quorum-sensing *Escherichia coli* regulator A: a regulator of the LysR family involved in the regulation of the locus of enterocyte effacement pathogenicity island in enterohemorrhagic *E. coli*, Infect. Immun. 70 (2002) 3085–3093.
[37] M. Ko, C. Park, H-NS-dependent regulation of flagellar synthesis is mediated by a LysR family protein, J. Bacteriol. 182 (2000) 4670–4672.
[38] G. Kellermann, F. Vicentin, E. Tamura, M. Rocha, H. Tolentino, A. Barbosa, A. Craievich, I. Torriani, The small-angle X-ray scattering beamline of the Brazilian Synchrotron Light Laboratory, J. Appl. Crystallogr. 30 (1997) 880–883.
[39] A.P. Hammersley, S.O. Svensson, M. Hanfland, A.N. Fitch, D. Hausermann, Two dimensional detector software: from real detector to idealised image or two-theta scan, High Pressure Res. 14 (1996) 235–248.
[40] O. Glatter, O. Kratky, Small Angle X-ray Scattering, Academic Press Inc. Ltd., London, 1982.
[41] P.V. Konarev, M.V. Petoukhov, V.V. Volkov, D.I. Svergun, ATSAS 2.1, a program package for small-angle scattering data analysis, J. Appl. Crystallogr. 39 (2006) 277–286.
[42] S. Doniach, Changes in biomolecular conformation seen by small angle X-ray scattering, Chem. Rev. 101 (2001) 1763–1778.
[43] G.V. Semisotnov, H. Kihara, N.V. Kotova, K. Kimura, Y. Amemiya, K. Wakabayashi, I.N. Serdyuk, A.A. Timchenko, K. Chiba, K. Nikaido, T. Ikura, K. Kuwajima, Protein

globularization during folding, a study by synchrotron small-angle X-ray scattering, J. Mol. Biol. 262 (1996) 559–574.
[44] D. Franke, D.I. Svergun, DAMMIF, a program for rapid ab-initio shape determination in small-angle scattering, J. Appl. Crystallogr. 42 (2009) 342–346.
[45] V.V. Volkov, D.I. Svergun, Uniqueness of *ab initio* shape determination in small-angle scattering, J. Appl. Crystallogr. 36 (2003) 860–864.
[46] The CCP4 suite: programs for protein crystallography, Acta Crystallogr. D: Biol. Crystallogr. 50 (1994) 760–763.
[47] A. Roy, A. Kucukural, Y. Zhang, I-TASSER: a unified platform for automated protein structure and function prediction, Nat. Protoc. 5 (2010) 725–738.
[48] Y. Zhang, I-TASSER server for protein 3D structure prediction, BMC Bioinforma. 9 (2008) 40.
[49] Y. Zhang, I-TASSER: fully automated protein structure prediction in CASP8, Proteins Struct. Funct. Bioinforma. 77 (2009) 100–113.
[50] T. Clark, S. Haddad, E. Neidle, C. Momany, Crystallization of the effector-binding domains of BenM and CatM, LysR-type transcriptional regulators from *Acinetobacter* sp. ADP1, Acta Crystallogr. D: Biol. Crystallogr. 60 (2004) 105–108.
[51] O.C. Ezezika, S. Haddad, T.J. Clark, E.L. Neidle, C. Momany, Distinct effector-binding sites enable synergistic transcriptional activation by BenM, a LysR-type regulator, J. Mol. Biol. 367 (2007) 616–629.
[52] O.C. Ezezika, S. Haddad, E.L. Neidle, C. Momany, Oligomerization of BenM, a LysR-type transcriptional regulator: structural basis for the aggregation of proteins in this family, Acta Crystallogr., Sect. F: Struct. Biol. Cryst. Commun. 63 (2007) 361–368.
[53] A. Lochowska, R. Iwanicka-Nowicka, D. Plochocka, M.M. Hryniewicz, Functional dissection of the LysR-type CysB transcriptional regulator — regions important for DNA binding, inducer response, oligomerization, and positive control, J. Biol. Chem. 276 (2001) 2098–2107.
[54] S. Muraoka, R. Okumura, N. Ogawa, T. Nonaka, K. Miyashita, T. Senda, Crystal structure of a full-length LysR-type transcriptional regulator, CbnR: Unusual combination of two subunit forms and molecular bases for causing and changing DNA bend, J. Mol. Biol. 328 (2003) 555–566.
[55] R. Tyrrell, K.H.G. Verschueren, E.J. Dodson, G.N. Murshudov, C. Addy, A.J. Wilkinson, The structure of the cofactor-binding fragment of the LysR family member, CysB: a familiar fold with a surprising subunit arrangement, Structure 5 (1997) 1017–1032.
[56] D.I. Svergun, C. Barberato, M.H.J. Koch, CRYSOL — a program to evaluate X-ray solution scattering of biological macromolecules from atomic coordinates, J. Appl. Crystallogr. 28 (1995) 768–773.
[57] M.B. Kozin, D.I. Svergun, Automated matching of high- and low-resolution structural models, J. Appl. Crystallogr. 34 (2001) 33–41.
[58] T.J. Clark, R.S. Phillips, B.M. Bundy, C. Momany, E.L. Neidle, Benzoate decreases the binding of cis, cis-muconate to the BenM regulator despite the synergistic effect of both compounds on transcriptional activation, J. Bacteriol. 186 (2004) 1200–1204.
[59] P.A. Zaini, A.C. Fogaça, F.G.N. Lupo, H.I. Nakaya, R.Z.N. Vêncio, A.M. da Silva, The iron stimulon of *Xylella fastidiosa* includes genes for type IV pilus and colicin V-like bacteriocins, J. Bacteriol. 190 (2008) 2368–2378.
[60] P.S. Stewart, J.W. Costerton, Antibiotic resistance of bacteria in biofilms, Lancet 358 (2001) 135–138.
[61] T.F. Mah, B. Pitts, B. Pellock, G.C. Walker, P.S. Stewart, G.A. O'Toole, A genetic basis for *Pseudomonas aeruginosa* biofilm antibiotic resistance, Nature 426 (2003) 306–310.
[62] K. Nishino, E. Nikaido, A. Yamaguchi, Regulation of multidrug efflux systems involved in multidrug and metal resistance of *Salmonella enterica* serovar *Typhimurium*, J. Bacteriol. 189 (2007) 9066–9075.
[63] K. Sauer, A.K. Camper, G.D. Ehrlich, J.W. Costerton, D.G. Davies, *Pseudomonas aeruginosa* displays multiple phenotypes during development as a biofilm, J. Bacteriol. 184 (2002) 1140–1154.
[64] M.S. Silva, A.A. de Souza, M.A. Takita, C.A. Labate, M.A. Machado, Analysis of the biofilm proteome of *Xylella fastidiosa*, Proteome Sci. 9 (2011) 58.
[65] L.M. Moreira, R.F. de Souza, L.A. Digiampietri, A.C. da Silva, J.C. Setubal, Comparative analyses of *Xanthomonas* and *Xylella* complete genomes, OMICS 9 (2005) 43–76.
[66] B.E. Miller, N.M. Kredich, Purification of the Cysb protein from *Salmonella–Typhimurium*, J. Biol. Chem. 262 (1987) 6006–6009.
[67] M.A. Schell, P.H. Brown, S. Raju, Use of saturation mutagenesis to localize probable functional domains in the NahR protein, a LysR-type transcription activator, J. Biol. Chem. 265 (1990) 3844–3850.

## DECLARAÇÃO

Declaro para os devidos fins que o conteúdo de minha dissertação de Mestrado/tese de Doutorado intitulada "Estudos estruturais e funcionais de proteínas relacionadas à patogenicidade de *Xylella fastidiosa*" :

(  ) não se enquadra no § 3º do Artigo 1º da Informação CCPG 01/08, referente a bioética e biossegurança.

Tem autorização da(s) seguinte(s) Comissão(ões):

( **X** ) CIBio – Comissão Interna de Biossegurança , projeto No. **15/2003**, Instituição: Universidade Estadual de Campinas.

(  ) CEUA – Comissão de Ética no Uso de Animais , projeto No. _____, Instituição: _____.

(  ) CEP - Comissão de Ética em Pesquisa, protocolo No. _____, Instituição: _____

** Caso a Comissão seja externa ao IB/UNICAMP, anexar o comprovante de autorização dada ao trabalho. Se a autorização não tiver sido dada diretamente ao trabalho de tese ou dissertação, deverá ser anexado também um comprovante do vínculo do trabalho do aluno com o que constar no documento de autorização apresentado.*

Aluno: Clelton Aparecido dos Santos

Orientador: Anete P. Souza

Para uso da Comissão ou Comitê pertinente:
(X) Deferido (  ) Indeferido

Carimbo e assinatura

Prof. Dr. MARCELO LANCELLOTTI
Presidente da Comissão Interna de Biossegurança
Instituto de Biologia - UNICAMP

Para uso da Comissão ou Comitê pertinente:
(  ) Deferido (  ) Indeferido

Carimbo e assinatura